ABSTRACT

Title of Dissertation: **INVESTIGATION OF SMOOTH MUSCLE CELL DEATH AND GENOME INSTABILITY IN HUTCHINSON-GILFORD PROGERIA SYNDROME**

Haoyue Zhang, Doctor of Philosophy, 2016

Dissertation directed by: Dr. Kan Cao
Department of Cell Biology and Molecular Genetics
University of Maryland

Hutchinson–Gilford progeria syndrome (HGPS) is a severe human premature aging disorder caused by a lamin A mutant named progerin. Death occurs at a mean age of 13 y from cardiovascular problems. Previous studies revealed loss of vascular smooth muscle cells (SMCs) from large arteries in HGPS patient and mouse models, suggesting a causal connection between SMC loss and cardiovascular malfunction. The primary aim of this dissertation is to elucidate the molecular mechanisms underlying the massive SMC loss in HGPS. To study this, I develop an *in vitro* differentiation protocol to generate HGPS SMCs from induced pluripotent stem cells (iPSCs). My results indicate that HGPS SMCs exhibit a profound cell death phenotype, potentially recapitulating the *in vivo* SMC loss. Mechanistically, I find

that HGPS SMCs bear deficient homologous recombination (HR). In addition, progerin accumulation strongly suppresses PARP1 and consequently triggers an activation of the error-prone non-homologous end joining (NHEJ) response during S/G2 phase. As a result, HGPS SMCs exhibit prolonged mitosis and mitotic catastrophe.

Mis-regulated DNA damage response (DDR) is proposed to induce genome instability and various cellular phenotypes in HGPS, including HGPS SMC cell death. To better understand HGPS DDR misregulation, I examine HR and NHEJ in HGPS fibroblasts at different cell cycle phases. My analysis indicates that HR is deficient in S/G2 phase, whereas NHEJ, the dominant G0/G1 phase DDR pathway, is impaired in G0/G1 phase but active in S/G2 phase HGPS fibroblasts. The mis-regulation of HR and NHEJ may jeopardize genome integrity in both G0/G1 and S/G2 phase HGPS cells. Mechanistic study reveals that γH2AX, a crucial upstream DDR signal, is reduced in G0/G1 but normal in S/G2 phase HGPS cells, implicating a potential cause of the cell cycle-dependent NHEJ mis-regulation. Furthermore, this reduction is correlated with impaired ATM activation and loss of H3K9me3 in HGPS. Restoration of H3K9me3 by methylene blue treatment can stimulate ATM activity, improve γH2AX signaling and rescue NHEJ in G0/G1 phase HGPS cells. This dissertation not only is the first mechanistic study on HGPS SMC loss but also provides a molecular basis and therapeutic approach for the HGPS DDR deficiencies.

INVESTIGATION OF SMOOTH MUSCLE CELL DEATH AND GENOME INSTABILITY IN HUTCHINSON-GILFORD PROGERIA SYNDROME

by

Haoyue Zhang

Dissertation submitted to the Faculty of the Graduate School of the
University of Maryland, College Park, in partial fulfillment
of the requirements for the degree of
Doctor of Philosophy
2016

Advisory Committee:
Professor Kan Cao, Chair
Professor David Mosser
Professor Wenxia Song
Professor Steven Fisher
Professor Leslie Pick, Dean's Representative

Dedication

To my dearest family, for their endless support and caring.

Acknowledgements

I would like to express my gratitude to all who have helped me accomplish this dissertation and fulfill my Ph.D. study, which I would cherish for the rest of my life.

Primarily, I would like to thank my advisor Dr. Kan Cao, for her enlightening inspiration, patient guidance, and unconditional support. You have done so much teaching me how to ask questions, how to test ideas and how to troubleshoot problems. You have spared no effort guiding me through my projects, inspiring me with new ideas, polishing my proposal and paper writing skills and preparing me as an independent researcher. This dissertation would not be possible without your instruction.

Secondly, I would like to give my special thanks to every professor on my committee. Especially, I would like to thank Dr. Steven Fisher for all the inspiring suggestions on the smooth muscle cell project. Your comments have greatly benefited the project and helped me circumvent many obstacles. I would like to thank Dr. David Mosser, Dr. Leslie Pick and Dr. Wenxia Song for all the advice on my projects and comments on my results. You have taught me how to be a critical researcher. I also thank you for your suggestions on my future career path.

Thirdly, I owe my gratitude to everyone who is currently or was previously a member in the Cao lab. I would like to thank Dr. Zheng-mei Xiong for teaching me most of the experimental skills when I first joined the lab. I would like to thank Christina Lanada for teaching me how to drive a car and being a fantastic friend. I would like to thank Eunae Ko, Mike O'Donovan, Mason Trappio and Megan Leung for creating a convenient and relaxed atmosphere in the lab. I would like to thank Di

Wu, Kun Wang, Julie Choi, Dr. Pratima Bharti and Dr. Linlin Sun for all the helpful discussions in lab meetings. I would like to thank Zeshan Tariq for your contagious scientific enthusiasm. I would like to thank Dr. Andrews Flannery and Dr. Christina Tan from Dr. Norma Andrews' lab for your help on my projects. I would like to thank Amy Beaver and Ken Class from the imaging and FACS core for your technical help.

Finally, I would like to thank my lovely family and friends. I want to thank my Mom and Dad for the endless support and love. I will never be able to come to U.S. and achieve this degree without your encouragement. I would like to thank my wife, Yangling Ou for her unconditional love and support. International long distance relationship is an extremely tough process. I am so glad that I made it! I would like to thank my peers here at UMD and all my friends. My life is much more cheerful with you all in the picture.

Table of Contents

List of Figures

Chapter I: Introduction

Chapter II: Differentiation and characterization of HGPS smooth muscle cells via induced pluripotent stem cells (iPSCs)

Chapter III: Mechanisms controlling the smooth muscle cell death in progeria via down-regulation of poly(ADP-ribose) polymerase 1

Chapter V: Reduced ATM activation and histone H2AX phosphorylation delay NHEJ in G0/G1 phase HGPS fibroblasts

Chapter VI: Summary and future perspectives

List of Abbreviations

53BP1	p53 binding protein 1
AFR	α-fetoprotein
AON	antisense oligonucleotide
AP	Alkaline phosphatase
ATM	Ataxia telangiectasia mutated
ATR	Ataxia telangiectasia and Rad3 related
BAC	Bacteria artificial chromosome
BAF	Barrier-to-autointegration
Bax	Bcl2-associted protein X
BRCA1/2	Breast cancer 1/2
CDK	Cyclin dependent kinase
CHK1	Checkpoint kinase 1
CPT	Camptothecin
CtIP	CtBP1 intracting protein
CTSL	Cathepsin L
DDR	DNA damage response
DIC	Differential interference contrast
DNAPKcs	DNA dependent protein kinase, catalytic subunit
Dox	Doxorubicin
DSBs	Double strand DNA breaks

EZH2	Enhancer of Zeste homolog 2
Ftase	Farnesyltransferase
FTI	Farnesyltransferase inhibitor
γH2AX	Phosphorylation of histone variant H2AX serine 139
H3K27me3	Trimethylation of histone H3 lysine 27
H3K9me3	Trimethylation of histone H3 lysine 9
H4K16ac	Acetylation of histone H4 lysine 16
H4K20me2	Dimethylation of histone H4 lysine 20
H4K20me3	Trimethylation of histone H4 lysine 20
HDAC	Histone deacetylase
HGPS	Hutchinson-Gilford progeria syndrome
HJ	Holiday junction
HP1α	Heterochromatin protein 1α
HR	Homologous recombination
hTERT	Human telomerase reverse transcriptase
ICMT	Isoprenylcysteine carboxyl methyltransferase
ILCs	DNA interstrand crosslinks
INM	Inner nuclear membrane
iPSC	Induced pluripotent stem cell
IR	Ionized radiation
KAT5	Lys acetlytransferase
MAD	Mandibuloacral dysplasia
MB	Methylene blue

MEF	Mouse embryonic fibroblast
MMP	Mitochondrial membrane potential
MRN	Mre11-Rad50-Nbs1
NAC	N-acetyl cysteine
NHEJ	Non-homologous end joining
NPC	Nuclear pore complex
NuRD	Nucleosome remodeling deacetylase
PAPR1/2	Poly-(ADP-ribose) polymerase 1/2
PCNA	Proliferation cell nuclear antigen
PFLD	Lipodystrophy
PGC1α	Peroxisome proliferator-activated receptor gamma coactivator 1 alpha
PI	Propidium iodide
Pol l	Polymerase λ
Pol m	Polymerase μ
PP1	Protein phosphatase 1
PTIP	PAX transactivation activation domain-interaction protein 1
RBBP4	Retinoblastoma binding protein 4
RBBP7	Retinoblastoma binding protein 7
RFC	replication factor C
RIF1	RAP interacting factor 1
ROS	Reactive oxygen species
RPA	Replication protein A

SA-β-gal	Senescence associated β-galactosidase
SILAC	Stable isotope labeling with amino acid
SIRT1	Surtuin 1
SMA	Smooth muscle α actin
SMC	Smooth muscle cell
smMHC	Smooth muscle myosin heavy chain
SSBs	Single strand DNA breaks
SUV39h1	Suppressor Of Variegation 3-9 Homolog 1
Xi	Inactivated X chromosome
XLB3	Xenopus major lamin B3
XPA	Xeroderma pigmentosum group A

Publication Information

The data from this thesis composed the following publications.

Zhang H, Xiong Z and Cao K (2014). Mechanism controlling smooth muscle cell death in progeria via down-regulation of Poly (ADP-ribose) polymerase 1. PNAS, 111I(2) : 2261-2270

Zhang H, Sun L, Wang K, Wu D, Trappio M, Witting C, and Cao K (2016). Loss of H3K9me3 impairs ATM activity and H2AX phosphorylation in Hutchinson-Gilford Progeria Syndrome (submitted to Plos One).

Chapter I: Introduction

1.1 Hutchinson-Gilford progeria syndrome (HGPS)

1.1.1 General description

Hutchinson-Gilford progeria syndrome (HGPS) is one of the most devastating segmental aging diseases, initially characterized by Hutchinson and Gilford in 1886 and 1897 respectively (Atkins, 1954). It is an extremely rare autosomal dominant disease, occurring at a rate of 1 in every 4-8 million of live births (Capell and Collins, 2006; Merideth et al., 2008). HGPS associated premature aging phenotypes include nutrition deficiency independent growth impairment, bone abnormalities, joint contractures, sclerotic skin, lipodystrophy, alopecia and systematic cardiovascular dysfunctions(Gordon et al., 2007; Merideth et al., 2008). Patients with HGPS are born normal, while start to display the above phenotypes at about 12-24 months after birth and eventually die in their early teens (average 13 years old) due to cardiovascular diseases such as stroke or myocardial infarction (Gordon et al., 2007).

1.1.2 Clinical features of HGPS

In 2008, a natural history study performed by Merideth et al., comprehensively examined the pathological features in 15 HGPS patients. The study revealed that HGPS patients exhibited severe growth retardation after birth (Merideth et al., 2008). Between 2 to 10 years of age, an average gain of body weight was only 0.65kg per year in HGPS patients compared to 1.80kg in healthy children. Similarly, HGPS patients displayed an average gain of 3.58cm per year while healthy individuals gained 5.84cm per year. Patients who received growth hormone treatment displayed

faster weight and height growth with average gain of 1.01kg and 3.98cm per year respectively.

Besides retarded growth, HGPS patients also showed a variety of musculoskeletal abnormalities such as abnormal peripheral joint motion range (every child older than 18 month of age), reduced spinal flexibility (11 out of 11 tested), stooped shoulder (11 out of 15), calcaneovalgus (9 out of 15), subluxed finger joints (7 out of 15), genu valgum (4 out of 15), kyphosis (3 out of 15) and calcaneo varus (1 out of 15) (Merideth et al., 2008).

Finally, Merideth et al. characterized a variety of cardiovascular abnormalities associated with HGPS (Merideth et al., 2008). For example, patients showed elevated systolic or diastolic blood pressure (7 out of 15), elevated pulse rate for age (5 of the oldest children), oxygen saturation (13 out of 13 tested), long QT intervals (5 out of 15), thickened aortic valve (2 out of 15), distal anteroseptum ischemia (1 out of 15) and adventitia thickening (14 out of 15). Additionally, two previous postmortal studies on three HGPS patients revealed severe depletion of smooth muscle cells from aortic media, maladaptive vascular remodeling, intima thickening, disrupted elastin, deposition of extracellular matrix and sclerotic plaques induced stenosis (Stehbens et al., 2001; Stehbens et al., 1999). These phenotypes resulted in reduced cardiovascular functionality with age and are of particular interest given that the majority of HGPS patient death are due to cardiovascular defects.

1.1.3 Loss of vascular smooth muscle cells (SMCs) in HGPS

A drastic phenotype that has repeatedly been observed in HGPS patients and animal models is the loss of media layer vascular smooth muscle cells (SMCs) in the major aortas. In the 2000s, two postmortem studies uncovered this phenotype in three HGPS patients (Stehbens et al., 2001; Stehbens et al., 1999) (Figure 1-1A). In an HGPS mouse model (BAC G608G), scientists observed a progressive loss of media layer smooth muscle cells in the descending aorta (Varga et al., 2006) (Figure 1-1B). This phenotype was later on recapitulated by a different HGPS mouse model, $lmna^{G609G}$ (Osorio et al., 2011) (Figure 1-1C). Interestingly, vascular SMC loss has been long considered as a contribution to the development of cardiovascular disorders such as atherosclerosis (Bennett, 1999; Clarke et al., 2006). Notably, SMC loss has been implied to increase plaque vulnerability and induce vessel plaque rupture (Bennett, 1999; Clarke et al., 2006). These studies strongly suggest a role of SMC loss in HGPS cardiovascular pathology. However, the molecular mechanism underlying this phenotype remains to be elucidated.

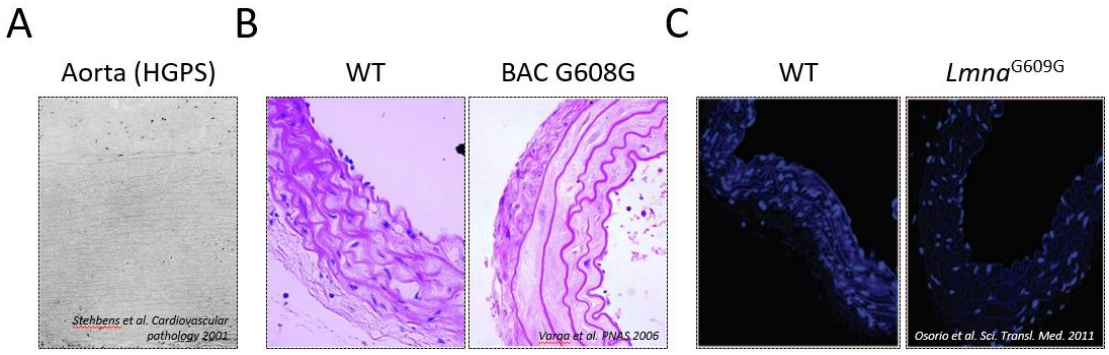

Figure 1-1: Vascular SMC depletion in HGPS. (A). Postmortem study of the atherosclerotic aorta from a male HGPS patient (adapted from Stehbens et al. *Cardiovascular Pathology 2001*). (B). H&E analysis of 12 month old mice aorta indicates loss of vascular SMCs in BAC G608G transgenic mice (adapted from Varga et al. *PNAS 2006*). (C). DAPI staining of aortic arch indicates depletion of vascular SMCs in $Lmna^{G609G}$ mice (adapted from Osorio et al. *Transl. Med. 2011*).

1.2 Causation: mutation in the *LMNA* gene

1.2.1 HGPS associated *LMNA* mutation

Given the fact that HGPS incidence did not show any family or sex preferences, it was initially difficult to genetically locate the mutated loci responsible for this specific disease. In 2003, Eriksson et al. successfully identified the prevalent (accounts for >80%) mutation for HGPS, using polymorphic microsatellite sequencing (Eriksson et al., 2003). This mutation is a spontaneous mutation in the *LMNA* gene on chromosome 1q21.2-q21.3 (Eriksson et al., 2003). It is a *de novo* mutation, which substitutes a single nucleotide (1824 C→T) in the exon 11 of the *LMNA* gene (Eriksson et al., 2003).

Under normal circumstances, *LMNA* gene mainly encodes two protein products: lamin A and lamin C (Capell and Collins, 2006). As a type V intermediate filament protein, lamin A consists of two globular domains at N terminus and C terminus respectively as well as a central α-helical rod domain. These domains allow lamin A to form homodimers and construct the nuclear lamina meshwork (see discussion in the next section) (Capell and Collins, 2006). At the C terminus of lamin A, there is a Ras-like-CAAX motif (C for cysteine, A for aliphatic amino acid and X for any

amino acid), which is indispensable for its maturation (Dechat et al., 2008; Zhang et al., 2013). With the CAAX motif, lamin A precursor undergoes a series of post-translational modifications, in which, every step is strictly dependent on the previous one and eventually becomes mature lamin A (Dechat et al., 2008; McCord et al., 2013; Zhang et al., 2013) (Figure 1-2A).

Among these modifications, the initial step is farnesylation of the cysteine residue on the CAAX motif by farnesyltransferase (Ftase) (Dechat et al., 2008; Zhang et al., 2013) (Figure 1-2A). Then, the last three amino acids (-AAX) are removed by a zinc metalloproteinase called Zmpste24/FACE1 (Figure 1-2A). The remaining cysteine at C terminus then undergoes carboxymethylation mediated by isoprenylcysteine carboxyl methyltransferase (ICMT) (Zhang et al., 2013) (Figure 1-2A). In the final step, the last 15 amino acids at C terminus including the farnesylated cysteine residue are removed by Zmpste24/FACE1, allowing the release of mature lamin A (Figure 1-2A). Mature lamin A, together with other nuclear lamina proteins (for example, B type lamins) form the nuclear lamina meshwork underneath the inner nuclear membrane (INM) (Capell and Collins, 2006).

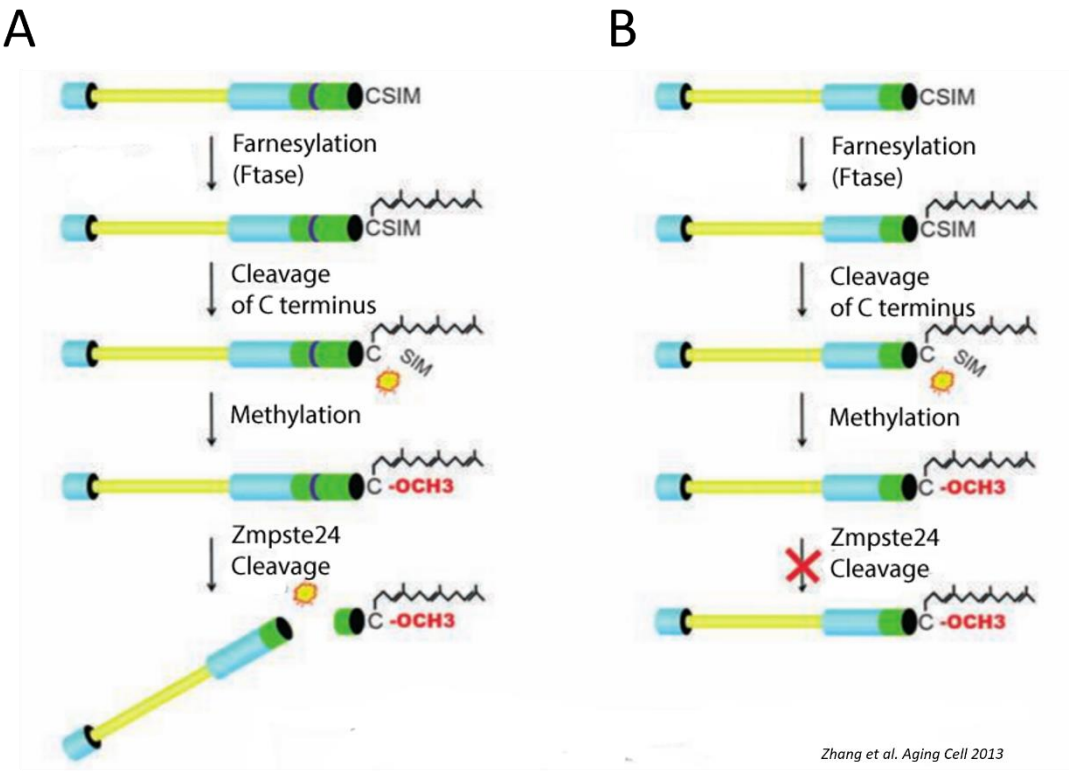

Figure 1-2: Post-translational processing of lamin A (A) and Progerin (B). Translation of the *LMNA* gene yields the prelamin A protein, which has the amino acids CSIM at the C-terminus. After farnesylation, a modification step that can be blocked by farnesyltransferase inhibitors (FTIs), the terminal three amino acids (SIM) are cleaved by the ZMPSTE24 endoprotease, and the terminal farnesylated cysteine undergoes carboxymethylation. A second cleavage step by the ZMPSTE24 endoprotease then removes the terminal 15 amino acids, including the farnesyl group. This final cleavage step is blocked in progerin (B) (adapted from Zhang et al. *Aging Cell* 2013).

In HGPS, the prevalent *de novo* mutation (1824 C→T) doesn't change the original amino acid sequence (G608G) (Figure 1-3). However, this mutation introduces a cryptic splicing donor site in exon 11 of *LMNA* gene (Zhang et al., 2013) (Figure 1-3). This splicing donor site can be recognized by spliceosome during transcription and yield a 150 nucleotides in frame deleted mRNA, which is eventually translated into a 50 amino acid deleted mutant protein termed progerin (Zhang et al.,

2013) (Figure 1-3). Progerin completely abolishes the Zmpste24/FACE1 cleavage site in wild type prelamin A and therefore retains a farnesyl tail on the C terminus (Capell and Collins, 2006; Zhang et al., 2013) (Figure 1-2B). This farnesyl tail permanently anchors progerin at the INM and functions in a dominant negative fashion and disrupts nuclear lamina meshwork (Capell and Collins, 2006).

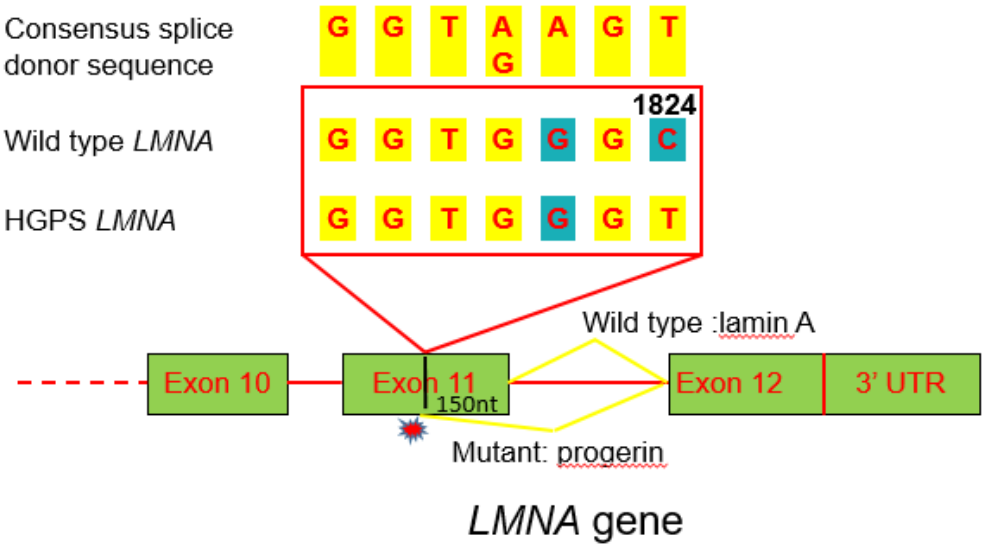

Figure 1-3: Scheme of the classic HGPS mutation in *LMNA* gene. The *LMNA* wild type sequence is similar to consensus splice donor site, with only two nucleotides different (indicated by blue). The 1824 cysteine in the wild type *LMNA* sequence was mutated into a thymine in HGPS, making the sequence closer to consensus splice donor site, with only one different nucleotide (indicated by blue). This mutation yields a cryptic splice donor site that can be recognized by spliceosome, resulting in a 150 nt in frame deletion and a mutant protein termed progerin.

1.2.2 Lamins and nuclear lamina

As discussed above, *LMNA* gene mainly encodes two A type lamins: lamin A, lamin C (Zhang et al., 2013). These two proteins are the two major products of *LMNA* gene and produced in roughly equal amounts(Capell and Collins, 2006). In addition,

LMNA also encodes another two minor products: laminAΔ10 and lamin C2 (Zhang et al., 2013). Lamin AΔ10 was only reported to be expressed in colon, lung and breast carcinomas and lamin C2 was confined in male germ cells (Burke and Stewart, 2013; Capell and Collins, 2006; Hutchison, 2002). Besides A type lamins, there are three B type lamin proteins: lamin B1 encoded by *LMNB*1, lamin B2 encoded by *LMNB*2 and lamin B3 encoded by *LMNB*2. Whereas A type lamins are highly regulated throughout mammalian development and exclusively expressed in differentiated somatic cells, B type lamins are present ubiquitously in all cell types (Burke and Stewart, 2013; Capell and Collins, 2006).

Both A and B type lamins belong to the type V intermediate filament proteins, which harbor a central α-helical coiled-coil rod domain flanked by an amino (N) terminal globular head domain and a carboxy (C) terminal globular tail domain (Burke and Stewart, 2013; Capell and Collins, 2006). The central rod domain allows A or B type lamins to form parallel coiled-coil homodimers in a head-to-tail fashion, which then align laterally to form anti-parallel protofilaments (Burke and Stewart, 2013; Capell and Collins, 2006). Eight protofilaments associate to form the intermediate filament structure (Capell and Collins, 2006). Lamin intermediate filaments then form a complex meshwork structure underneath the inner nuclear membrane (INM) termed nuclear lamina (Burke and Stewart, 2013). Nuclear lamina was initially considered to be little more than a structural apparatus, which only provides mechanical rigidity to support nuclear envelope. However, increasing evidences have recently revealed that nuclear lamina plays far more complex roles maintaining cellular homeostasis and is involved in critical cellular processes such as

chromatin organization, cell cycle regulation, DNA replication, DNA damage repair and etc. (Burke and Stewart, 2013; Capell and Collins, 2006; Dechat et al., 2008; Hagting et al., 1999; Stuurman et al., 1998).

Nuclear lamina in chromatin organization: nuclear lamina is suggested to provide anchoring points for chromatin domains and thereby regulate chromatin structure and histone modifications. The initial evidence supporting this idea is that A type lamins have been shown to directly interact with core histones and DNA through their tail domain (Andres and Gonzalez, 2009; Parnaik, 2008; Shoeman and Traub, 1990; Taniura et al., 1995). A type lamins also indirectly bind to chromatin through interacting with lamin binding proteins such as Lap2a and barrier-to-autointegration (BAF) (Andres and Gonzalez, 2009; Dechat et al., 2009; Vlcek and Foisner, 2007). Microscopic study provided evidence that lamin A was able to interact with Lap2α and locate heterochromatin to the nuclear envelope and potentially suppress gene transcription (Dechat et al., 2009; Reddy et al., 2008; Verstraeten et al., 2007). Moreover, evidence consolidating the functional importance of A type lamins in regulating chromatin structure come from reports on *LMNA* mutations. Loss of functions studies by knocking out lamin A from *C. elegans* or Drosophila have revealed abnormal chromatin organizations and developmental aberrations (Andres and Gonzalez, 2009; Parnaik, 2008). Cardiomyocytes from *LMNA* deficient ($Lmna^{-/-}$) mouse have been shown to display dissociated heterochromatin from nuclear envelope (Nikolova et al., 2004). In addition, patient cells from multiple laminopathies (diseases caused by mutations associated with lamin encoding genes such as *LMNA*, *LMNB1* and *LMNB2*) including HGPS, Mandibuloacral dysplasia

(MAD) and familial partial lipodystrophy (PFLD) all exhibit general loss of heterochromatin (Capanni et al., 2003; Capell and Collins, 2006; Filesi et al., 2005).

Nuclear lamina in cell cycle regulation: at the onset of mitosis, nuclear lamina is phosphorylated by cyclin B/CDK1, which leads to its disassembly and allows mitotic spindles to interact with kinetochores (Hagting et al., 1999; Stuurman et al., 1998). During this process, B type lamins are associated with disassembled nuclear envelopes while A type lamins are soluble and distributed evenly in the entire cell till the end of mitosis (Dechat et al., 2008; Goldman et al., 2002). Interestingly, it is unclear whether lamins play a role in nuclear envelope reassembly at the end of mitosis. There is evidence suggesting that de-phosphorylation of B type lamins by protein phosphatase 1 (PP1) that targets the nuclear envelope is a prerequisite for their reassembly (Steen et al., 2000; Thompson et al., 1997). Alternatively, there are also studies claiming that lamins don't participate in nuclear envelope reassembly, but were transported into the nuclear vesicles around chromatins through nuclear pore complexes (Meier et al., 1991; Newport et al., 1990).

Nuclear lamina in DNA replication: Both lamin A and B participate in regulating DNA replication. Unlike B type lamins which exclusively locates at the nuclear periphery and associates with the nuclear envelope, A type lamins are partially distributed in the nucleoplasmic region. This part of A type lamins are believed to play a role in the initiation of DNA replication (Dechat et al., 2008; Kennedy et al., 2000). In early S phase, the nucleoplasmic lamin A/C structures are associated with the replication origin sites in primary fibroblasts (Kennedy et al., 2000). During S phase, lamin B1 co-localizes with the proliferating cell nuclear

antigen (PCNA) in the replication machinery in 3T3 cells (Dechat et al., 2008; Moir et al., 1994). Moreover, studies in Xenopus egg extracts revealed that immuno-depletion of Xenopus major lamin XLB3 or introduction of XLB3 dominant negative mutant will inhibit DNA replication (Dechat et al., 2008; Meier et al., 1991; Newport et al., 1990). Introduction of dominant negative XLB3 mutant will result in redistribution of endogenous XLB3 foci along with PCNA and replication factor C (RFC) (Moir et al., 2000; Spann et al., 1997). Interestingly, re-establishment of normal lamin structure by transferring these foci into fresh extracts would resume DNA replication, suggesting an essential role of appropriate lamin structure in DNA replication (Moir et al., 2000).

Nuclear lamina in DNA damage repair: several recent studies have enlightened the important role of lamin A/C in DNA damage repair. For instance, lamin A/C deficient cells exhibited elevated sensitivity to DNA inter-strand crosslinks (ICLs) and replication stress. When treated with ICLs agents, lamin A/C deficient cells displayed decreased recruitment of FANCD2 (a DNA damage repair factor), delayed γH2AX (DNA double strand break marker) clearance and increased aberrant chromosomes (Singh et al., 2013). Similar effects were also observed in cells treated with hydroxyurea (a replication stress inducing agent) (Singh et al., 2013). In addition, lamin A also stabilizes DNA damage repair foci by engaging into chromosome through histone variant H2AX (Mahen et al., 2013). Lamin A/C favor both non-homologous end joining (NHEJ) and homologous recombination (HR) DNA repair pathways by regulating DNA repair protein homeostasis. Depletion or shRNA mediated suppression of lamin A results in cysteine protease Cathepsin L

(CTSL) mediated degradation of p53 binding protein 1 (53BP1) (an important NHEJ promoting factor) and transcriptional reduction of breast cancer 1 (BRCA1) and RAD51 (two key HR regulators) (Gibbs-Seymour et al., 2015). Consequently, deletion of lamin A/C inhibits both NHEJ and HR and renders persistent DNA breaks, chromosome aberrations and increased radio-sensitivity (Gibbs-Seymour et al., 2015; Singh et al., 2013). Mechanistically, 53BP1 binds to lamin A/C via its Tudor domain in undamaged human dermal fibroblasts, suggesting a role of lamin A/C maintaining a nucleoplasmic pool of 53BP1 (Gibbs-Seymour et al., 2015). Collectively, these studies illustrate a crucial role of lamin A/C in DNA repair.

Given such physiological importance, mutations in lamin encoding genes may disrupt organism homeostasis and lead to pathological consequences. As a matter of fact, there are over 180 mutations in these genes that are associated with at least 13 diseases (termed as the laminopathies), including HGPS (Capell and Collins, 2006). In HGPS, the presence of progerin disrupts the structure and function of the nuclear lamina and results in a variety of pathological phenotypes. At the systematic level, progerin induces severe premature aging phenotypes as described in 1.1. At the cellular level, progerin disrupts nuclear morphology, perturbs heterochromatin organization and interfere with numerous critical cellular processes such as DNA damage repair，mitochondrial respiration etc. (Capell and Collins, 2006; Dechat et al., 2008).

1.3 HGPS cellular and molecular phenotypes

1.3.1 Nuclear "blebbing" in HGPS

Abnormal nuclear morphology is one of the most frequently observed phenotypes in HGPS. Primary fibroblasts from HGPS patients display a lobulated nuclear morphology termed as nuclear blebbing (Eriksson et al., 2003; Goldman et al., 2004). The abnormal nuclear shape is usually accompanied by a disrupted spatial distribution of nuclear pore complex (NPC) (Goldman et al., 2004). Interestingly, as progerin gradually builds up inside the cell, the "nuclear blebbing" phenotype becomes more severe, suggesting a role of progerin in this phenotypical development (Driscoll et al., 2012; Goldman et al., 2004). In fact, the farnesyl tail of progerin within the CAAX motif, enhances its affinity with SUN1, a component of the LINK (links the nucleoskeleton and cytoskeleton) complex, results in SUN1 accumulation at the nuclear envelope and potentially impacts nuclear structure (Chen et al., 2012; Chen et al., 2014). However, studies need to be done to further reveal the molecular and physical mechanisms underlying this phenotype.

Structural abnormalities in the nucleus are often coupled with functional alterations. For example, NPC is a critical structure that spans across both inner and outer nuclear membranes and governs protein nuclear transportation (Kelley et al., 2011). It is also a multi-functional apparatus that regulates a variety of other cellular processes including RNP assembly, mRNA quality control and SUMOylation (Kelley et al., 2011). Disruption of NPC organization in HGPS potentially impacts its interaction with nuclear import and export receptors, interferes with nuclear-

cytoplasmic Ran gradient and impedes nuclear transportation of numerous proteins (Kelley et al., 2011; Zhang et al., 2014).

1.3.2 Abnormal chromatin structure and epigenetic modifications in HGPS

Progerin has been shown to interfere with chromatin organization in HGPS cells. Particularly, HGPS cells display a passage dependent progressive loss of peripheral heterochromatin, a highly organized and transcriptionally repressive chromatin structure that is mainly associated with nucleoli and nuclear lamina (Figure 1-4). This loss is accompanied by progerin accumulation and nuclear lamina thickening (Goldman et al., 2004; McCord et al., 2013). Moreover, we have previously shown that there is a global loss of spatial chromatin compartmentalization in late passage HGPS cells by genome wide chromosome conformation capture (Hi-C), suggesting additional structural abnormalities in HGPS (Goldman et al., 2004; McCord et al., 2013).

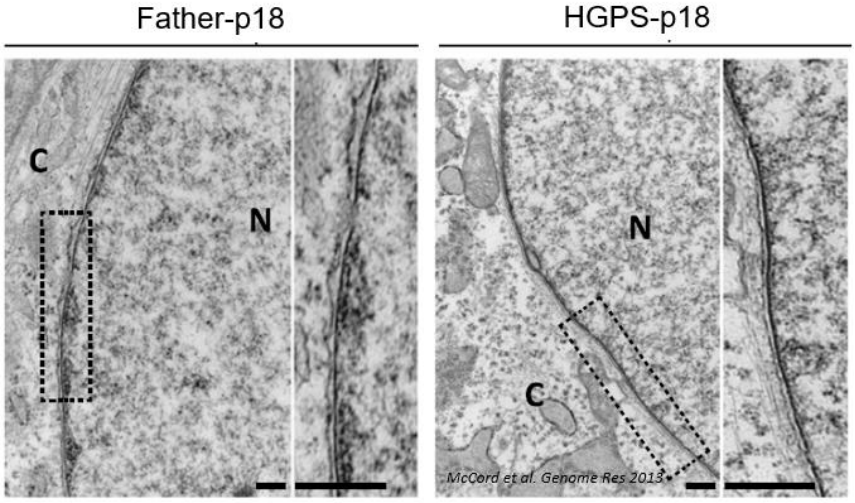

Figure 1-4: Loss of peripheral heterochromatin in HGPS fibroblasts. Electronic microscopy analysis of HGPS fibroblasts at passage 18 and normal control fibroblasts (father of HGPS patient) at passage 18, showing a loss of peripheral heterochromatin in HGPS nucleus. Regions cropped by dot boxes were illustrated by higher magnification views on the right. C and N indicate cytoplasm and nucleus respectively (adapted from McCord et al. *Genome Res*. 2013).

Multiple lines of evidence have suggested abnormal histone modifications in HGPS cells (McCord et al., 2013; Scaffidi and Misteli, 2005; Shumaker et al., 2006). Specifically, progressive changes in histone methylations that mark heterochromatin were most frequently observed. These methylations are: facultative heterochromatin marker, trimethylation of histone H3 lysine 27 (H3K27me3) and constitutive heterochromatin markers, trimethylation of histone H3 lysine 9 (H3K9me3) and trimethylation of histone H4 lysine 20 (H4K20me3) (McCord et al., 2013; Shumaker et al., 2006). To date, H3K27me3 and H3K9me3 are found to be down-regulated in HGPS cells, while H4K20me3 has been shown to be down-regulated. These changes are not only observed in HGPS primary fibroblasts, but also seen in cells ectopically expressing progerin, suggesting a direct role of progerin in this abnormalities (Dechat et al., 2008). Significantly, the change in H3K27me3 happens as an early event, before the appearance of other cellular defects such as nuclear blebbing, and therefore is considered to be an upstream mechanism responsible for various cellular defects in HGPS (McCord et al., 2013; Shumaker et al., 2006). Indeed, our previous study illustrated that the association between lamin A/C and chromatin was reduced in regions with low H3K27me3 abundance in HGPS (McCord et al., 2013). Mechanistically, H3K27me3 was able to physically interact with lamin A/C. Therefore, depletion of H3K27me3 reduces the association between lamin A/C and

chromatin (McCord et al., 2013). These findings provided a mechanistic explanation of the heterochromatin loss phenotype in HGPS.

Besides structural changes, abnormal epigenetic modifications also led to functional compromises in HGPS cells. For example, we have previously shown that local changes in H3K27me3 enrichment at specific gene promoters were significantly correlated with gene expression alterations in HGPS cells (McCord et al., 2013). Loss of H3K27me3 on the inactive X chromosome (Xi) results in partial decondensation of the X chromosome and can potentially cause transcriptional activation in those regions (Dechat et al., 2008; Shumaker et al., 2006). In addition to histone methylation, abnormal histone acetylation pattern is observed Zmpste24$^{-/-}$ mouse embryonic fibroblasts, a MEF that mimics HGPS by producing unprocessed prelamin A. Krishnan et al, reported that there was a down-regulation of acetylation on histone H4 lysine 16 in Zmpste24$^{-/-}$ MEFs. This down-regulation rendered a more condensed chromatin structure which created a physical barrier preventing DNA repair factors from access to the damaged DNA lesions (Krishnan et al., 2011).

Over the past decade, scientists have revealed some mechanistic insights underlying these abnormal histone modifications in HGPS. For example, the loss of H3K27me3 is possibly due to a down-regulation of enhancer of zeste homolog 2 (EZH2), a methyltransferase responsible for its maintenance (McCord et al., 2013; Shumaker et al., 2006). The mechanism that manifests H3K9me3 loss still remains to be uncovered. However, scientists reported a significant down-regulation of heterochromatin protein 1α (HP1α), a histone binding protein that associated with H3K9me3 and maintained its abundance (Dechat et al., 2008; Scaffidi and Misteli,

2005; Xiong et al., 2015). Knockdown of HP1α results in a significant loss of H3K9me3, supporting the critical role of HP1α in H3K9me3 maintenance (Zhang et al., 2015). This information together highlights HP1α down-regulation as a potential candidate responsible for H3K9me3 loss in HGPS.

1.3.3 Defective DNA damage repair and genome instability in HGPS

As I discussed in 1.2.1, nuclear lamina serves as an important regulator in DNA damage repair. Deletion of lamin A/C leads to deficient DNA repair upon various types of DNA damages. Given such importance, functional disruption of the nuclear lamina by progerin may impact DNA damage repair and increase genome instability. Indeed, HGPS fibroblasts display a variety of phenotypes that can be caused by sustained DNA damage, such as reduced proliferative capacity, premature direct evidence demonstrating the defective DNA damage repair in HGPS was reported in 2005. In that study, Liu et al. showed that upon the insult of excessive DNA damage by ionized irradiation, HGPS fibroblasts and Zmpste24$^{-/-}$ MEFs displayed a delayed recruitment of 53BP1, an important NHEJ regulator, towards the damaged DNA lesions (Liu et al., 2005). In addition, the recruitment of Rad51, a critical player in HR DNA damage repair pathway was also shown to be delayed in HGPS fibroblasts and Zmpste24$^{-/-}$ MEFs (Liu et al., 2005). As a result, HGPS fibroblasts or Zempste24-/- MEFs displayed significantly higher sensitivity to DNA damage inducing agent and slower rate of recover compared to normal control (Liu et al., 2005). Notably over expressing of progerin in HeLa cells was able to recapitulate this phenotype,

supporting a direct role of progerin impairing DNA damage repair (Manju et al., 2006).

Mechanistically, progerin was proposed to disrupt DNA damage repair by interfering with lamin A/C functionality. For example, Krishnan et al. reported that in Zmpste24$^{-/-}$ MEFs, unprocessed prelamin A interferes with the interaction between lamin A and the histone acetyltransferase Mof, disrupts Mof retention at nuclear matrix, and impairs 53BP1 foci formation at DNA lesions (Krishnan et al., 2011). In another study from the same group, unprocessed prelamin A and progerin was also shown to disrupt the interaction between lamin A and the NAD^+-dependent deacetylase, Sirtuin 1 (SIRT1) (Liu et al., 2012). Given the importance of SIRT1 in DNA damage repair, this study points out a potential mechanism through which progerin impacts DNA damage repair. Epigenetic alterations are also proposed to impact DNA damage repair in HGPS or Zmpste24$^{-/-}$ cells. For example, loss of H4K16ac induced by prelamin A was considered to render a more condensed chromatin structure and create a physical barrier preventing DNA repair factors to access to the damaged foci in Zmpste24$^{-/-}$ MEFs (Krishnan et al., 2011). In addition, progerin was shown to reduce retinoblastoma binding protein 4 and 7 (RBBP4 & RBBP7) and histone deacetylase (HDAC), all of which were components of nucleosome remodeling deacetylase (NuRD) complex and played critical roles in chromatin modification. Importantly, loss of these proteins corresponded with DNA repair defects in HeLa cells, suggesting an alternative mechanism through which progerin perturbed DNA repair by impacting chromatin modifications (Pegoraro et al., 2009).

Not only, does progerin block DNA damage repair, its accumulation also increases the source of DNA damage. Specifically, it has been reported to induce DNA breaks by increasing the level of reactive oxygen species (ROS) (Richards et al., 2011; Xiong et al., 2015). It is well established that ROS is an important contributor to genome instability. By reacting with the double strand bonds, ROS is able to induce more than 20 types of DNA breaks (Cooke et al., 2003). If not properly repaired, single strand breaks (SSBs) created by ROS will turn into double strand breaks (DSBs) and threaten genome integrity. Importantly, it was previously reported that ROS accumulates in HGPS cells (Richards et al., 2011). Accumulated ROS was shown to correlate with impaired proliferation capacity in HGPS cells, in agreement with the inhibitory role of DNA damage in cell cycle progression (Richards et al., 2011). Moreover, treatment with ROS scavenger N-acetyl cysteine (NAC) was able to alleviate their DNA damage basal level and improved population doubling times (Richards et al., 2011).

Taken together, progerin jeopardizes genome integrity not only by disrupting proper DNA damage repair, but also by introducing more DNA damage. As a result, HGPS cells exhibit an elevated basal level of DNA damage (Liu et al., 2008). Un-repaired DNA damage is proposed to be responsible for a variety of cellular defects in HGPS, including growth defects, premature senescence and genome instability (Krishnan et al., 2011; Liu et al., 2012; Liu et al., 2005; Liu et al., 2013a; Liu et al., 2013b; Liu et al., 2008; Zhang et al., 2014).

1.3.4 Mitochondrial deficiencies in HGPS

ROS production is highly correlated with mitochondrial functionality. Disruption of mitochondrial function could result in oxidative stress under various pathological situations (Murphy, 2009; Xiong et al., 2015). Studies performed by our group and others have confirmed a progerin induced mitochondrial disruption in HGPS cells (Rivera-Torres et al., 2013; Xiong et al., 2015). To begin with, a recent SILAC (stable isotope labeling with amino acid) analysis revealed that the mitochondrial oxidative phosphorylation proteins were down-regulated in HGPS patients compared to normal subjects (Rivera-Torres et al., 2013). Similar reductions were also observed in fibroblasts obtained from adult progeroid mouse models: $Zmpste24^{-/-}$ and $Lmna^{G609/G609}$ (a mouse progerin knock-in model) (Rivera-Torres et al., 2013). As expected, mitochondrial ATP synthesis was also found to be reduced HGPS fibroblasts (Pagano et al., 2014). Recently, our group showed that HGPS fibroblasts bear swollen and fragmented mitochondria (Xiong et al., 2015). Functional wise, HGPS fibroblasts and progerin expressing normal controls displayed slower mitochondria movement, disrupted mitochondrial membrane potential (MMP) and increased ROS (Xiong et al., 2015). Interestingly, HGPS cells displayed a significant down-regulation of the peroxisome proliferator-activated receptor gamma coactivator 1α (PGC1α), a central regulator of mitochondrial biogenesis which controlled the expression of many mitochondrial proteins, suggesting a potential mechanism underlying mitochondrial deficiencies in HGPS (Xiong et al., 2015). Notably, over expression of progerin was shown to induce the above defects and

directly inhibit PGC1α expression, validating a negative effect of progerin on mitochondrial structure and functionality (Xiong et al., 2015).

1.3.5 Therapeutic approaches

Based on HGPS pathology, several therapeutic approaches have been developed to either alleviate the toxic effects of progerin or reduce the amount of progerin. As I mentioned in 1.2.1, progerin retains a permanent farnesyl tail, resides on the inner nuclear membrane and disrupts nuclear structure. Therefore, one representative attempt to counteract progerin's toxic effects is to block its farnesylation by using farnesyltransferase inhibitors (FTIs). Treating HGPS fibroblasts or normal fibroblasts over expressing progerin with FTIs was able to improve their nuclear morphologies (Capell et al., 2005). Moreover, *in vivo* studies on HGPS mouse models confirmed that FIT treatment was able to rescue a variety of disease phenotypes including growth retardation, bone sickness and vascular SMC loss (Capell et al., 2008; Yang et al., 2006). The positive results from these studies have led to a clinical trial of FTIs on HGPS patients (Gordon et al., 2012).

Progerin has been shown to disrupt mitochondrial functionality, increase ROS and cause DNA damage (Rivera-Torres et al., 2013). Based on this information I proposed a novel approach to counter act progerin by targeting its defective mitochondria. Specifically, we adopted methylene blue (MB) a mitochondrial targeting antioxidant (Xiong et al., 2016). Our study showed that MB treatment not only rescued HGPS associated mitochondrial defects, but also significantly delayed premature senescence, improved cell proliferation and restored nuclear morphology

and histone modifications (Xiong et al., 2016). Further analysis confirmed MB treatment drove a release of progerin from inner nuclear membrane. These results indicated MB as a promising therapeutic approach to treat HGPS.

The second type of attempts aims at reducing the level of progerin and thereby reduce toxicities. For example, Scaffidi et al. were able to reduced progerin mRNA level by using sequence specific morpholino antisense oligonucleotides (AONs), which blocked the cryptic splicing sites. HGPS fibroblasts treated with AONs displayed improved nuclear morphology and fixed gene expression profile (Scaffidi and Misteli, 2005). *In vivo* study performed by Osorio et al. confirmed that morpholino treatment was able to alleviate disease phenotypes in an HGPS mouse model (*lmna*^{G609G}) (Osorio et al., 2011). However, the dosage of morpholino in these studies was relatively high (micromolar level). Therefore, attentions should be paid to off-target effects.

Approaches have also been taken to directly reduce progerin protein level. In 2011, Cao et al. showed that rapamycin, a macrolide antibiotic, was able to decrease the formation of insoluble progerin aggregates and stimulate progerin degradation by an autophagic mechanism in HGPS cells. *In vitro* study revealed that treatment with rapamycin was able to rescue HGPS nuclear morphology, delay cellular senescence and improve cell proliferation (Cao et al., 2011b).

1.4 Connections between HGPS and normal aging

Whether progeriod disease such as HGPS resembles an accelerated form of normal aging is under debate for decades. Recent progresses on HGPS have identified phenotypical and mechanistic similarities between HGPS and normal aging process. For example, HGPS patients and conventional geriatric individuals share many common aspects in terms of cardiovascular pathology (Olive et al., 2010). Immunohistochemistry study on the artery of two HGPS patients who died from myocardial infarction identified a series of classical features that observed in normal aging atherosclerosis (Olive et al., 2010). In addition, several normal aging associated cellular phenotypes have been observed in HGPS including: cellular senescence, altered heterochromatin structure, defective DNA damage repair, disrupted mitochondrial function and etc., suggesting that there are common mechanisms shared between normal aging and HGPS (Burtner and Kennedy, 2010).

The connection between HGPS and normal aging is strengthened by the discovery that progerin accumulates in normal senior individuals. Scaffidi et al. reported that primary cells from normal senior individuals displayed a sporadic use of the classic HGPS cryptic splice donor site, resulting in accumulation of progerin (Scaffidi and Misteli, 2006). Moreover, Olive et al. observed an age associated (1 month to 97 years) progerin deposit that accumulates at a rate of 3.34% per year in the coronary arteries of normal individuals, suggesting that progerin may participate in normal cardiovascular pathology (Olive et al., 2010). Together, these evidences emphasize the similarities between HGPS and normal aging and suggest that

elucidating molecular mechanism underlying HGPS will benefit our understanding of normal aging processes.

1.5 DNA damage responses (DDRs)

1.5.1 DNA damage response, senescence, and aging

Nuclear DNA is under constant attacks by endogenous or exogenous damaging inducing agents such as ROS, UV light, irradiation, chemical drugs etc. (Zhang et al., 2014). These agents create multiple types of DNA damages including single strand DNA break (SSB), double strand DNA break (DSB), DNA inter-strand crosslinks (ICLs) etc. Among them, DSB is the most severe type of DNA damage, causing chromatin rearrangement, genome instability, cell death or cancer (Jackson, 2002). To properly handle DSBs, eukaryotic cells developed sophisticated mechanisms to sense and response to DSBs. Failure to properly fix DSBs will result in sustained DDR and form observable DDR foci, where DDR proteins are recruited to form aggregates and transduce DDR signals (d'Adda di Fagagna, 2008). Initial DDR signals at DNA break lesions are passed on to distant nuclear regions by diffusible checkpoint proteins such as CHK1 and CHK2. p53, then is activated and mediates cell cycle arrest by transcriptionally activating p21, a CDK inhibitor (d'Adda di Fagagna, 2008). This arrest is transient if DSBs are properly fixed. However, if DNA damage is severe, sustained DDR may induce a status of permanent cell cycle arrest termed cellular senescence (d'Adda di Fagagna, 2008).

At the organism level, senescent cells are observed to accumulate within tissues. For example, senescence associated β-galactosidase analysis revealed an increased percentage of senescent skin cells in aged healthy individuals (Dimri et al., 1995). A potential mechanism driving cellular senescence *in vivo* is through DDR activation. Indeed, DDR positive cells were observed more in the skin of baboons with age. These DDR foci (γH2AX and 53BP1) were located at telomeric regions, suggesting telomere de-protection and replicative exhaustion during age (Herbig et al., 2006; Jeyapalan et al., 2007). The presence of senescent cells within tissues is considered to disrupt normal tissue homeostasis and contribute to physiological aging (Campisi, 2001). Removal of p16 positive senescent cells from mice was shown to delay aging associated disorders (Baker et al., 2011).

Given the role of DDR in cellular senescence, it is widely accepted that defective DNA damage repair causes accumulation of DSBs in HGPS cells and is responsible for their premature senescence phenotypes (Krishnan et al., 2011; Liu et al., 2005; Liu et al., 2013a; Liu et al., 2013b; Liu et al., 2008).

1.5.2 Initiation and amplification of DDR signals upon DSBs

DSBs can be directly recognized by proteins in a sequence independent manner (Polo and Jackson, 2011). For example, poly-(ADP-ribose) polymerase 1 and 2 (PARP1 and PARP2) are among the most efficiently recruited proteins and severe as the sensor of DNA breaks (Polo and Jackson, 2011). They were shown to directly bind to DNA through their N terminal Zinc finger domain and basic N terminal domain respectively (Ame et al., 1999; Menissier-de Murcia et al., 1989). This

binding will trigger their catalytic activity and mediate poly ADP-ribosylation at DNA breaks, initiating down-stream repair signals (Polo and Jackson, 2011). Other DNA break sensor proteins include Ku70-Ku80 complex and Mre11-Rad50-Nbs1 (MRN) complex. Ku70-Ku80 complex binds to DSB break ends with high affinity and then recruits a variety of down-stream factors through protein-protein interaction (Polo and Jackson, 2011). Recognizing similar structures, Ku70-Ku80 complex and PAPR1 compete at DNA break ends to mediate different DNA repair programs (Polo and Jackson, 2011; Wang et al., 2006).

After break detection, down-stream signaling proteins and repair factors are subsequently recruited to DSBs through protein-protein interaction with sensors. For example, DNA dependent protein kinase, catalytic subunit (DNA-PKcs) binds to the C terminus of Ku80 and is recruited to DSBs to mediate NHEJ (see next section) (Polo and Jackson, 2011). Another critical DDR signal protein is ataxia telangiectasia mutated (ATM). Through interacting with the MRN complex, ATM is recruited to DSBs, where it undergoes auto-phosphorylation and self-activation (d'Adda di Fagagna, 2008). Activated ATM, then phosphorylate histone variant H2AX at serine 139, yielding γH2AX, a modification widely viewed as a marker of DSBs (Bouquet et al., 2006; Burma et al., 2001; d'Adda di Fagagna, 2008). γH2AX can be recognized by MDC1, whose join triggers the additional accumulation of MRN complex and ATM (d'Adda di Fagagna, 2008). Newly recruited ATM is able to phosphorylate adjacent H2AX and thereby create a positive feedback loop to amplify DDR signals (Bouquet et al., 2006; d'Adda di Fagagna, 2008; Polo and Jackson, 2011). In mammals, this spreading of γH2AX signals occupies several megabases beyond the

original broken DNA lesion (Polo and Jackson, 2011) (Rogakou et al., 1999). This process concentrates MDC1, which serves as a platform for the loading of various signal and repair factors such as 53BP1, RNF8, Nbs1, Rad51 etc (d'Adda di Fagagna, 2008; Polo and Jackson, 2011).

1.5.3 The error-prone NHEJ DSB repair pathway

There are two major DSB repair pathways: non-homologous end joining (NHEJ) and homologous recombination (HR). NHEJ is the prevalent DSB repair pathway and is active throughout the cell cycle, although favored in G1 phase (Chapman et al., 2012). Unlike HR, which relays on the presence of sister chromatid as DNA template, NHEJ operates in a template independent manner. NHEJ mediates the direct ligation of two random DNA break ends at proximity and therefore is often error prone, resulting in small insertions or deletions of chromatin (Chapman et al., 2012; Polo and Jackson, 2011). At the beginning of NHEJ, Ku70 and Ku80 form a ring-shaped heterodimer complex and encircles the duplex DNA ends with a strong equilibrium dissociation constant (~10^{-9} M) (Lieber, 2010; Polo and Jackson, 2011). Ku70-Ku80 complex serves as a dock to load additional kinase, nuclease and polymerases (Lieber, 2010).

One of these factors is DNA-PKcs, a kinase that specifically binds to blunt end double strand DNA (Lieber, 2010). Once recruited, DNA-PKcs undergoes an initial auto-phosphorylation and acquires serine and threonine kinase activity (Lieber, 2010). DNA-PKcs interacts, phosphorylates and activates with a variety of proteins, one of which is the endonuclease Artemis. The Artemis-DNA-PKcs complex

possesses 5’ exonuclease, 5’ endonuclease and 3’ endonuclease activities and is able to mediate break end resection on a wide range of DNA end configurations to create micro-homology (Lieber, 2010; Ma et al., 2002). However, this process is largely restricted, with a nucleolytic resection amount ranging from 0 to 14 nucleotides in most cases (Lieber, 2010).

Polymerases μ (Pol μ) and λ (Pol λ) are directly recruited to Ku at DSBs through their BRCT domain (Lieber, 2010; Ma et al., 2004). Both Pol μ and Pol λ are much more flexible than most other polymerases during poly-nucleotide synthesis (Lieber, 2010). Pol μ is particularly important for NHEJ as it mediates both template dependent and independent DNA synthesis (Gu et al., 2007; Lieber, 2010). Moreover, Pol μ is able to incorporate rNTP into DNA strands which is important for NHEJ during G1 phase, when dNTP level is low and rNTP level is high (Gu et al., 2007; Lieber, 2010). Pol μ is able to add random nucleotides to DNA blunt ends in a template independent fashion and create a 3’ single strand overhang, which will significantly enhance ligation efficiency (Lieber, 2010). However, due to this randomness, Pol μ activity introduces heterogeneity during NHEJ even with a pair of relatively homogenous DNA ends to start with (Lieber, 2010).

The final step of NHEJ is DNA ligation. DNA-PKcs is able activate the ligation activity of XRCC4-Ligase IV complex, which mediates the rejoining of two break ends (Lieber, 2010). Unlike other ligases, XRCC4-Ligase IV complex has very high enzymatic flexibility. It is capable of ligating complex DSB ends such as incompatible ends and nicking ends. In summary, enzymes (nuclease, polymerases and ligase) involved in NHEJ are efficient, yet flexible and are able to process

different DNA conformations. These flexibility creates high mutation probability and therefore renders NHEJ as an error prone DSB repair pathway.

1.5.4 The error-free HR DSB repair pathway

As discussed above, NHEJ is favored in G1 phase although active during the entire cell cycle. In contrast, HR is mostly observed in S/G2 phase, when sister chromatid is accessible (Chapman et al., 2012; Mao et al., 2008; San Filippo et al., 2008). Unlike NHEJ, which is error-prone, HR is mutation free and can accurately fix DSBs that arise from various sources including ionized irradiation, inter-strand cross linking, replication fork collapse (San Filippo et al., 2008). Particularly, HR but not NHEJ is capable of fixing replication fork collapse induced DSBs (San Filippo et al., 2008). The necessity of HR in genome integrity maintenance is highlighted in two levels. At the cellular level, mutations in HR associated genes could result in hypersensitivity to DSB inducing agents such as ionized irradiation (Game and Mortimer, 1974; San Filippo et al., 2008). At organism level, heritable mutations associated with HR deficiency often lead to cancer or cancer prone diseases such as breast and ovarian cancers or Fanconi anemia and Bloom's syndrome, (Kennedy and D'Andrea, 2006; Mathew, 2006; San Filippo et al., 2008; Sung and Klein, 2006).

The substrate of HR machinery is single strand DNA (Sung and Klein, 2006). To achieve this, DSB ends (if blunt) have to be nucleolytically catalyzed to generate a 3' overhang in a process termed DNA end resection (Chapman et al., 2012). Unlike NHEJ, whose end resection is tightly restricted, the resection in HR tends to be more excessive, with up to 3.5kb from the DNA lesion (Zhou et al., 2014). To initiate

resection, the 3'-5' endonuclease activity of Mre11 (a member of MRN complex) is required to create a nick on the DNA duplex at up to 300 nucleotides away from the break lesion (Chapman et al., 2012) (Figure 1-5). MRN complex then, proceeds to degrade DNA toward the 5' break ends and dissociates Ku from DSB end (Chapman et al., 2012) (Figure 1-5). Meanwhile, the 5'-3' endonuclease Exo1 is activated and mediate DNA degradation in the opposite direction as Mre11 (Chapman et al., 2012) (Figure 1-5).

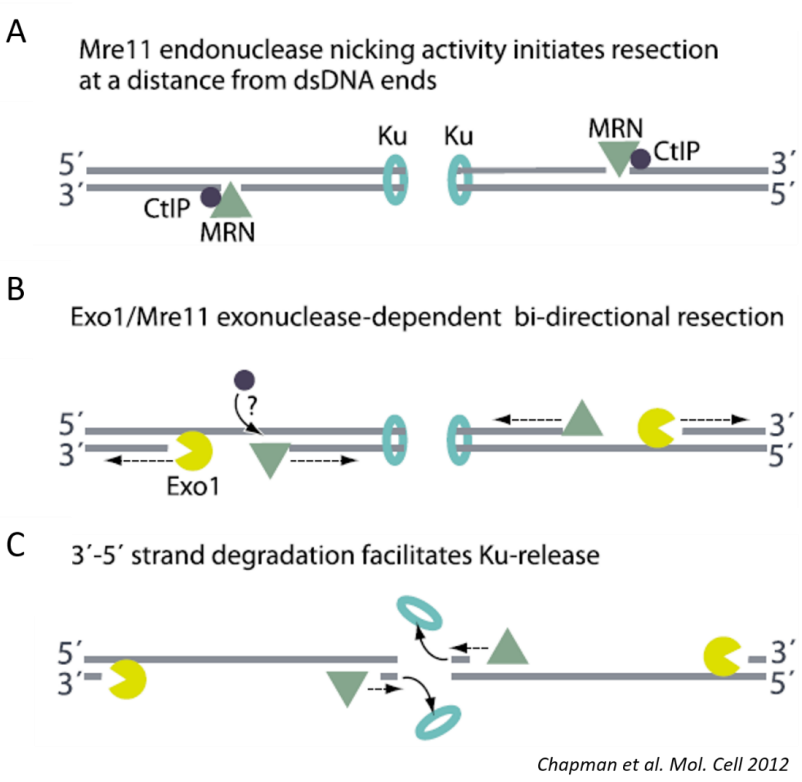

Figure 1-5: Model of MRN and CtIP dependent initiation of resection. (A). The Mre11 endonuclease within the MRN complex cleaves the 5' strand at a distance that is far away (~300nt) from DSB ends. (B). DNA resection by MRE11 (3' to 5') and endonuclease Exo1 (5' to 3'). (C). MRN complex counteracts Ku complex, releases Ku complex from DSB end and inhibits NHEJ.

The resulting 3' single strand DNA overhangs are quickly coated by replication protein A (RPA) with high affinity (Chapman et al., 2012; Li and Heyer, 2008; Polo

and Jackson, 2011). In vertebrates, RPA is then substituted by Rad51, a eukaryotic Rec A homolog, with the help of other mediator proteins including, Rad51 paralogs (Rad51B, Rad51C, Rad51D, Xrcc2 and Xrcc3) and BRCA2 (Li and Heyer, 2008; Polo and Jackson, 2011). The single strand DNA coated by Rad51 forms a structure termed nucleofilament. Rad51 together with other HR factors then mediate nucleofilament homology search and strand invading, a process when resected nucleofilament searches for and invades into the corresponding homologous template in the sister chromatid (Li and Heyer, 2008; Polo and Jackson, 2011). The invading strand anneals with its homologous template and drives off the original anti-sense strand forming a structure termed D loop (Li and Heyer, 2008). This anti-sense strand then forms duplex DNA with the second DNA break end either through annealing or a second invading event. Two break ends, together with sister chromatid forms an intermediate structure termed holiday junction (HJ) (Li and Heyer, 2008). HJ is then cleaved and resolved by enzymes to generate an intact error-free double strand DNA (Li and Heyer, 2008; Polo and Jackson, 2011).

1.5.5 NHEJ vs. HR: a cell cycle-dependent regulation

NHEJ and HR are two antagonizing mechanisms that compete to repair DSBs. The key event that determines the choice between these two pathways is DSB end resection, which is restricted in NHEJ while more excessive in HR (Polo and Jackson, 2011). DSB end resection is largely regulated by the interplay between two proteins: 53BP1 and BRCA1, both of which are recruited to DSBs by DDR signals (see in 1.5.2 and next section). 53BP1 play an inhibitory role on DSB end resection and thus

inhibit HR and promote NHEJ, while BRCA1 does the opposite (Chapman et al., 2012; Zimmermann et al., 2013). Loss of 53BP1 has been shown to extensively increase DSB end resection (Bothmer et al., 2011; Bunting et al., 2010). In addition, dominant negative 53BP1 mutant expression was reported to increase HR efficiency, confirming the negative role of 53BP1 on HR (Xie et al., 2007a). Mechanistically, 53BP1 undergoes an ATM mediated phosphorylation and then recruits two additional effectors: RAP interacting factor 1 (RIF1) and PAX transactivation activation domain-interaction protein 1 (PTIP) (Panier and Boulton, 2014). Then 53BP1-RIF1 complex binds to local H4 dimethylated on lysine 20 (H4K20me2) around DSBs to form a chromatin barrier and block resection machinery (Bothmer et al., 2010; Chapman et al., 2012). In addition to inhibiting DSB end resection, 53BP1 also promote NHEJ through its ability to increase DSB end mobility and tether distinct DSB ends to proximity for ligation (Chapman et al., 2012; Dimitrova et al., 2008).

In a way to compete with NHEJ, HR adopts BRCA1 to promote DSB end resection. The exact mechanism underlying this BRCA1 mediated HR promotion remains unclear. However, multiple studies have revealed that depletion of 53BP1 is able to alleviate the detrimental phenotypes associated with BRCA1 deficiency in mouse models, suggesting that BRCA1 likely to promote HR by antagonizing with 53BP1 (Bouwman et al., 2010; Bunting et al., 2012; Bunting et al., 2010; Cao et al., 2009).

As I mentioned before, HR is mostly active in S/G2 phase. Therefore, cells are likely to maintain a mechanism to reinstate HR and inhibit NHEJ during that period. To begin with, the expression of BRCA1 and its co-factors is much more prevalent

during S/G2 phase (Chen et al., 2008). In addition, when cells enter S phase, cyclin dependent kinase (CDK) phosphorylates the CtBP interacting protein (CtIP), which in turn binds to BRCA1 and MRN complex to reinforce DSB end resection and antagonize 53BP1-RIF1 complex (Chapman et al., 2012; Escribano-Diaz et al., 2013; Panier and Boulton, 2014). Meanwhile, Lys acetyltransferase 5 (KAT5) carries out local histone acetylation events and generates histone H4 acetylated on lysine 16 (H4K16ac), a marker that has been shown to reduce the binding between 53BP1 and H4K20me2 (Panier and Boulton, 2014; Tang et al., 2013).

Proper regulation of NHEJ and HR pathway choice is critical for cells to maintain homeostasis. Disruption of this process could result in chromatin relocation, genome instability and cell death. For example, PARP1 inhibitors are lethal on BRCA1 deficient cells by introducing excessive DSBs and inappropriately activating the error-prone NHEJ, leading to chromatin aberrations and cell death (Bunting et al., 2010; Patel et al., 2011). Deletion of 53BP1 inhibits NHEJ, restores HR and completely removes the toxicity of PARP inhibitors, suggesting a toxic effect of NHEJ on genome integrity (Bunting et al., 2010).

1.5.6 Impact of γH2AX signals on NHEJ and HR

As discussed in 1.4.2, ATM mediated H2AX phosphorylation plays a central role coordinating DDR signal amplification (Chapman et al., 2012; Kinner et al., 2008). The major significance of γH2AX is its ability to attract down-stream DNA repair factors through direct or indirect mechanisms (Chapman et al., 2012; Kinner et al., 2008). For example, MDC1 directly recognizes and binds to the phosphorylated

tail on γH2AX through its BRCT domain repeats. The enrichment of MDC1 recruits MRN complex and ATM at DSBs. ATM phosphorylates MDC1, initiating further recruitment of RNF8 and RNF168, two E3 ubiquitin ligases (Kinner et al., 2008; Kolas et al., 2007). With the help from E2 conjugating enzyme UBC13, RNF8/RNF168 mediate the poly-ubiquitination of histone H2A and H2AX, which reinforce the efficient and stable recruitment of 53BP1 and BRCA1 (Fradet-Turcotte et al., 2013; Kolas et al., 2007; Mailand et al., 2007). Therefore, γH2AX serves as upstream signals to promote NHEJ and HR. Notably, the association equilibrium between MDC1 and γH2AX are relatively low (~10^{-6} M). Therefore, a widespread of γH2AX signals is likely to help stabilize the DDR machinery at DSBs. Depletion of H2AX has been shown to disrupt 53BP1 recruitment (Ward et al., 2003). To this end, it is proposed that γH2AX dependent 53BP1 recruitment functions to block DSB end resection during class-switch recombination in immune cells (Chapman et al., 2012; Reina-San-Martin et al., 2004). Besides 53BP1, depletion of H2AX was also shown to impede BRCA1 and RAD51 recruitments (Bassing et al., 2002; Paull et al., 2000). Mouse embryonic stem cells lacking H2AX displayed elevated genome instability and sensitivity to ionized irradiation (Bassing et al., 2002).

1.6 Significance of this dissertation

As discussed in 1.1.3, vascular smooth muscle cell loss is a drastic phenotype observed in HGPS patient and mouse models. Moreover, this phenotype has been implied to be associated with cardiovascular disorders, the driving force of HGPS patient lethality. In this dissertation, my primary goal is to elucidate the molecular

mechanism underlying this phenotype of SMC loss in HGPS. In chapter II, I begin by establishing a differentiation protocol to generate HGPS SMCs via induced pluripotent stem cells (iPSCs). I fully characterize these cells and provide the first evidence that HGPS SMCs undergo elevated basal level cell death. In chapter III, I aim to illustrate the mechanism of HGPS SMC cell death. PARP1 is shown to be significantly down-regulated in the HR deficient HGPS SMCs, resulting in over-activation of NHEJ during S/G2 phase, leading to chromosome aberrations and mitotic catastrophe. Chapter IV characterizes the efficiencies of both HR and NHEJ at different cell cycle stages in HGPS fibroblasts. Microscopy analysis reveals that both HR and NHEJ are abnormally regulated in G0/G1 phase or S/G2 phase HGPS fibroblasts. This is the first cell cycle dependent analysis of NHEJ and HR in HGPS cells. Chapter V focuses on investigating the molecular mechanism underlying NHEJ mis-regulation. I provide evidence showing that ATM activity and H2AX phosphorylation are differentially regulated between G0/G1 phase and S/G2 phase HGPS cells. The disruption of these upstream DDR signals is associated with mis-regulated NHEJ. Moreover, my data suggests that loss of H3K9me3 in HGPS cells plays a role in these defects. Together, my study demonstrates an attenuated early DDR signal of ATM activation and H2AX phosphorylation and provides a plausible connection between the classic H3K9me3 loss phenotype and mis-regulated NHEJ in HGPS.

Chapter II: Differentiation and characterization of HGPS smooth muscle cells via induced pluripotent stem cells (iPSCs)

2.1 Introduction

Hutchinson-Gilford progeria syndrome (HGPS), the most drastic form of premature aging diseases, is characterized by multiple aging-related clinical features including growth retardation, lipodystrophy, alopecia, bone abnormalities and severe cardiovascular defects (Capell and Collins, 2006; Merideth et al., 2008). Patients with HGPS typically start to display premature onset of aging-related pathologies at 12-24 month of age and die in their early teens of heart attacks or strokes (Capell and Collins, 2006; Merideth et al., 2008). Over 80% HGPS cases are caused by a de novo mutation (1824 C→T) in exon 11 of the human *LMNA* gene. This mutation activates an alternative splice donor site, leading to a truncated lamin A mutant termed "progerin", which bears a 50 aa deletion near the C terminus (Capell and Collins, 2006). This internal deletion interferes with lamin A processing and causes a permanent farnesylation of progerin. As a dominant negative protein, the accumulation of progerin inside the nucleus causes various cell biological phenotypes including a misshapen nuclear morphology, loss of peripheral heterochromatin, global changes in gene transcription and disrupted mitotic progress (Capell and Collins, 2006; Zhang et al., 2013).

Among all of the clinical features associated with HGPS, the cardiovascular disease is the cause of death in almost all patients. Despite its great importance, investigation of the HGPS arterial pathology has been extremely limited mainly due to the low incidence of HGPS. One postmortem study on an HGPS patient found a severe loss of SMCs in the aorta and carotid arteries (Atkins, 1954). Moreover, two independent *in vivo* studies on HGPS transgenic mouse models (the BAC G608G and

Lmna^{G609G} models, respectively) confirmed the loss of SMCs in large vessels (Osorio et al., 2011; Varga et al., 2006). Significantly, this SMC loss could be largely rescued by treating the mice with farnesyltransferase inhibitors (FTIs) or progerin suppressing morpholinos, indicating a causal connection between the presence of progerin and the SMC loss phenotype (Capell et al., 2008; Osorio et al., 2011). Loss of vascular SMCs (aortic arch and carotid arteries) has been proposed to induce aortic dilation and atherosclerosis plaque rupture (Bennett, 1999; Clarke et al., 2006). Thus elucidating the molecular mechanism underlying HGPS SMC loss is of great importance to understand the cardiovascular pathology and develop new therapeutic approaches in HGPS.

To investigate how progerin induces cell death in HGPS SMCs, *in vitro* culture of primary SMCs from HGPS patients is an ideal system. However, there are several challenges hurdling this strategy. First of all, HGPS is an extremely rare disease with an incidence rate of one in every four to eight million of population (Capell and Collins, 2006; Zhang et al., 2013). It is difficult to find the source of HGPS primary SMCs. Secondly, dissection of SMCs from *in vivo* large vessels is impractical compared with other cell types such as dermal fibroblasts. In recent years, with the emerge of induced pluripotent stem cells (iPSCs), there is an increasing interest in using iPSCs as a new source to study specific diseases. With pluripotency, iPSCs are able to differentiate into multiple lineages including SMC. Therefore, in this chapter, I developed a lineage specific differentiation protocol and generated HGPS SMCs from HGPS iPSCs. Physiological examinations suggested that HGPS SMC exhibit muscle contractility in response to vasoconstrictor. Moreover, the cellular and

molecular analysis suggested that HGPS SMCs faithfully recapitulated classic HGPS cellular phenotypes such as premature senescence and proliferation defects. Significantly, HGPS SMCs displayed a drastically elevated basal level of cell death, strongly indicating a cellular mechanism underlying the SMC loss phenotype *in vivo*.

2.2 Results

2.2.1 Normal and HGPS iPSC show comparable differentiation potency into SMC lineage.

To study HGPS SMC defects, SMCs were generated from iPSCs derived from HGPS and normal skin fibroblasts. Analysis of HGPS iPSCs revealed the expression of Oct4, Nanog, SSEA4 and Tra1-60, indicating that these HGPS iPSCs contain essential pluripotency factors, as well as normal chromosome number and size (Figure 2-1A-C). Alkaline phosphatase (AP) staining and EB formation assay further demonstrated the undifferentiated state and the differentiation potential of iPSCs (Figure 2-1A-E). In accordance with previous reports, the expression of lamin A/C was repressed in both normal and HGPS iPSCs (Figure 2-1D).

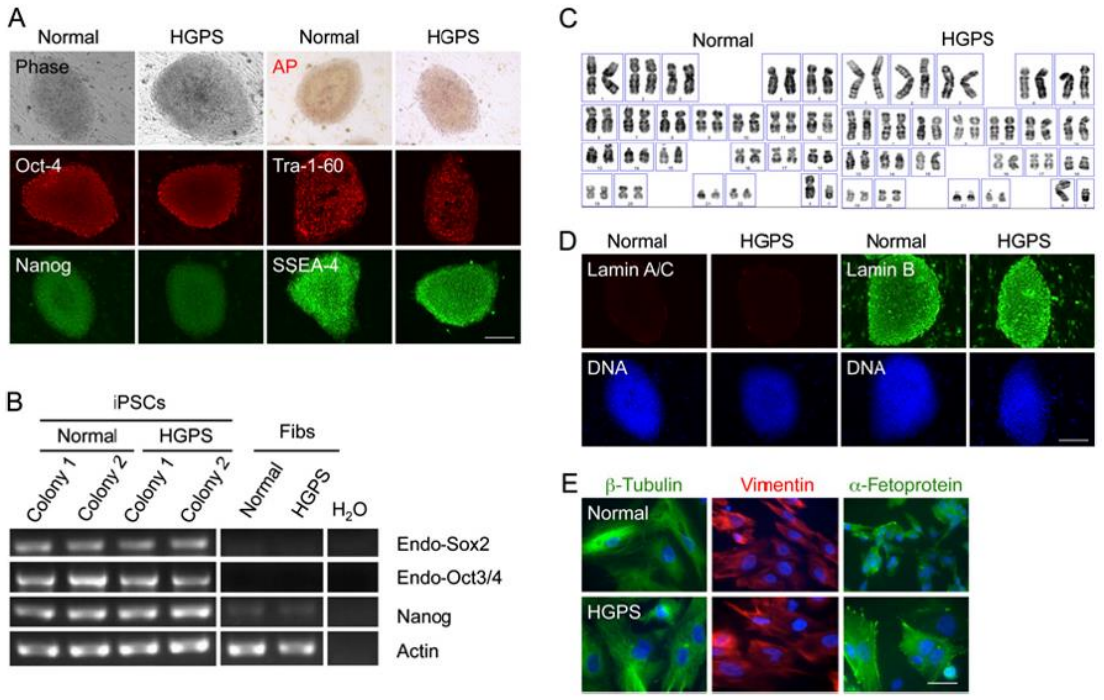

Figure 2-1: Characterization of HGPS iPSCs. (A). Representative images of phase contrast, alkaline phosphatase (AP) staining, and pluripotency marker immunofluorescence staining of normal and HGPS iPSC colonies. (Scale bar, 200 μm) (B). RT-PCR with denoted pluripotency gene primers in the samples of normal and HGPS iPSCs and the parent fibroblasts (Fibs). PCR products of each indicated gene in various samples were run together on a single gel. Representative normal and HGPS samples were cropped and aligned together, separated by white lines. (C). Normal karyotypes of normal and HGPS iPS colonies. (D). Representative images of immunofluorescence staining with anti-lamin A/C and anti-lamin B antibodies on normal and HGPS iPSC colonies. DNA was stained by Hoechst 33342. (Scale bar, 200 μm.) (E). Representative images of immunofluorescence staining with anti–β-tubulin, Vimentin and α-fetoprotein (AFP) antibodies on normal and HGPS EBs. Immunofluorescence signal of β-tubulin, vimentin, and AFP confirmed the differentiation of ectodermal, mesodermal, and endodermal layers, respectively. (Scale bar, 50 μm.)

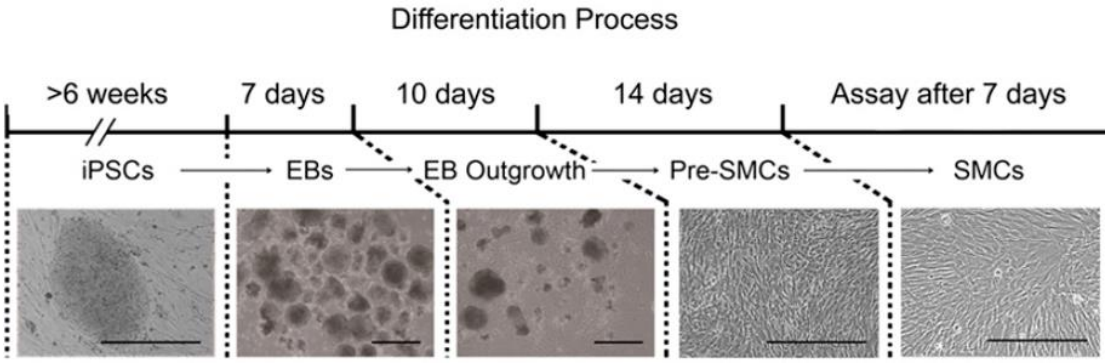

Figure 2-2: Schematic diagram of SMC differentiation timeline and representative phase contrast images underneath each denoted stage. EB, embryoid body. (Scale bar, 400 μm.)

SMCs were differentiated from iPSCs using a previously established protocol (Figure 2-2, see details in Methods) (Xie et al., 2007b). After 7 d in the SMC differentiation medium, immunofluorescence revealed the expression of SMC-specific markers SMC-α-actin (SMA) and calponin in both normal and HGPS lines (Figure 2-3A). In accordance with the immunofluorescence observation, Western blotting analysis and RT-quantitative PCR (RT-qPCR) showed a significant up-regulation of SMA, calponin and SM22-a in SMCs relative to iPSCs, fibroblasts and pre-SMCs (Figure 2-3B & C and 2-4A). Notably, the expression of smooth muscle myosin heavy chain (smMHC), a marker for terminally differentiated SMCs, was not up-regulated in normal and HGPS SMCs, suggesting that SMCs in my system were not terminally differentiated (Figure 2-3B). FACS analysis using fluorescence-labeled SMA or calponin revealed that, after 14 d in SMC differentiation medium, >80% of the cells were induced to express SMA and calponin (Figure 2-4B). Western blotting analysis suggested that the expression of these SMC markers was stable for at least two weeks in SMC differentiation medium (from day 14 to day 28) (Figure 2-3C).

Next, I carried out contractility analysis on normal and HGPS SMCs. Cells at day 14 and 21 were treated with a vasoconstrictor, angiotensin II. More than 70% of the SMCs displayed various levels of contraction 30min after stimulation (Figure 2-4C & D). Taken together, these results indicated that both normal and HGPS iPSCs were differentiated into SMCs with similar high efficiency.

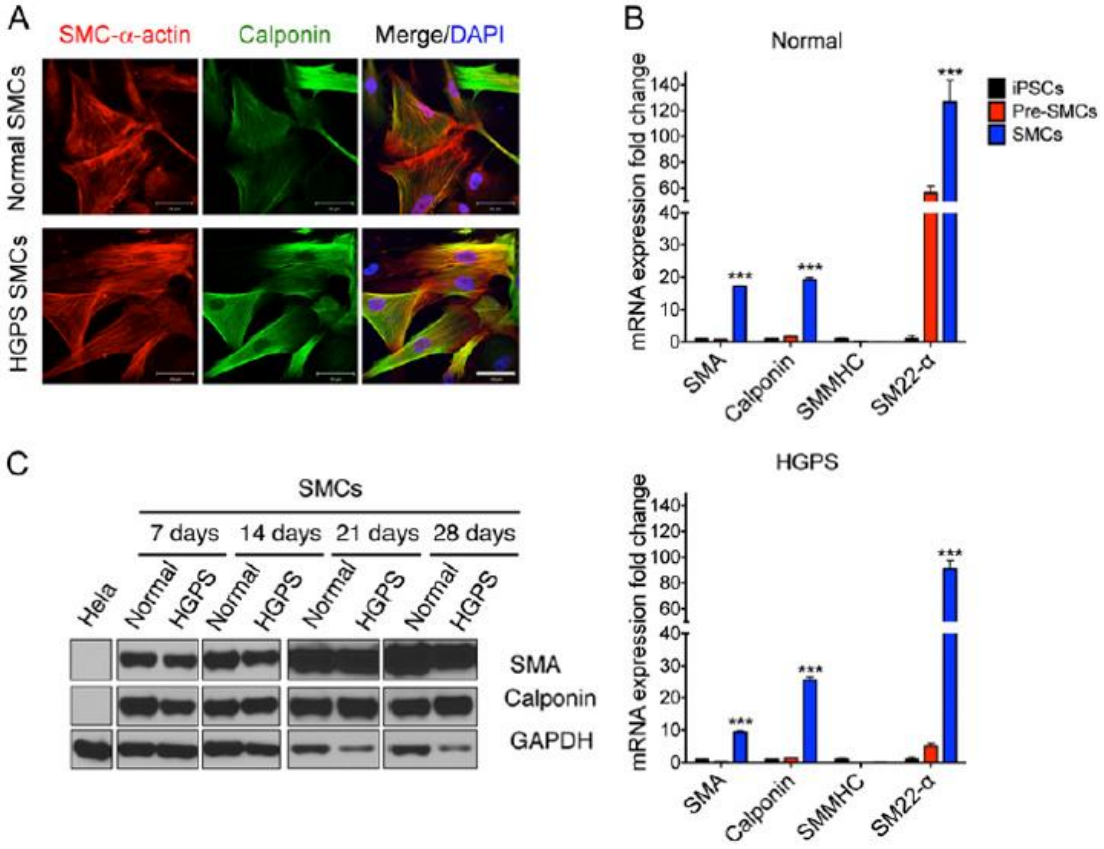

Figure 2-3: Expression of SMA and calponin in normal and HGPS SMCs. (A). Representative images of immunofluorescence staining with anti-SMA and anti-calponin antibodies on normal and HGPS SMCs. (Scale bar, 50 μm.) (B). RT-qPCR with SMA, calponin, smMHC, and SM22-α–specific primers on normal and HGPS iPSCs, pre-SMCs, and SMCs. ***P < 0.001. (C). Western blot with anti-SMA, calponin, and GAPDH antibodies on normal and HGPS SMCs at indicated time points during

SMC differentiation. SMC samples at various time points were run separately and are denoted by white lines.

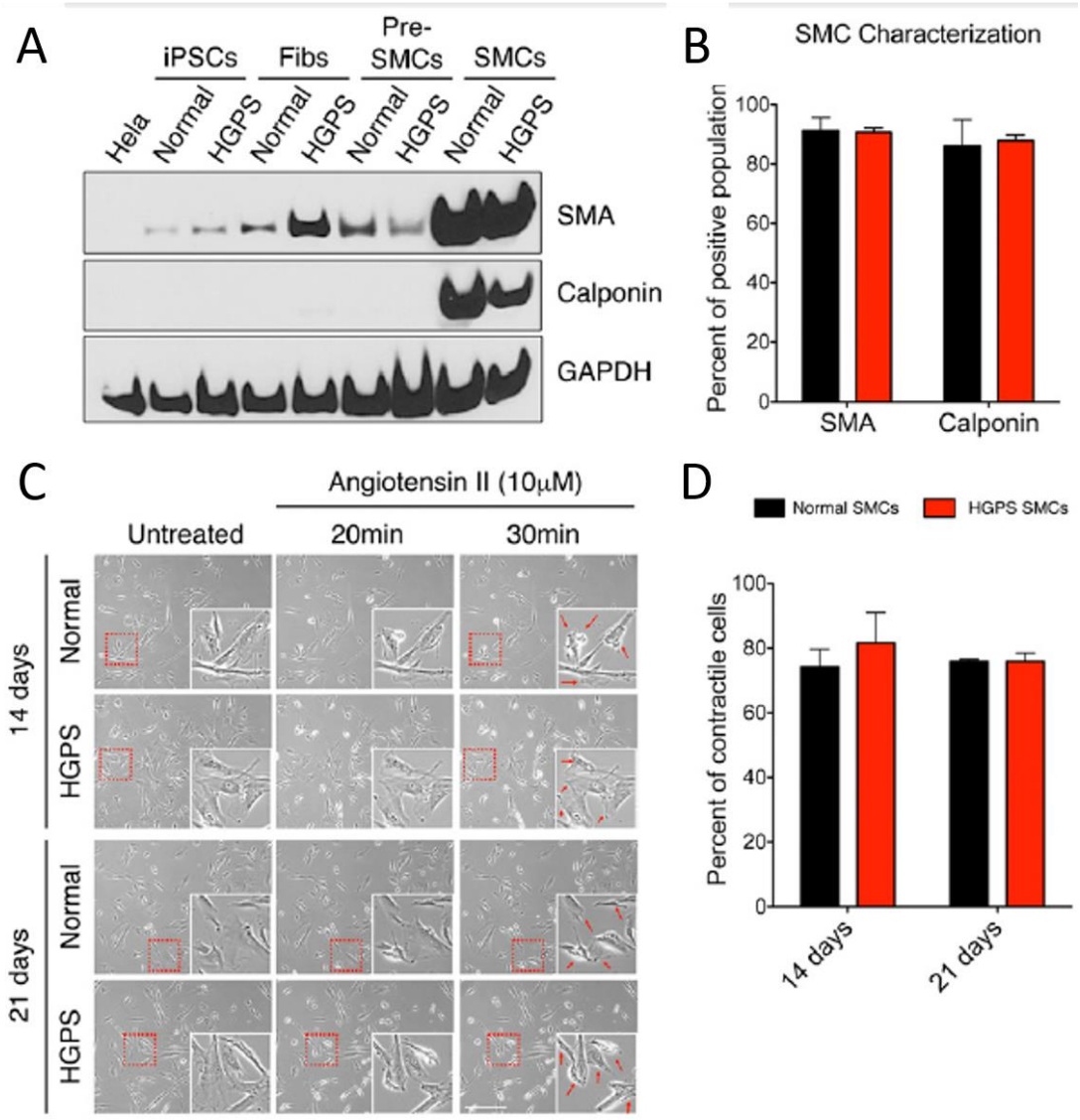

Figure 2-4: Normal and HGPS SMCs express SMC markers. (A). Western blot with anti-SMA, calponin, and GAPDH antibodies on the cell samples at various differentiation stages. (B). Percentages of SMA and calponin positive population in normal and HGPS SMCs at day 14. Results were generated from two biological replicates. (C). Representative phase control images showing the contraction of normal and HGPS SMCs at days 14 and 21 upon angiotensin II treatment. Cell contraction at 30 min after stimulation was indicated by red arrows in the enlarged images. (Scale bar,

400 μm.) (D). Quantification of C, showing the percentage of contracted SMCs upon stimulation. Results were generated from three independent experiments.

To measure progerin amounts during SMC differentiation, western blotting analysis and immunofluorescence were conducted and revealed a gradual accumulation of progerin in HGPS cells during SMC differentiation (Figure 2-5A-C). Senescence-associated β-galactosidase (SA-β-gal) staining suggested that HGPS SMCs were more senescent than normal SMCs at similar stages (Figure 2-6A). Interestingly, p16ink4a, a senescence marker and cyclin-dependent kinase inhibitor, was found to be up-regulated in HGPS SMCs relative to the normal controls (Figure 2-6B & C) (Baker et al., 2011). Next, I examined whether the senescence in HGPS SMCs was related to shortened telomeres in HGPS, as suggested previously (Liu et al., 2011). RT-PCR using a pair of human telomerase reverse transcriptase (hTERT)-specific primers revealed that hTERET was robustly expressed in iPSCs but undetectable in both normal and HGPS SMCs (Figure 2-6D), indicating that telomerase expression was significantly inhibited upon SMC differentiation. Using quantitative telomere PNA-FISH, as described before by Cao et al (Cao et al., 2011a), I found no evidence of shortened telomeres in HGPS SMCs as well as in primary vascular SMCs isolated from G608G transgenic mice, in which the SMC loss was first discovered (Figure 2-6E & F) (Varga et al., 2006).

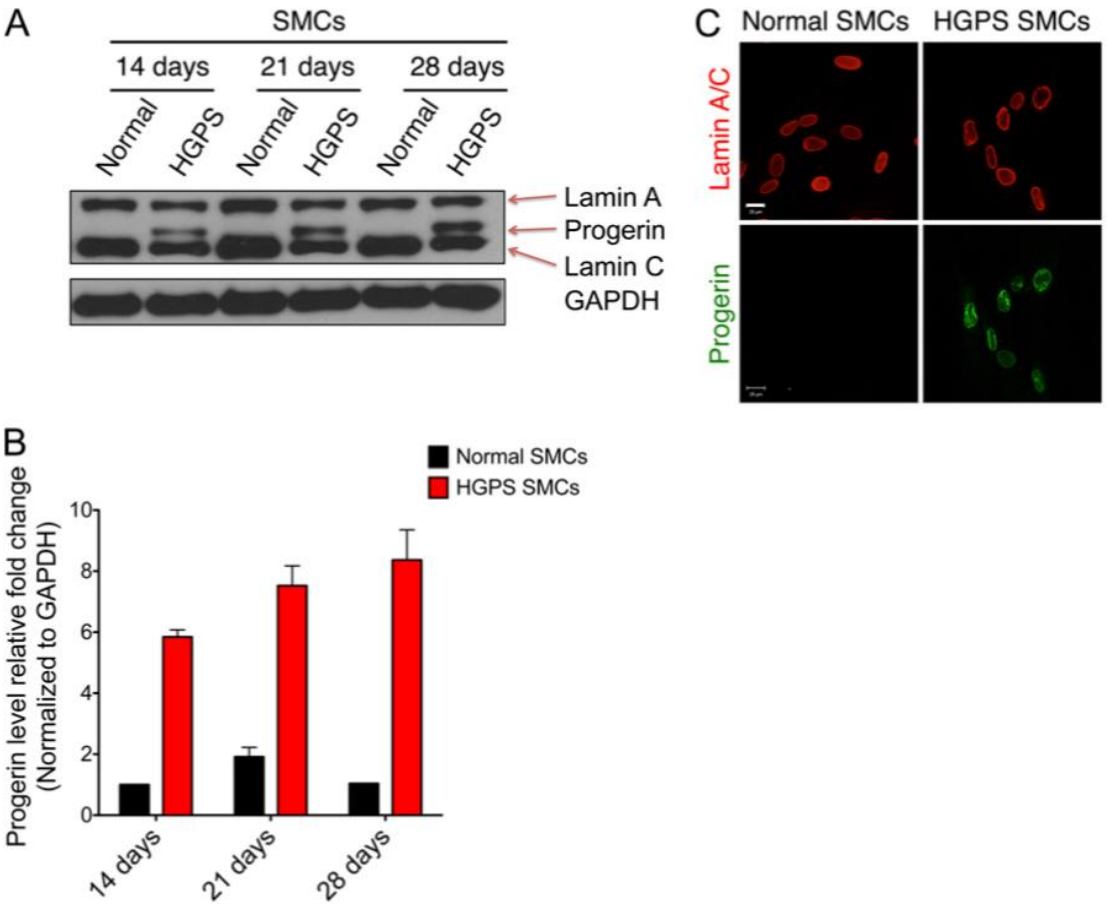

Figure 2-5: Expression of progerin in HGPS SMCs. (A). Western blot with anti-lamin A/C and anti-GAPDH antibodies on normal and HGPS SMCs at indicated time points during differentiation. Lamins A and C were detected in all SMC samples, and progerin was only observed in HGPS SMCs. (B). Quantification of A, showing gradual increases of progerin in HGPS SMCs with culturing time. Results were generated from two independent experiments. (C). Representative images of immunofluorescence staining with anti-lamin A/C and progerin antibodies on normal and HGPS SMCs at day 14. (Scale bar, 20 μm.)

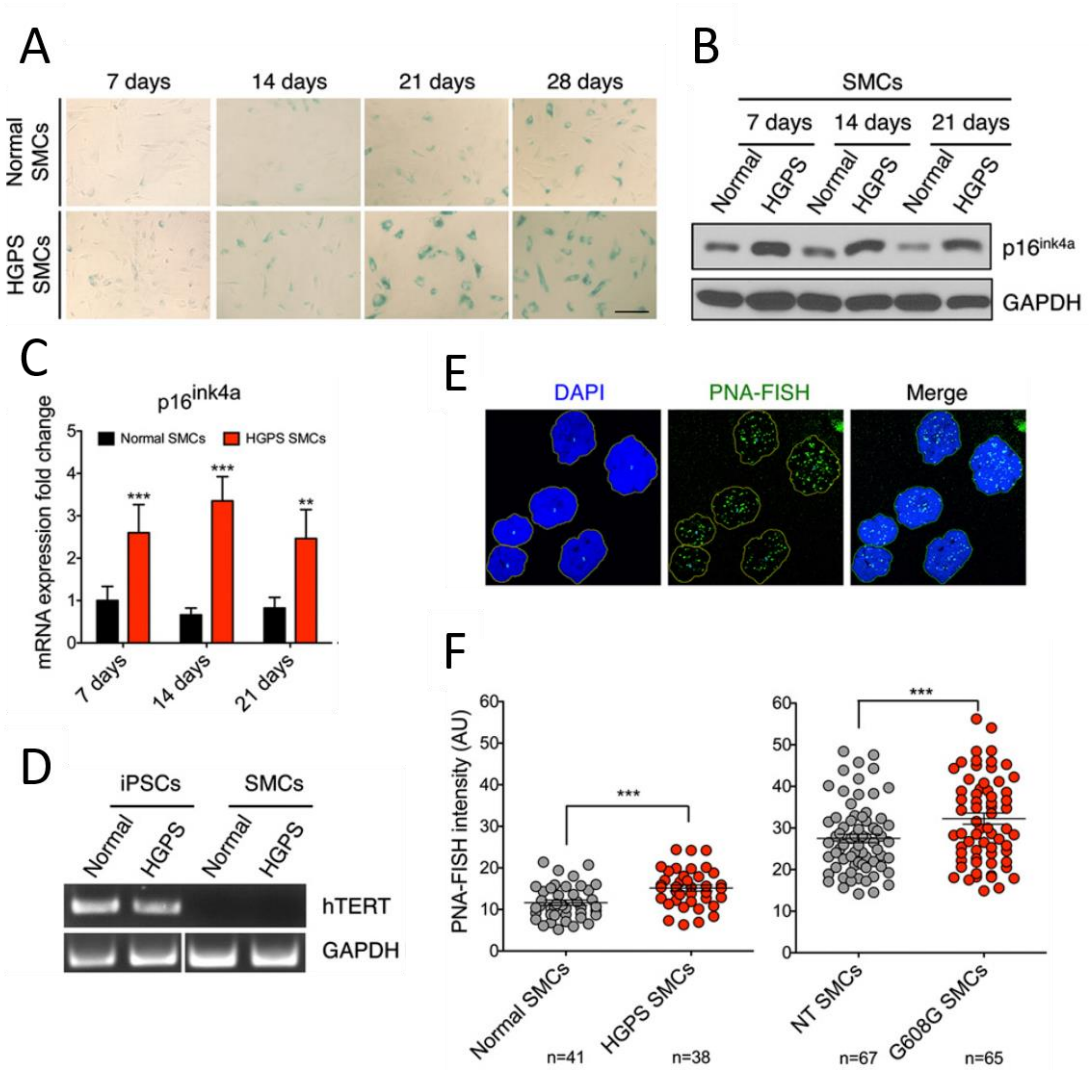

Figure 2-6: Premature senescence in HGPS SMCs. (A). Representative images of SA–β-Gal staining on normal and HGPS SMCs at indicated time points during differentiation. (Scale bar, 200 μm.) (B). Western blot with anti-p16ink4a and GAPDH antibodies on normal and HGPS SMCs at indicated time points during differentiation. (C). RT-qPCR with p16ink4a-specific primers on normal and HGPS SMCs at indicated time points during differentiation. **P < 0.01, ***P < 0.001. (D). RT-PCR with human TERT and GAPDH-specific primers on normal and HGPS iPSCs and SMCs. The expression of TERT was undetectable by RT-PCR in normal and HGPS SMCs. SMC samples at various time points were run separately and are denoted by white lines. (E). Representative images of telomere PNA-FISH staining. (F). Quantification of telomere PNA-FISH fluorescence intensity in the indicated cell types. The HGPS (G608G) and control (nontransgenic, NT) mouse samples were age, sex, and passage matched. In both differentiated human SMCs and primary mouse vascular SMCs, HGPS samples showed slightly but significantly stronger PNA-FISH signals (***P < 0.001). I found no evidence of shortened telomeres in HGPS samples.

2.2.2 HGPS SMCs exhibit proliferation defects and elevated basal level of cell death.

To evaluate cell proliferation potential, growth curves were plotted for HGPS and normal SMCs (Figure 2-7A & B). This experiment showed that, where as normal SMC kept a constant proliferation rate, the cell number of HGPS SMCs stopped increasing after day 14. I reasoned that this proliferative defect could be caused by either premature senescence or progerin induced cell death. To distinguish these two possibilities, I conducted a cell cycle analysis at day 14. If premature senescence of HGPS SMCs was the dominant cause, the majority of HGPS SMCs should be arrested in the G0/G1 phase of the cell cycle. To my surprise, cell cycle analysis revealed that the percentage of the G0/G1 population of HGPS SMCs showed no significant changes compared with the control (~70% in both), but there was an obvious increase in the mitotic population (G2/M) in HGPS SMCs (Figure 2-7C). This result suggested that despite being more senescent than normal SMCs, HGPS SMCs did not lose their proliferative ability. Thus, I speculated that the proliferation defect in HGPS SMCs was likely caused by cell death occurring during cell division.

To analyze cell death, next, I carried out propidium iodide (PI)-annexin V assay in both normal and HGPS SMCs at weekly time points during SMC differentiation. Indeed, HGPS-SMCs displayed 8- to 10- fold increase in cell death compared with normal controls at days 14, 21 and 28 (Figure 2-7D & E). Notably, at the early time point day 7, when no obvious growth defect was detected (Figure 2-7B), both normal and HGPS SMCs showed a similar percentage of cell death, implying a relatively healthy state of HGPS SMCs at the beginning of SMC differentiation (Figure 2-7D &

E). These results strongly supported my speculation that the proliferation defect in HGPS SMCs was caused by cell death. Furthermore, these results provide a plausible explanation for the *in vivo* SMC loss phenotype in HGPS.

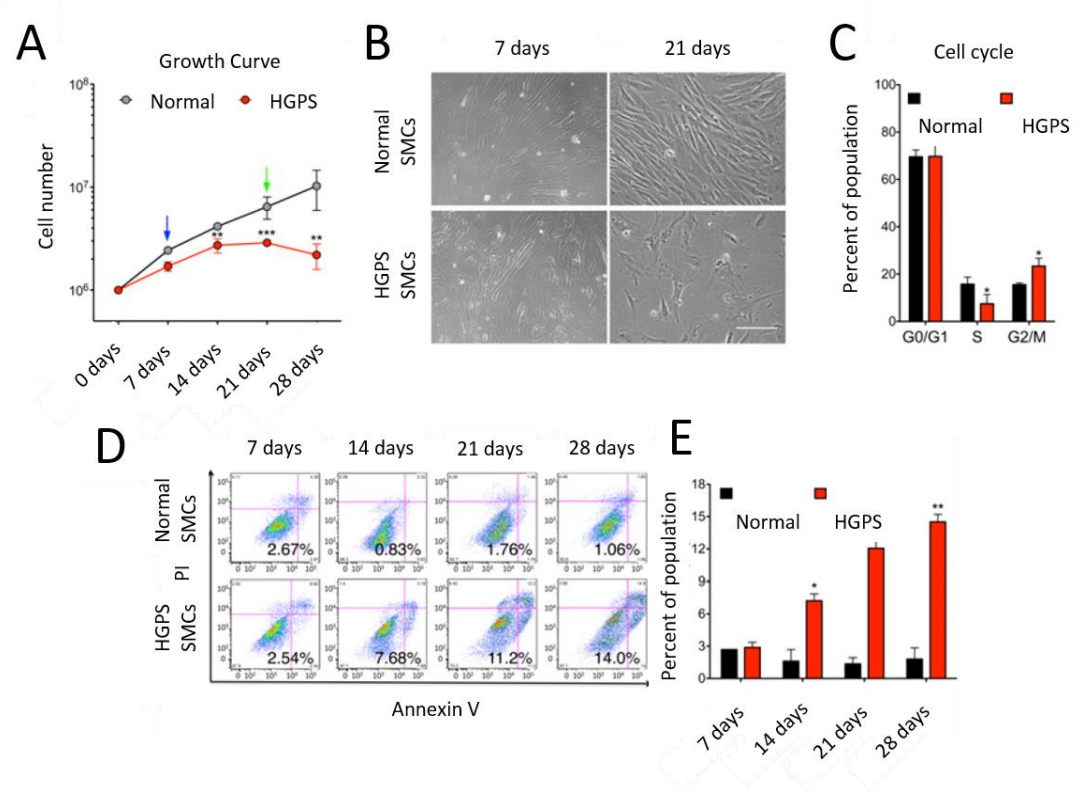

Figure 2-7: Increased cell death in HGPS SMCs. (A) Growth curve of normal and HGPS SMCs during differentiation. Results were generated from three biological replicates. *P < 0.05, **P < 0.01. Blue and green arrows referred to the images at days 7 and 21 in B, respectively. (B) Representative phase contrast images of normal and HGPS SMCs at days 7 and 21 during SMC differentiation. (Scale bar, 200 μm.) (C) Cell cycle analysis of normal and HGPS SMCs at day 14, illustrating the distribution of G0/G1, S, and G2/M phases. Results were generated from three biological replicates. *P < 0.05. (D) PIannexin V flow cytometry analysis on normal and HGPS SMCs at various time points during SMC differentiation. The gates were set according to the positive and negative controls as suggested by the manufacturer. The cells in the Lower Right quadrant were scored as the dying cell population. (E) Quantification of D, showing the percentage of dying population based on the PI-annexin V assay. Results were generated from three biological replicates. *P < 0.05, **P < 0.01. (F) RT-qPCR analysis with Bax specific primers on normal and HGPS SMCs at different time points during SMC differentiation.

2.3 Discussion

2.3.1 iPSCs based SMC differentiation model

Children with progeria die almost exclusively from cardiovascular disease. In 2006, Varga et al. reported the first evidence of progressive vascular SMC loss in large vessels of an HGPS transgenic mouse model (G608G BAC) (Varga et al., 2006). SMC loss might undermine vessel architecture and induce inflammation, vessel calcification, and excessive atherosclerosis (Lopez-Candales et al., 1997). The mechanisms underlying progerin-induced SMC loss had not been explored, which was at least partially due to the technical difficulties in obtaining sufficient amounts of vascular SMCs from progeria patients or animal models.

In this chapter, the problem was overcome by the iPSCs-mediated differentiation system that generated a large amount of patient SMCs. I found that these differentiated cells were induced to express some established SMC markers and exhibited functional characteristics of SMCs (Figure 2-3 and Figure 2-4). However, the expression of smMHC, a marker for fully differentiated SMCs, was undetectable (Figure 2-3B), which suggested that the SMCs in my experiments were not terminally differentiated. Indeed, the proliferation assay (Figure 2-7A & B) showed that the normal SMCs could proliferate in SMC differentiation medium for at least 28 days. *In vivo*, SMC proliferation is a characteristic of synthetic SMCs, and contractile SMCs do not proliferate (Rensen et al., 2007; Rzucidlo et al., 2007). Under pathological conditions, SMCs switch from the contractile to the synthetic phenotype (Rensen et al., 2007; Rzucidlo et al., 2007). Thus, I speculate that by using these iPSCs generated

SMCs, I may be studying how progerin affects SMCs responses to pathological conditions *in vivo*.

2.3.2 The proliferative defect in HGPS SMCs is primarily caused by cell death, not by premature senescence.

The HGPS SMCs expressed progerin, a hallmark of HGPS cells (Figure 8), and stopped proliferating after two weeks in SMC culture (Figure 2-7A & B). Initially, I had hypothesized that this severe growth defect was caused by premature senescence, as previously suggested by Liu and colleagues and supported by my senescence analysis with SA–β-Gal assay and p16 expression (Figure 2-6A-C) (Liu et al., 2011). However, to my surprise, cell cycle analysis indicated that the HGPS SMCs did not rest at G0, but actively reentered the cell cycle (Figure 2-7C). Moreover, I found a significant delay in G2/M phase in the HGPS SMCs (Figure 2-7C). Additional experiments revealed a time-dependent increment of cell death in HGPS SMCs in culture (Figure 2-7D & E). Based on these results, I concluded that the cell death phenotype accounted for the proliferation phenotypes in HGPS SMCs.

Chapter III: Mechanisms controlling the smooth muscle cell death in progeria via down-regulation of poly(ADP-ribose) polymerase 1

3.1 Introduction

DNA damage often arises as a result of normal cellular processes. Reactive oxygen species (ROS), the byproducts of cellular metabolism, can damage DNA bases and block the progression of replication, leading to replication fork collapse and double-strand breaks (DSBs). DSBs can also be induced by environmental factors including irradiation, chemical agents, or UV light (Rothkamm et al., 2003). A gradual accumulation of DSBs and a decline in DNA repair capacity are suggested to play a causative role in normal physiological aging (Chen et al., 2007). Defects in DNA damage repair result in at least three premature aging diseases: xeroderma pigmentosum, Cockayne syndrome, and trichothiodystrophy (Kraemer et al., 2007). In addition, impaired DNA repair has also been implicated in the development of age-related neurodegenerative diseases such as Alzheimer's disease, Parkinson disease, and Huntington disease (Lin and Beal, 2006).

At the cellular level, DSBs are potent inducer of cell death, if left unrepaired, DSBs can trigger p53-mediated cell cycle arrest and programmed cell death; on the other hand, if repaired inaccurately, DSBs can cause small or large scale chromosome alterations, which can lead to premature entry into mitosis and mitotic cell death (mitotic catastrophe) (Vakifahmetoglu et al., 2008). Two separate pathways control the repair of DSBs: homologous recombination (HR) and non-homologous end joining (NHEJ). HR repairs DSBs using the undamaged sister chromatid as a template, during S/G2 phase and effectively protects genome integrity. In contrast, NHEJ repairs DSBs by connecting two free chromosome ends together with litter requirement for sequence homology, which leads to a high frequency of chromosome

mis-arrangements (Rothkamm et al., 2003). Normally these two pathways antagonize each other to fix DSBs and the choice between these two is under precise control by a group of regulators including 53BP1, BRCA1 and poly(ADP-ribose) polymerase 1 (PARP1) (Bunting et al., 2010; Patel et al., 2011).

Among these regulators, PARP1 acts as an essential molecular switch controlling activities of HR and NHEJ pathways. The classic function of PARP1 is involved in sensing initiating DNA single-strand break (SSB) repair (Caldecott, 2008). A previous study demonstrated that treating an HR-deficient cell line with a PARP1 inhibitor led to abnormal chromosome karyotypes and significantly reduced cell survival, suggesting that PARP1 mediates the suppression of NHEJ upon DSBs (Bunting et al., 2010). This sensitivity to a PARP1 inhibitor in the HR-deficient cells could be a combined effect of the PARP1's dual roles in DNA damage repair. First, inhibition of PARP1 hinders SSB repair and the unrepaired SSBs develop into DSBs. More importantly, inhibition of PARP1 removes the suppression of NHEJ which results in chromosome aberrations and subsequent cell death in these HR-deficient cells (Bunting et al., 2010).

Depletion of smooth muscle cells from the major vessels is a frequently observed phenotype in HGPS patients and animal models (Atkins, 1954; Osorio et al., 2011; Varga et al., 2006). It has been previously shown that vascular SMC loss plays a positive role in the development of cardiovascular disorders such as aortic dilation and atherosclerosis, making it an interesting target to understand the cardiovascular pathology in HGPS (Bennett, 1999; Clarke et al., 2006). To model this phenotype, I established an *in vitro* differentiation system to generate HGPS SMCs from iPSCs

(see Chapter II). HGPS SMCs displayed classic HGPS cellular phenotypes such as proliferation defects and premature senescence. More importantly, HGPS SMCs bear an elevated basal level of cell death, suggesting a plausible cellular mechanism to explain the *in vivo* SMC loss. However, the molecular mechanism underlying this HGPS SMC cell death phenotype remains largely unknown.

In this chapter, I aim to investigate how progerin accumulation induces cell death in HGPS SMCs. Insightfully, deficiencies in DNA damage repair have been reported in HGPS fibroblasts and various progeria animal models, suggesting a likely involvement of genome instability in the manifestation of this drastic premature aging disease (Krishnan et al., 2011; Liu et al., 2005; Liu et al., 2013a; Liu et al., 2013b; Osorio et al., 2011). More specifically, HR DSB repair pathway has been shown to be impaired in HGPS fibroblasts, allowing us to speculate a similar HR deficiency in HGPS SMCs (Liu et al., 2005).

Here I present data showing that HR activity was almost completely blocked in HGPS SMCs during S/G2 phase. Moreover, I demonstrate that the accumulation of progerin directly down-regulates PARP1. Consistent with previous reports that PARP1 inhibition was lethal to HR deficient cells (Bunting et al., 2010; Patel et al., 2011), down-regulation of PARP1 by progerin in the HR deficient HGPS SMCs stimulated the error-prone NHEJ responses in S/G2 phase. Consequently, HGPS SMCs encounter chromosome aberrations and cell division problems and die in mitosis through a caspase-independent mitotic catastrophe pathway.

3.2 Results

3.2.1 HGPS SMCs underwent caspase 3 independent cell death

Previously, I have shown that HGPS SMCs bear an elevated basal level of cell death using PI-annexin V assay, which has been frequently applied in apoptosis study (Figure 2-7D & E). I next wondered whether HGPS SMCs death was caused by classic apoptosis pathway. To test this, I measured the mRNA level of Bcl2-associated protein X (Bax), a major proapoptotic gene acting upstream of caspase (Oltvai et al., 1993). Interestingly, no significant change in Bax expression was observed in HGPS SMCs compared with the normal control (Figure 3-1A), implying that caspase was not activated in HGPS SMCs. To further investigate this, I checked the activity of caspase 3. Activity assay revealed that caspase 3 was not activated but slightly suppressed in HGPS SMCs (Figure 3-1B). Consistently, I did not detect any cleaved PARP1 protein, a well-known substrate of caspases, in either sample (Figure 3-1C). Moreover, I did not find any obvious sub-G1 population in HGPS SMCs, indicating that there was no DNA fragmentation (Figure 3-1D). Taken together, these data suggested that cell death in HGPS SMCs may be executed in a caspase-independent manner.

It has been shown that treatment with high dosages (micro molar) camptothecin (CPT), a topoisomerase I inhibitor, can induce caspase-dependent apoptosis in normal cells (Ulukan and Swaan, 2002). Thus, as a positive control to the above experiments, I treated both normal and HGPS SMCs with 20mM CPT. In control SMCs, I detected an up-regulation of Bax mRNA by four folds and caspase 3 activity by nearly ten

folds after 72h in CPT treatment (Figure 3-1E & F). Consistently, cleaved PARP1 was clearly detected by western blotting in these cells (Figure 3-1G). However, HGPS SMCs appeared quite unresponsive to CPT induction, which failed to activate Bax expression and exhibited a delay over 48h in caspase 3 activation and PARP1 cleavage (Figure 3-1E-G). PI-annexin V assay further confirmed no significant increase in cell death in HGPS SMCs after CPT treatment (Figure 3-1H). These results suggest that, in the presence of progerin, caspase become less responsive to apoptotic stimuli like CPT. Collectively, I concluded that progerin accumulation in SMCs led to increased cell death, likely via caspase-independent pathways.

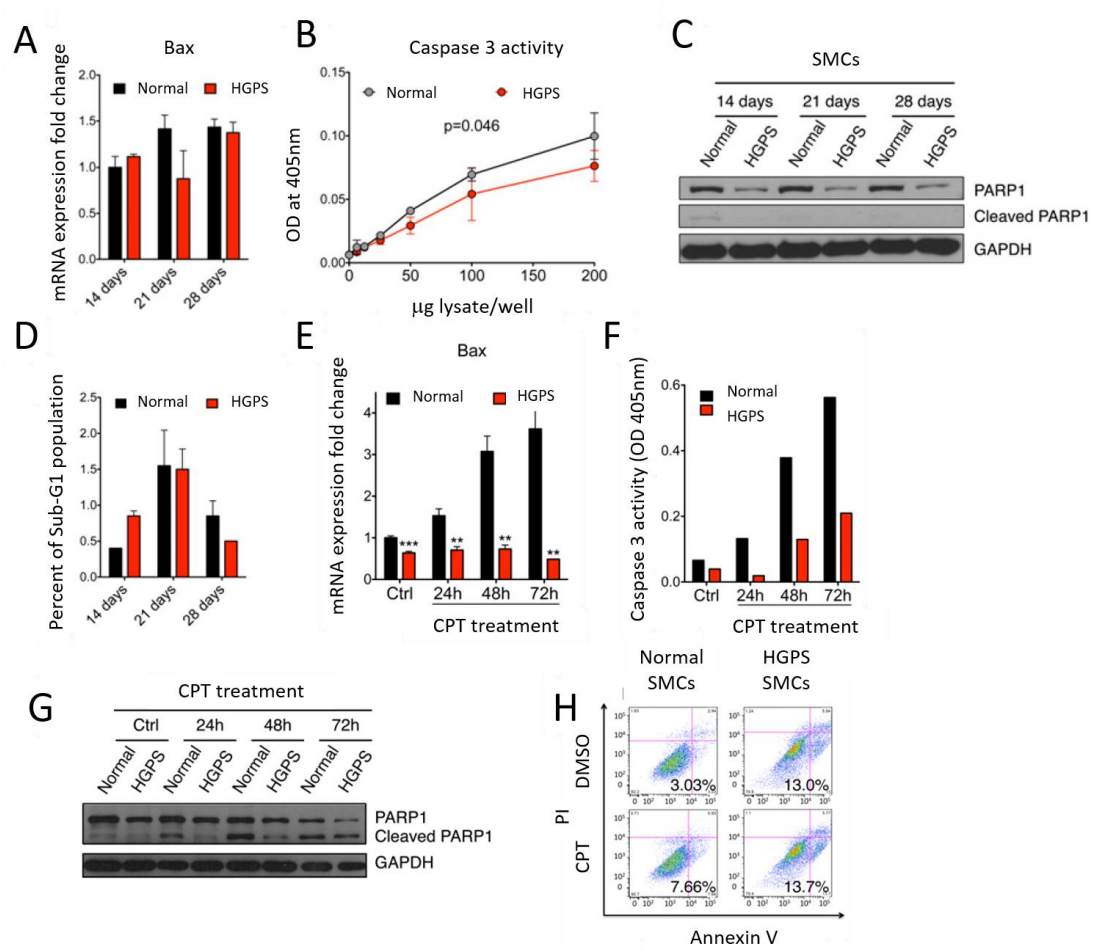

Figure 3-1: HGPS SMC cell death is caspase 3 independent. (A). RT-qPCR analysis with Bax specific primers on normal and HGPS SMCs at different time points during SMC differentiation. (B) Basal caspase 3 activity of normal and HGPS SMCs at day 14. Results were generated from two independent biological replicates. (C). Western blot with anti-PARP1 and GAPDH antibodies on normal and HGPS SMCs at indicated time points during differentiation. (D). Percentage of the sub-G1 population in normal and HGPS SMCs at days 14, 21, and 28. (E). RT-qPCR with Bax-specific primers on normal and HGPS SMCs after treatment with 20 μM CPT for the indicated period, respectively. **P < 0.01, ***P < 0.001. (F). Caspase 3 activity assay on normal and HGPS SMCs after treatment with 20 Mm CPT for the indicated period, respectively. (G). Western blot with anti-PARP1 and GAPDH antibodies on normal and HGPS SMCs after treatment with 20 μMCPT for the indicated period, respectively. (H). Representative plot of PI-annexin V FACS analysis on normal and HGPS SMCs after 24-h treatment with 20 μM CPT.

3.2.2 Progerin accumulation down-regulates PARP1 in HGPS SMCs

When probing PARP1 cleavage in the caspase studies, I observed that the levels of PARP1 protein were always lower in HGPS SMCs compared to the normal controls at days 14, 21 and 28 (Figure 3-1C & G), whereas no obvious changes were detected at day 7 (Figure 3-2A). To confirm this observation, I measured PARP1 levels in two different HGPS SMC lines at day 14 and found that the PARP1 levels in both were decreased by at least 75% relative to the control (Figure 3-2B). Immunofluorescence showed a significant decrease in PARP1 nuclear staining in HGPS SMCs at day 14 compared with the normal control (Figure 3-2C & D). Moreover, in primary skin fibroblasts from HGPS patients and a transgenic animal model G608G (Varga et al., 2006), similar PARP1 reduction was found in late passage cells (Figure 15 A & B). Resembling the cell cycle analysis in HGPS SMCs (Figure 2-7C), a significant increase in the G2/M population was detected in late passage HGPS fibroblasts (Figure 3-3C-F). Notably, there was no significant change in PARP1 protein or cell cycle distribution in early passage HGPS fibroblasts, similar

to the day 7 HGPS SMCs (Figure 3-2A). This suggests that the PARP1 reduction phenotype is not exclusive for SMCs, but a consequence of progerin accumulation in each cell type. As an initial executor of SSB repair and a key mediator of DNA DSB repair, PARP1 plays a crucial role in maintaining genome stability. Thus, I next examined whether PARP1 reduction was relative to increased cell death in progerin expressing SMCs.

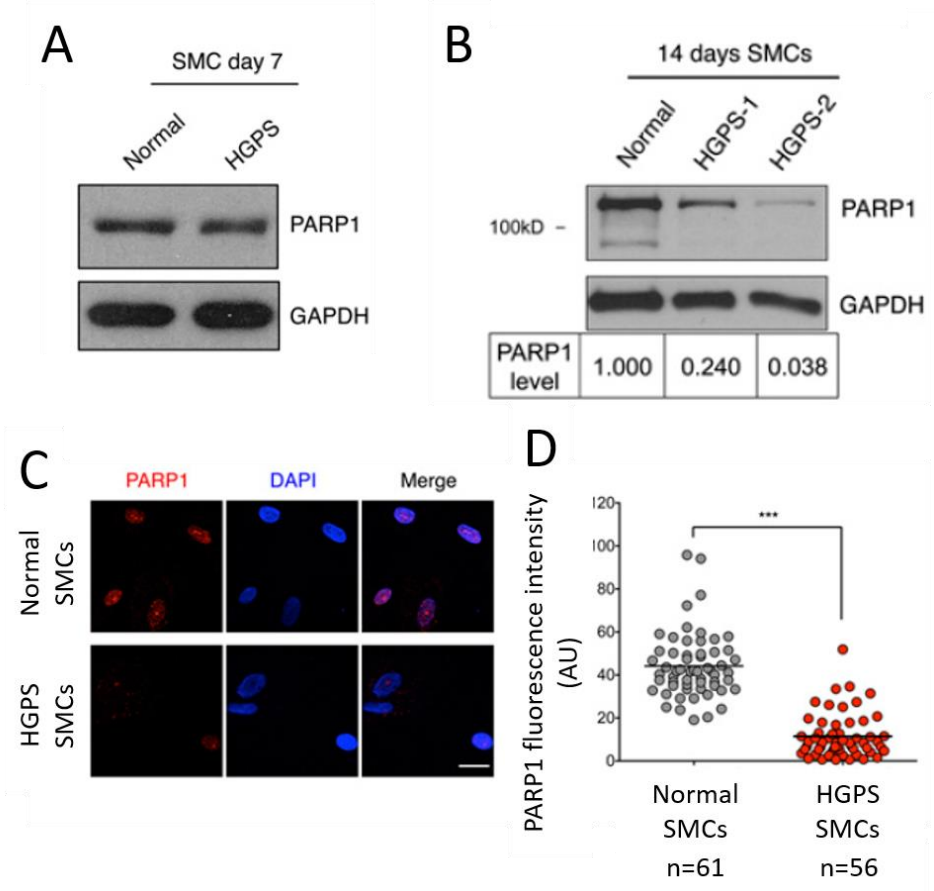

Figure 3-2: PARP1 is down-regulated in HGPS SMCs. (A). Western blot with anti-PARP1 and GAPDH antibodies on normal and HGPS SMCs at day 7 during SMC differentiation. (B, Upper) Western blot with anti-PARP1 and GAPDH antibodies on two HGPS SMC lines (HGADFN167 and HGADFN164) and a normal control SMC line at day 14. (Lower) Quantification of PARP1 in each sample. The intensity of PARP1 was first normalized to the corresponding GAPDH and then normalized to the control SMC. (C). Representative images of immunofluorescence staining with anti-

PAPR1 antibody in normal and HGPS SMCs at day 14. (Scale bar, 50 μm.) (D). Quantification of B, showing the PARP1 red fluorescence intensity. ***P < 0.001.

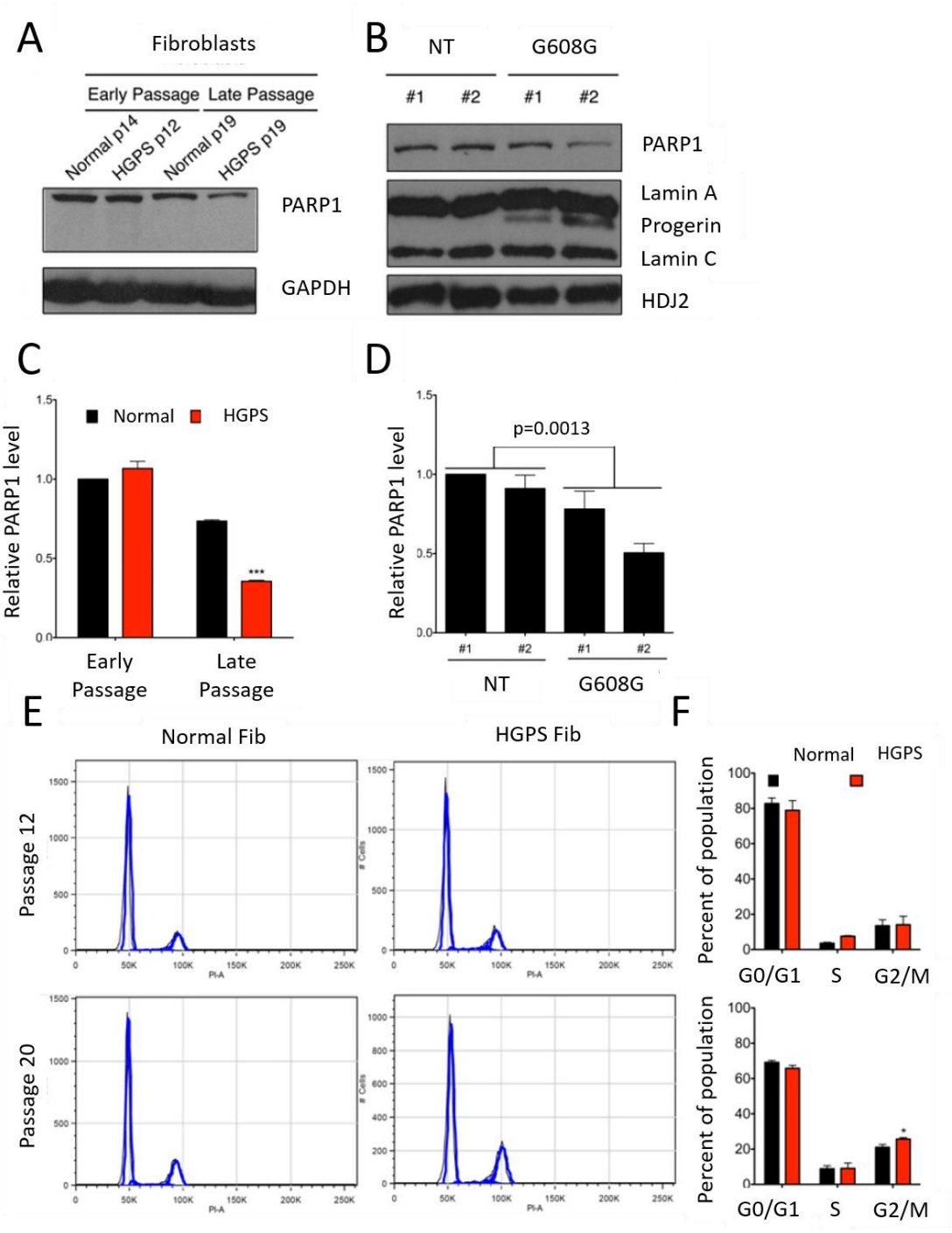

Figure 3-3: PARP1 is down-regulated in HGPS fibroblasts and BACG608G MEFs. (A). Western blot with anti-PARP1 and GAPDH antibodies on normal and HGPS fibroblasts at early (passages 14 and 12) and late (passage 19) cellular stages. (B). Quantification of A. Data was first normalized to loading control GAPDH, then to the early passage normal fibroblast. Results were generated from three independent experiments. ***P < 0.001. (C) Western blot with anti-mouse PARP1, lamin A/C, and HDJ2 antibodies on nontransgenic (NT) or G608G transgenic mouse fibroblast samples. Two mice were included for each genotype. (D) Quantification of D. Data were first normalized to loading control GAPDH, then to WT mouse 1. Results were generated from at least three independent experiments. (E) Cell cycle analysis on normal and HGPS fibroblasts at early and late passages, respectively. (F) Quantification of cell cycle analysis in E from two independent experiments. *P < 0.05.

To determine the effect of progerin on PARP1, normal SMCs were transfected with EGFP-progerin (EGFP-HG) or EGFP lamin A (EGFP-LA) and subsequently stained with an anti-PARP1 antibody. As shown in Figure 3-4A, the PAPR1 staining intensities were similar in the non-transfected cells (white arrows) as those in the cells expressing EGFP-LA or low amounts of EGFP-HG (green arrows). In contrast, in high expressers of EGFP-HG, PARP1 signals were significantly reduced (Figure 3-4A). Quantification of fluorescence intensity further indicated that, as the amounts of EGFP-HG increased, PARP1 decreased at a significantly faster rate than when EGFP-LA amounts increased (Figure 3-4B), supporting the belief that PARP1 reduction is associated with the amount of progerin.

Next, to directly investigate the causative relationship between progerin accumulation and PARP1 down-regulation, increasing amounts of EGFP-HG were transfected and expressed in normal SMCs. I found that the levels of PARP1 gradually decreased as the amounts of EGFP-HG increased (Figure 3-4C). Quantification confirmed a negative linear relationship between the amounts of

PARP1 and EGFP-HG (R^2 = 0.9818, Figure 3-4D). Notably, when progerin was ectopically expressed, a corresponding decrease of endogenous lamin A and C was observed (Figure 3-4C), implying a potential feedback loop in SMCs to control the total amount of A type lamins. Taken together, these results show that progerin resulted in PARP1 reduction in SMCs. In an attempt to address the functional importance of PARP1 in progerin-expressing cells, I applied a PARP1 inhibitor to the early passage HGPS fibroblasts, which expressed similar amounts of PARP1 as the control cells (Figure 3-3A). As shown in Figure 16E, HGPS fibroblasts showed much higher sensitivity to PARP1 inhibitor than normal control fibroblasts, suggesting an indispensable role of PARP1 in progeria cell survival.

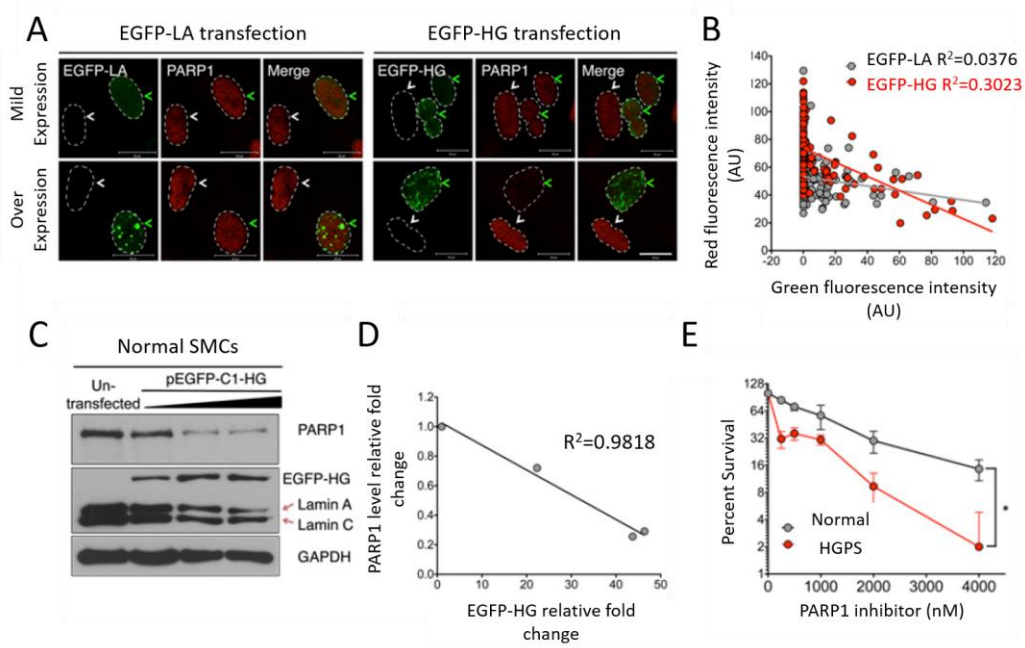

Figure 3-4: Progerin down-regulates PARP1. (A). Representative images of immunofluorescence staining with anti-PARP1 in normal SMCs transfected with pEGFP-C1-LA or pEGFP-C1-HG plasmids. The transfected and untransfected cells are indicated by green and white arrows, respectively. The nuclei were outlined by white dashed lines. (Scale bar, 20 μm.) (B). Quantification of A, showing the correlation between EGFP-HG or EGFP-LA fluorescence intensity (x axis) and PARP1 fluorescent intensity (y axis). More than 100 cells were randomly picked for each group. (C). Western blot with anti-PARP1 and GAPDH antibodies on normal SMCs transfected with different amounts of pEGFP-C1-HG plasmid. (D). Quantification of F, showing a negative-linear relationship between PARP1 (y axis) and progerin (x axis) protein amounts. Signals were normalized to the untransfected control. (E). Survival curve of early passage normal and HGPS fibroblasts upon a PARP1 inhibitor (Olaparib) treatment. Results were generated from two independent experiments. *$P < 0.05$.

3.2.3 PARP1 mis-localization is associated with disrupted Ran gradient in HGPS SMCs.

To investigate how progerin down-regulated PARP1, I compared PARP1 mRNA levels in normal and HGPS SMCs using RT-qPCR. Furthermore, I overexpressed progerin in normal SMCs and examined its effect on PARP1 transcription (Figure 3-5A & B). These data revealed no major changes in mRNA levels of PARP1 in those progerin-expressing SMCs, suggesting the observed down-regulation of PARP1 might result from compromised protein maintenance.

To examine how progerin may affect PARP1 protein stability, I overexpressed PARP1-GFP as described previously (Haince et al., 2008), together with DsRed-LA or DsRed-HG in normal SMCs. As expected, PARP1-GFP was localized inside the nucleus when co-expressed with the vector control or DsRed-LA (Figure 3-6A). In addition, consistent with a previous study (Boamah et al., 2012), I observed that PARP1-GFP became concentrated in the nucleoli when over expressed (Figure 3-6A), reflecting its roles in ribosome biogenesis. However, in DsRed-HG transfected with SMCs, more than 30% of the cells showed cytoplasmic localization of PARP1-

GFP (Figure 3-6A & B). These results implied that accumulated progerin excluded a fraction of PARP1 from the nucleus, and this fraction might be subjected to protease/proteasome mediated degradation.

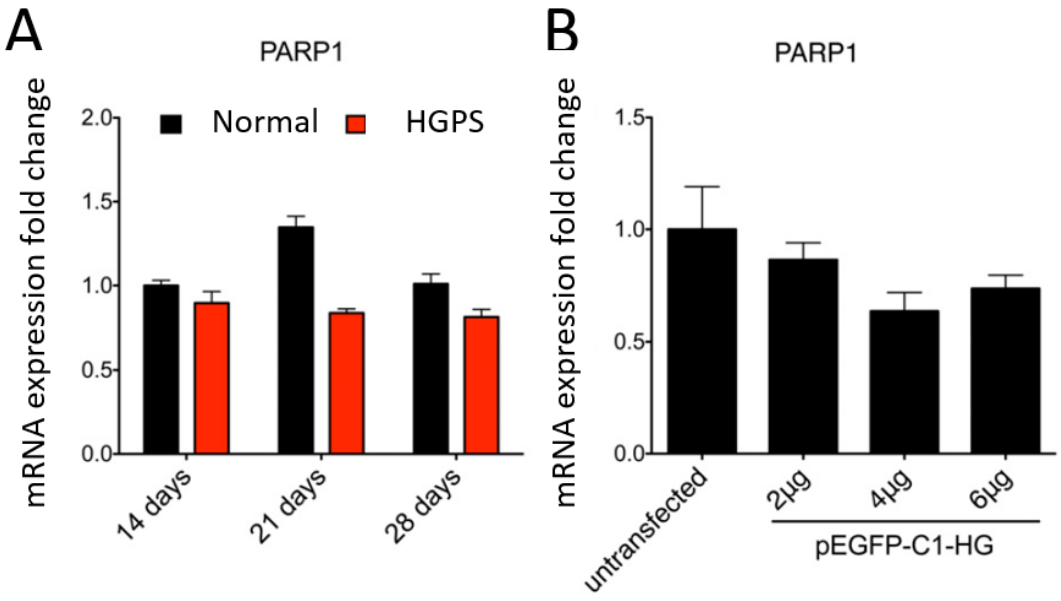

Figure 3-5: PARP1 mRNA level was not significantly affected by progerin. (A). RT-qPCR with PARP1-specific primers on normal and HGPS SMCs at days 14, 21, and 28. No significant changes of PARP mRNA levels were detected. (B). RT-qPCR with PARP1-specific primers on normal SMC samples transfected with indicated amounts of pEGFP-C1-HG plasmids. No significant changes of PARP1 mRNA levels were detected.

Next, I tested whether blocking farnesylation of progerin could restore PARP1's normal localization. To study this possibility, I used HG-SSIM, a non-farnesylatable mutant of progerin that carries a cysteine to serine mutation on the CSIM motif at the C terminus (Capell et al., 2005), and co-expressed it with PARP1-GFP in normal SMCs. As reported previous (Capell et al., 2005), DsRed-HG-SSIM no longer located at the inner nuclear membrane but was sequestered in giant aggregates in the

nucleoplasm (Figure 3-6A). Importantly, in the majority of the DsRed-HG-SSIM-transfected cells, I observed that the normal nuclear localization of PARP1-GFP was restored (Figure 3-6A). Quantification revealed that the percentage of PARP1-mislocalized cells was significantly decreased to 10% in the DsRed-HG-SSIM-expressing cells, compared with roughly 30% in DsRed-HG-expressing cells (Figure 3-6B). To further confirm this result, a FTI was used to treat DsRed-HG-expressing cells. As expected, the FTI treatment also rescued the mis-localization phenotype of PARP1-GFP and significantly reduced the mis-localized population (Figure 3-6A & B). These data suggested that the abnormal anchorage of progerin to the nuclear envelope was the main cause of the PARP1 mis-localization.

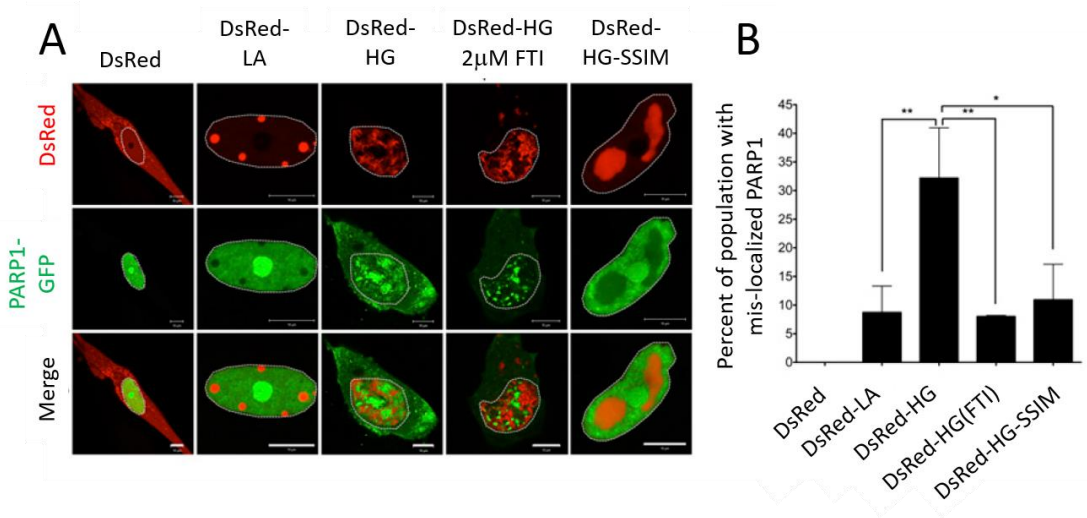

Figure 3-6: Progerin induces PARP1 mis-localization. (A) Representative images showing normal SMCs coexpressing PARP1-GFP with DsRed, DsRed-LA, DsRed-HG (with or without 2 μM FTI), or DsRed-HG-SSIM. Nuclei were outlined by white dashed lines. (Scale bar, 10 μm.) (B) Quantification of A, showing the percentage of PARP1-GFP– mislocalized cells under indicated conditions. More than 100 cells were counted for each group. Results were generated from three independent experiments. *P < 0.05, **P < 0.01.

I speculated that the PARP1 mis-localization in HGPS SMCs might be caused by a compromised nuclear import system mediated by a disrupted Ran gradient, which has been reported in HGPS fibroblasts (Kelley et al., 2011; Snow et al., 2013). To test this idea, I first examined the Ran gradient in normal and HGPS SMCs at days 7, 14, and 21 using immunofluorescence. As shown in Figure. 3-7A, HGPS SMCs displayed significantly decreased Ran signals in the nucleus, compared with the control cells, indicating that the Ran gradient [nuclear/cytoplasmic (N/C) ratio, (Figure 3-7B)] was disrupted in HGPS SMCs. Moreover, HGPS SMCs at days 14 and 21 exhibited even lower N/C ratios than the same cells at day 7 (Figure 3-7B), which is in agreement with the observation of a gradual reduction of PARP1 levels over time in HGPS SMCs. To further test the correlation between Ran gradient disruption and PARP1 mis-localization, HGPS SMCs at day 14 were transfected with PARP1-GFP and subsequently stained with Ran antibody. About 30% of the transfected HGPS SMCs displayed the PARP1 mis-localization phenotype (Figure. 3-8A). Importantly, these cells also showed significantly lower N/C ratios compared with the cells with normal nuclear PARP1-GFP (Figure 3-8B). Similar to Figure 18A, I examined the Ran gradient in normal SMCs transfected with DsRed-HG or DsRed-LA. Unlike LA, which did not interfere with the Ran gradient (Fig. 21A), HG expression significantly weakened nuclear signals of Ran (Figure 3-9A). Quantification revealed that the N/C ratios of Ran negatively correlated with progerin amounts (Figure 3-9B). Furthermore, inhibition of progerin farnesylation through FTI or HG-SSIM mutant rescued the Ran gradient disruption (Figure 3-9A & B). Collectively, these data suggested that abnormal anchorage of progerin to the nuclear

envelope disrupted Ran gradients, thereby affecting the nuclear import of PARP1 in HGPS SMCs.

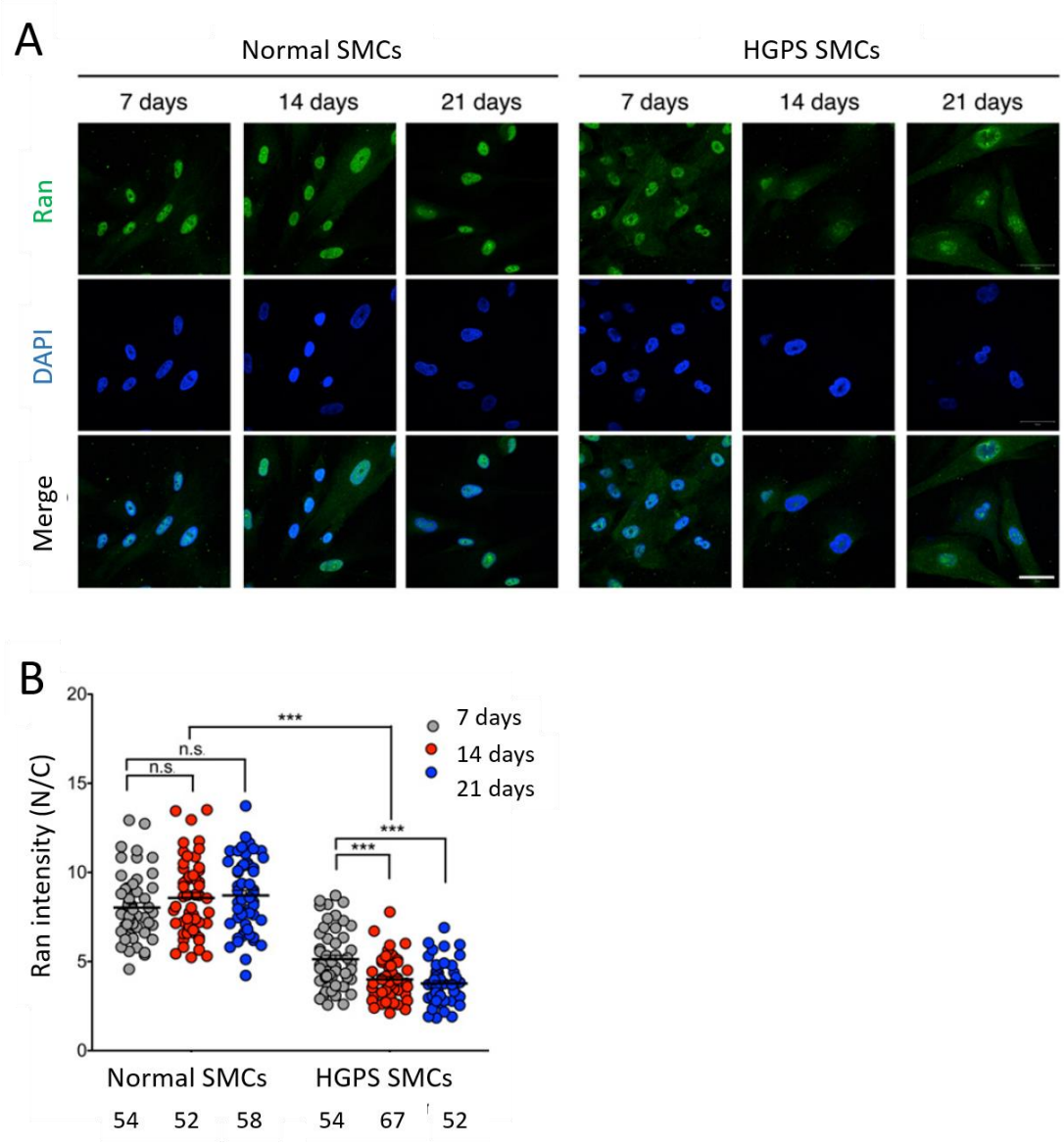

Figure 3-7: HGPS SMC display disrupted Ran gradient. (A) Representative images of immunofluorescent staining with an anti-Ran antibody on normal and HGPS SMCs at days 7, 14, and 21. Ran gradient was denoted as Ran (N/C). N and C refer to the nucleus and cytoplasm, respectively. (Scale bar, 50 μm.) (B) Quantification of Ran gradient in A. ***P < 0.001.

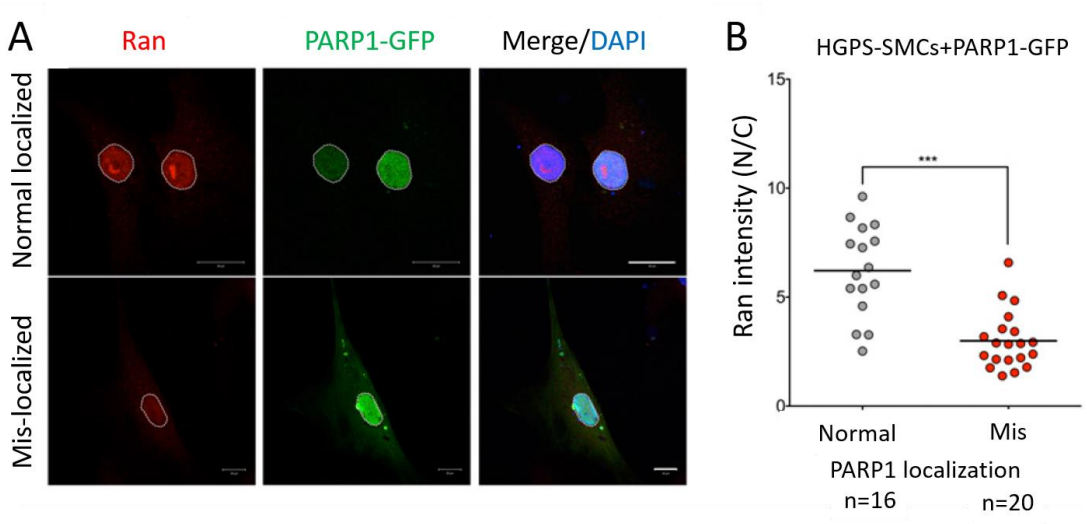

Figure 3-8: PARP1 mis-localization is associated with Ran gradient disruption in HGPS SMCs. (A). Representative images of immunofluorescence staining with anti- Ran antibody on HGPS SMCs transfected with PARP1- GFP. Cells with both normally or mislocalized PARP1- GFP were shown. The nuclei were outlined by white dashed lines. (Scale bar, 20 μm.) (B). Quantification of C, showing the Ran gradient in HGPS SMCs transfected with PARP1-GFP. ***P < 0.001.

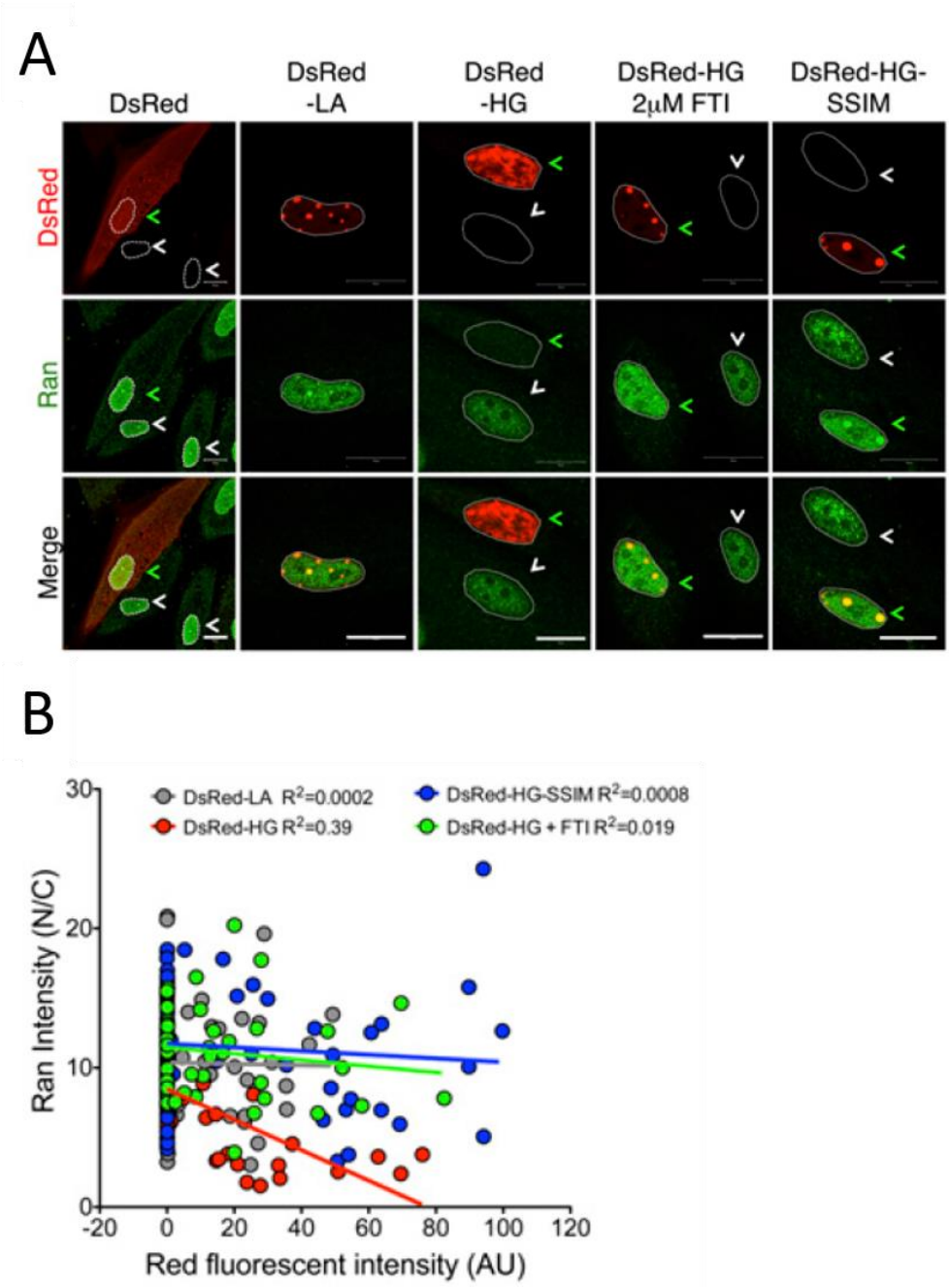

Figure 3-9: Progerin disrupts Ran gradient. (A). Representative images of immunofluorescence staining with anti- Ran antibody in normal SMCs transfected with DsRed, DsRed-LA, DsRed-HG (with or without 2 μM FTI) or DsRed-HG-SSIM. The transfected and untransfected cells were indicated by green and white arrows, respectively. The nuclei were outlined by white dashed lines. (Scale bar, 20 μm.) (B). Quantification of E, showing the correlation between DsRed fluorescent intensity and Ran gradient (Ran N/C) in N and C refer to the nucleus and cytoplasm, respectively. More than 50 cells were randomly picked for each group.

3.2.4 Compromised HR and activated NHEJ in S/G2 phase HGPS SMCs.

Previous studies reported that inhibition or silencing of PARP1 could lead to cell death in HR-deficient cells, due to NHEJ activation and consequent chromosome mis-arrangements (Bunting et al., 2010). Given PARP1's essential function in HR-deficient cells, I next examined the repair efficiencies of HR and NHEJ in HGPS SMCs.

Because HR is the major mechanism for replication-associated DSB repair in S/G2 phase, I induced DNA damage with CPT again to mimic replication fork collapse (Rothkamm et al., 2003). Different from the CPT experiment shown in Figure 3-1, here, CPT was used at a very low concentration (100 nM), thus only S/G2 phase cells were affected and no global apoptosis was induced (Ray Chaudhuri et al., 2012). At 10 min, 30 min, 120 min, and 720 min after CPT treatment, γH2AX and Rad51 signals were examined using immunofluorescence. After 10 min of CPT treatment, γH2AX foci were clearly identified in both normal an HPGS-SMCs, indicating that CPT had induced DSBs in both (Figure 3-10A). Rad51 plays an essential role in HR-mediated DSB repair. In normal SMCs, the formation of Rad51 foci started to appear at the 30-min time point, and at 720 min, most of these foci became co-localized with γH2AX foci (Figure 3-10A). Conversely, no distinct Rad51 foci were observed in HGPS SMCs throughout the whole time course (Figure 3-10A). To elucidate this phenomenon, over 100 cells were randomly picked at each time point, and each cell was plotted according to the numbers of γH2AX and co-localized Rad51 foci (as x and y). In normal SMCs, Rad51 foci became increasingly co-localized with γH2AX foci as shown by an increase in the slope of the trend line

during the time course. However, in HGPS SMCs, the slope of the trend line remained around 0 at all every point (Figure 3-10B), revealing a completely defective HR in these HGPS SMCs. Notably, the percentage of γH2AX-positive nuclei in Figure 3-10C is reduced in HGPS SMCs compared with normal controls under 100nM CPT treatment, probably due to the reduced S phase cell population in HGPS SMCs (Figure 2-7C).

With decreased PARP1 and a completely defective HR, DSBs will be fixed through the error-prone mechanism NHEJ. Indeed, in HGPS SMCs, the percentile of γH2AX-positive nuclei and the average number of γH2AX foci in each nucleus were gradually reduced after CPT treatment (Figure 3-10B & C), suggesting the NHEJ pathway was active in repairing these DSBs caused by CPT. 53BP1 can promote an NHEJ response to DNA damage (Bothmer et al., 2010). To assay the activity of NHEJ in S/G2 phase HGPS SMCs, I checked the formation of 53BP1 foci after 100nM CPT treatment. I found that, whereas no apparent 53BP1 foci formed in normal SMCs, distinct 53BP1 foci started to co-localize with γH2AX at 10 min after treatment in HGPS SMCs (Figure 3-11A & B), suggesting that normal SMCs used HR to fix DSBs at S phase, whereas HGPS SMCs repair DSBs through NHEJ.

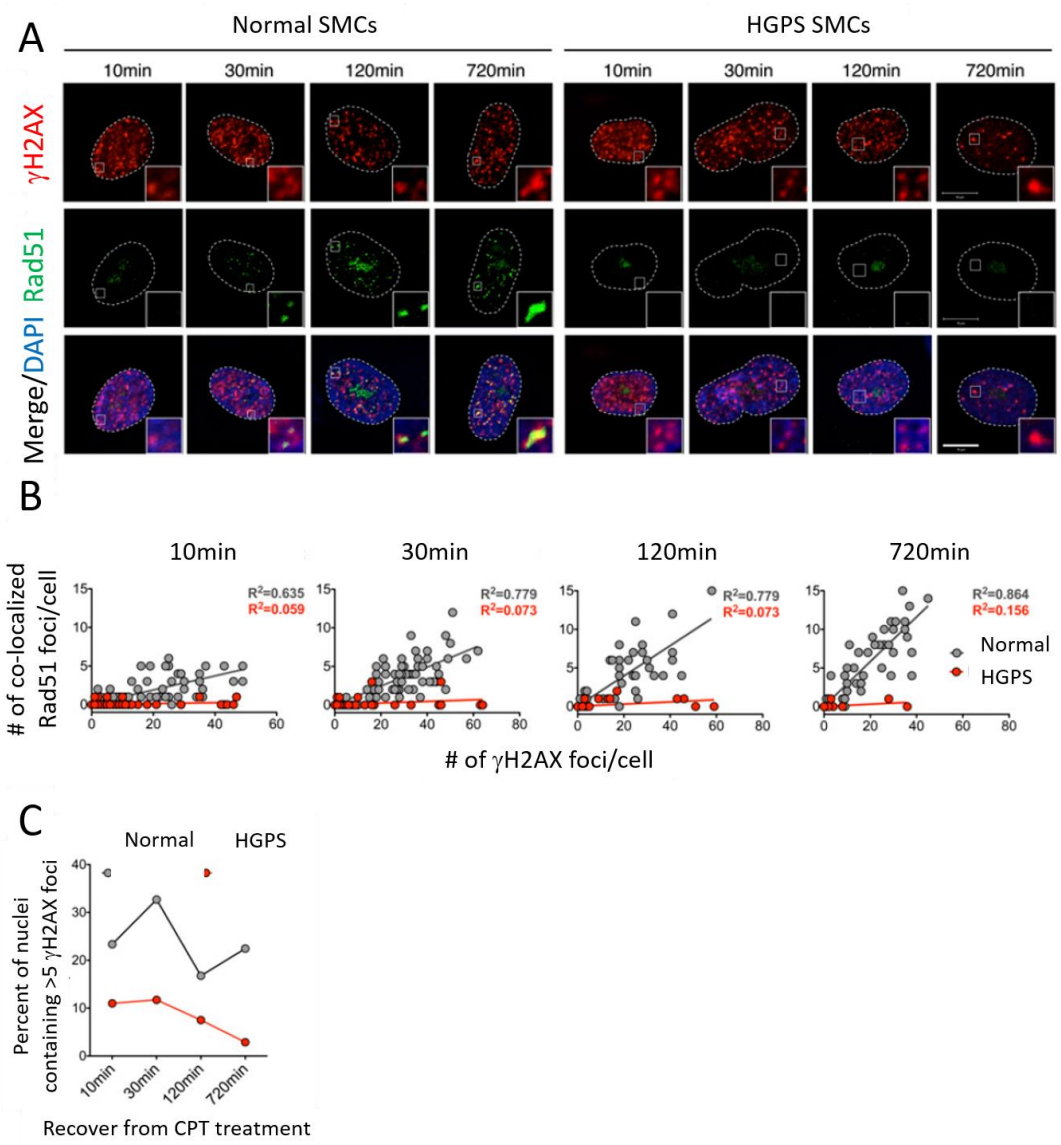

Figure 3-10: HGPS SMCs show impaired HR and activated NHEJ. (A). Representative image showing immunofluorescence staining with anti-γH2AX and Rad51 antibodies on normal and HGPS SMCs recovered for various amounts of time after 100 nM CPT treatment. (Scale bar, 10 μm.) (B). Quantification of A, showing the number of γH2AX (x axis) and colocalized Rad51 (y axis) foci in normal and HGPS SMCs at different time points. More than 100 cells were counted for each case. The trend lines of normal (in gray) and HGPS (in red) SMCs were also presented. (C). The percentage of nuclei containing more than five γH2AX foci in normal and HGPS SMCs at each indicated time point after 100 nM CPT treatment.

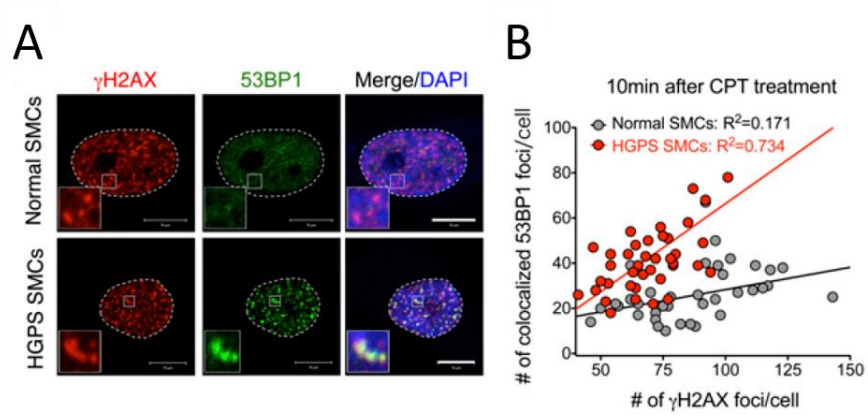

Figure 3-11: NHEJ is over-activated in HGPS SMCs during S/G2 phase. (A). Representative images of immunofluorescence staining with anti-γH2AX and 53BP1 antibodies on normal and HGPS SMCs at 10 min after 100 nM CPT treatment. (Scale bar, 10 μm.) (B). Quantification of D, showing the number of γH2AX (x axis) and colocalized 53BP1 (y axis) foci in normal and HGPS SMCs at different time points. Over 50 cells were analyzed.

3.2.5 Mitotic catastrophe in HGPS SMCs

Based on the observations of increased caspase-independent cell death, down-regulated PARP1, defective HR, and activated NHEJ, I hypothesized that DSBs were repaired incorrectly by NHEJ, which resulted in problems during mitotic division, leading to a mitotic catastrophe of HGPS SMCs. To test this hypothesis, cell cycle analysis was performed at days 14, 21, and 28 in SMC differentiation medium. Consistent with the data shown in Figure2-7, at each time point, I observed a significant increase in the G2/M population and a corresponding reduction in S phase population in HGPS SMCs compared with the normal control (Figure 3-12). This observation further supported the notion that mitosis is defective in HGPS. Taken together, this result indicated prolonged mitosis in HGPS SMCs, reflecting mitotic defects.

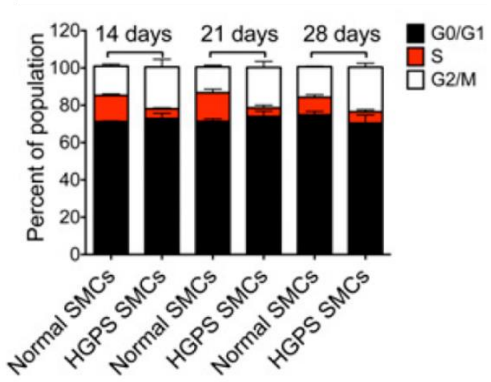

Figure 3-12: HGPS SMCs arrest at G2/M phase. Cell cycle analysis of the normal and HGPS SMCs at denoted time points. Results were generated from two biological replicates.

Next, to directly visualize the M phase of HGPS SMCs, I performed differential interference contrast (DIC) live cell imaging. Whereas all normal SMCs proceeded through mitosis smoothly (Figure 3-13A, top), HGPS SMCs either died and were destroyed during cell division (mitotic catastrophe) or exited mitosis without dividing but survived (Figure 3-13A, middle and bottom, respectively). Statistical analysis confirmed that about 50% of the HGPS SMCs displayed mitotic catastrophe, and the rest failed to divide (Figure 3-13B). In support of this observation, metaphase spectral karyotyping revealed ~6.7% aneuploidy and 20% polyploidy in dividing HGPS SMCs (Figure 3-14A & B). Next, a BrdU pulse-chase experiment was conducted to follow the fate of S phase SMCs. 48 and 96 h after the BrdU pulse, immunofluorescence staining of BrdU was carried out. In normal SMCs, the percentage of the BrdU positive nuclei gradually increased from 20% to 80%, reflecting normal cell division. In contrast, the BrdU-positive nuclei in HGPS SMCs gradually decreased from 6% at time 0 h to less than 2% at 96 h after the pulse

(Figure 3-15). This result indicated that over 60% of the S phase HGPS SMCs were not able to proceed through the cell division and died during cell division.

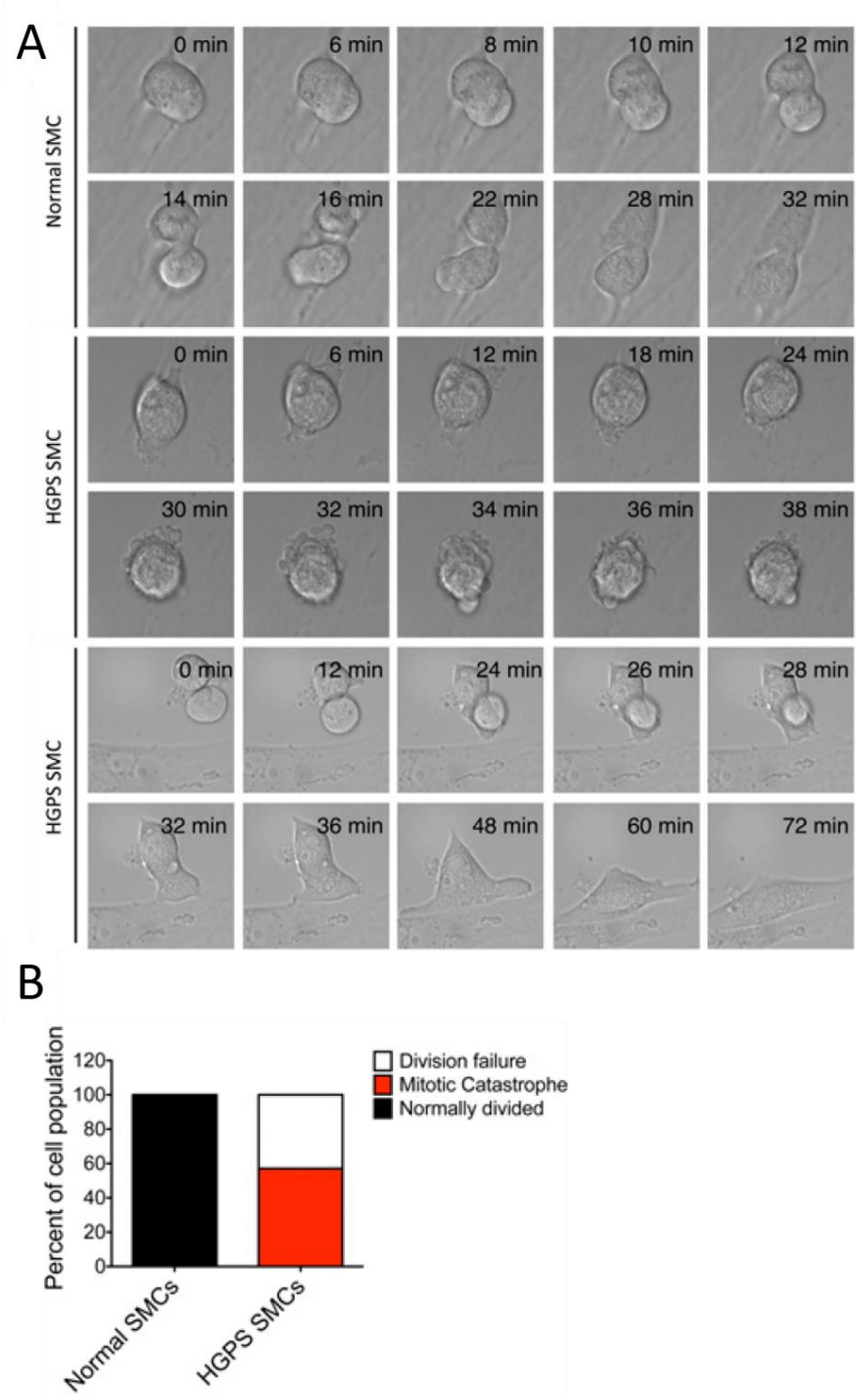

Figure 3-13: Mitotic catastrophe in HGPS SMCs. (A). DIC live cell imaging of normal and HGPS SMCs at day 21. (Top) Normal mitotic division of a normal SMC; (Middle) mitotic catastrophe of an HGPS SMC; and (Bottom) failed mitosis of an HGPS SMC. (b). Percentage of normal and defective mitosis in normal and HGPS SMCs. n = 4 and 7 for normal and HGPS SMCs, respectively.

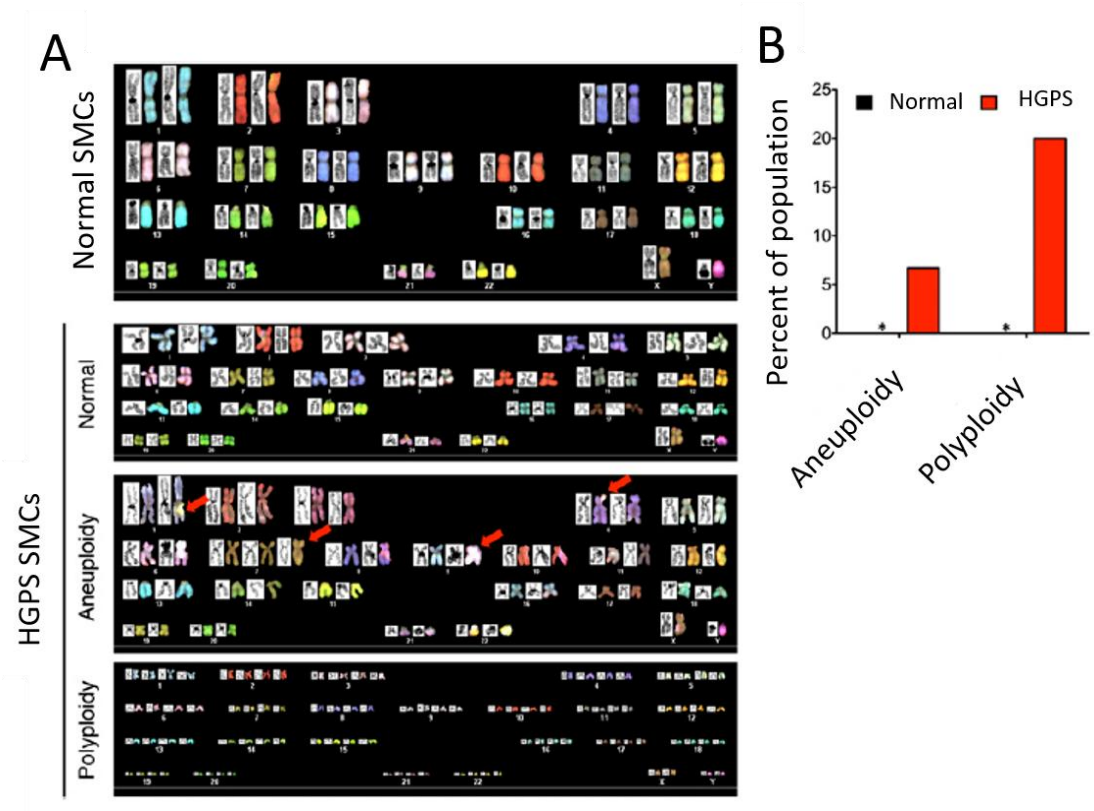

Figure 3-14: HGPS SMCs bear abnormal karyotype. (A). Representative spectral karyotypes of normal and HGPS SMCs at day 14. Red arrows refer to chromosome re-arrangements and aneuploidy in HGPS SMCs. (B). Quantification of A, showing the percentage of aneuploidy and polyploidy in normal and HGPS SMCs. The asterisk indicated 0% of aneuploidy or polyploidy in normal SMCs. A total of 20 metaphase cells were analyzed for each sample.

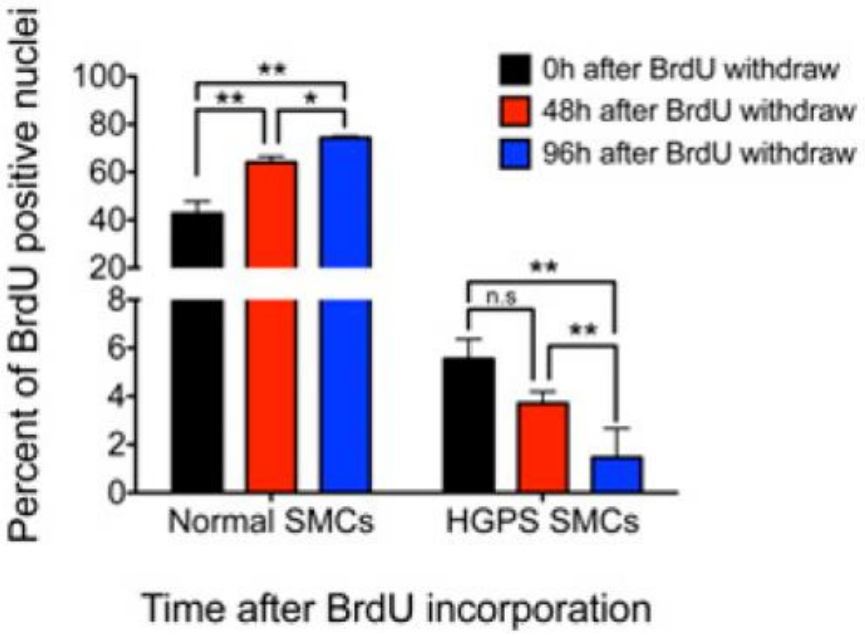

Figure 3-15: HGPS SMCs fails to proceed through cell division. Quantification of the percentages of BrdU-positive nuclei at 48 h and 96 h after BrdU pulse in normal and HGPS SMCs at day 14. Results were generated from two independent experiments. *P < 0.05 and **P < 0.01.

3.3 Discussion

3.3.1 PARP1 is a key regulator of SMC survival in Progeria

Efforts to test the role of caspase 3 in HGPS SMC cellular death led to negative results, suggesting that this phenotype was carried out through caspase 3 independent mechanisms (Figure 3-1). However, during this process, I found that PARP1, an important protein involved in DNA damage repair and cellular homeostasis, was significantly reduced in HGPS SMCs (Figure 3-1C) (Luo and Kraus, 2012). Given

this important role of PARP1, I wondered whether its down-regulation contributed to the cell death phenotype in HGPS SMCs.

In addition to its well-recognized role in DNA SSB repair, several studies revealed a new role of PARP1 in protecting HR and suppressing NHEJ (Hochegger et al., 2006; Patel et al., 2011). Here, I found that the PARP1 protein levels were reduced in HGPS SMCs after day 14 in SMC culture as well as in late passage HGPS fibroblasts (Figure 3-1C & G and Figure 3-2A & B). Importantly, the progerin overexpression (Figure 3-4A-D) revealed a direct inverse relationship between the amounts of PARP1 and progerin, indicating that progerin is a powerful suppressor of PARP1. The PARP1 inhibitor experiment in HGPS fibroblasts further revealed an essential role of PARP1 in cell survival (Figure 3-1E). I speculate that the sensitivity of PARP1 to progerin may vary in different cell types. In fibroblasts, PARP1 may be less influenced by progerin accumulation than in SMCs. Therefore PARP1 down-regulation was not obvious until late passage fibroblast cells. These data also suggest that PARP1 is indispensable in all progerin-expressing cell types, and the levels of PARP1 reduction may be positively correlated with the severity of phenotypes in HGPS patients.

My next question was how does progerin inhibit PARP? Quantitative RT-PCR analysis showed a slight, insignificant reduction in PARP1 mRNA in the presence of progerin, suggesting that progerin likely affects PARP1 post-translationally (Figure 3-5). Microscopy analysis further revealed that a fraction of PARP1 was mis-localized to the cytosol in the presence of large amounts of progerin (Figure 3-2), and this progerin-mediated PARP1 mis-localization was likely due to the abnormal anchorage

of progerin to the nuclear envelope (Figure 3-2). Previous studies demonstrated abnormal nuclear pore clustering and a disrupted Ran gradient across the nuclear membrane in HGPS fibroblasts (Kelley et al., 2011; Snow et al., 2013). I speculated that this mis-localization of PARP1 was a novel effect of the disrupted RanGTP gradient. Indeed, a weakened Ran gradient (Figure 3-7) and a strong correlation between these two (Figure 3-9) were found in HGPS SMCs.

It has been shown that NHEJ is active in all cell cycle phases, whereas HR is particularly important in S/G2. Moreover, DSBs produced by replication fork inhibitors are primarily repaired by HR. Using a topoisomerase I inhibitor (CPT) at a nanomolar concentration that only affects S/G2 phase cells, my analysis revealed a completely deficient HR and an elevated NHEJ response in S phase HGPS SMCs (Figure 3-10 and Figure 3-11). When the error-prone NHEJ pathway is used in DNA repair, irreversible chromosome aberrations can occur, resulting in complicated consequences (Bunting et al., 2010; Patel et al., 2011). Most commonly, cells will spend more time in M phase, attempting to resolve the problems (Vitale et al., 2011). If entangled chromosomes are unresolvable, cells will die through mitotic catastrophe (Vitale et al., 2011). Indeed, my cell cycle analysis revealed a palpable G2/M delay in HGPS SMCs (Figure 3-12) and late passage fibroblasts (Figure 3-3E & F), suggesting that these cells were encountering problems during cell division. Live cell imaging and spectral karyotyping experiments further demonstrated that HGPS SMCs either died in mitosis or failed to divide, forming bi-nucleated cells (Figure 3-13 and Figure 3-14). An additional line of supportive evidence arose from a BrdU pulse-chase assay, which indicated that most of the labeled S phase HGPS SMCs could not

proceed through the M phase (Figure 3-15). Previous studies also have shown mitotic delay and bi-nucleation in HGPS fibroblast cells (Cao et al., 2007). Again, the mitotic delay and cell death in HGPS SMCs were more prominent than those observed in HGPS fibroblasts, possibly due to a greater PARP1 reduction in HGPS SMCs.

DNA damage has long been implicated in HGPS pathogenesis. In 2005, the Zhou group published a study elucidating a deficient HR, an overactive NHEJ, and defective DNA damage repair in primary HGPS fibroblasts and mouse embryonic fibroblasts (MEFs) from a progeria model (Liu et al., 2005). In 2011, Zhang and colleagues generated the first iPS cell model for HGPS and reported increased DNA damage in differentiated HGPS SMCs (Zhang et al., 2011). In addition, Liu et al. reported a decrease of DNA PKCs in differentiated HGPS SMCs, an enzyme with an established role in the NHEJ response (Liu et al., 2011). In line with these previous reports, I reported a previously unidentified and essential role of PARP1 in mediating DNA damage repair and SMC survival in HGPS. My data can be summarized in a model: the accumulation of progerin causes PARP1 down-regulation, which results in the activation of the NHEJ pathway in the HR deficient HGPS SMCs. The error-prone NHEJ further leads to chromosome aberrations and mitotic catastrophe in HGPS SMCs

3.3.2 Insights into future therapeutics of HGPS and normal vascular aging.

Based on my model, to rescue the SMC loss in HGPS, one solution is to restore normal HR function. Whereas the precise pathway for progerin to interfere with HR remains to be understood, previous studies have provided some valuable insights.

One emerging hypothesis is that progerin disrupts chromatin remodeling after DSBs, hence blocking the access of DNA damage repair factors to damaged regions. This idea is supported by a number of studies demonstrating global changes in genome organization and the epigenome in HGPS cells (McCord et al., 2013; Shumaker et al., 2006). Importantly, recent studies have suggested that changes in H3K9me3 levels in HGPS cells can affect genome maintenance and the compromised ATM-mediated phosphorylation of KAP-1 impairs DNA repair in Zmpste24-deficient MEFs (Liu et al., 2013a; Liu et al., 2013b), providing a possible molecular connection between chromatin modifications and the DNA repair machinery. Other lines of studies have suggested a role of Xeroderma pigmentosum group A (XPA) protein in excluding normal access of DNA repair machinery to DSBs in HGPS cells (Musich and Zou, 2009, 2011). Whereas the detailed mechanisms underlying HR deficiency in HGPS are still being elucidated, I predict that specific treatments that promote targeting of HR repair proteins to DSB termini are expected to reduce or diminish the SMC loss phenotype associated with progerin accumulation.

Increasing evidence suggests the involvement of progerin in the normal aging process (Cao et al., 2011a; McClintock et al., 2007; Scaffidi and Misteli, 2006). Significantly, overlapping cardiovascular pathology was identified in HGPS and geriatric patients (Olive et al., 2010). Additional studies demonstrated an accumulation of unprocessed farnesylated prelamin A (a longer version of progerin) in the vasculature (Liu et al., 2013c; Ragnauth et al., 2010). It will be of great interest to determine whether HR becomes partially impaired in the aged vasculature and whether a similar PARP1-mediated mitotic cell death mechanism also contributes to

normal vascular aging. In summary, the present study uncovers what I believe is the first study to elucidate the DNA damage response pathway underlying the vascular disease in HGPS.

Chapter IV: Cell cycle dependent characterization of homologous recombination and non-homologous end joining efficiencies in HGPS.

4.1 Introduction

Non-homologous end joining (NHEJ) and homologous recombination (HR) are the two major pathways used by eukaryotic cells to repair DSBs (Branzei and Foiani, 2008). The choice between these two pathways is largely decided by the specific cell cycle phase (Branzei and Foiani, 2008). For example, NHEJ is the predominant DSB repair pathway during the G0/G1 phase, due to the nature of more condensed chromatin and the absence of sister chromatid as repairing template (Branzei and Foiani, 2008; Chapman et al., 2012). On the other hand, HR activity is mostly observed in S/G2 phase cells, where chromatin structure is less compact and sister chromatids are available (Branzei and Foiani, 2008; Chapman et al., 2012). During S/G2 phase, the Ku70-Ku80 heterodimer complex can still bind to DSB ends with extremely high affinity, which is in favor of NHEJ upon DSBs (Branzei and Foiani, 2008). Interestingly, HR manages to compete with NHEJ during S/G2 phase with the help from additional factors including BRCA1, CtIP, PARP1 and CDKs (Branzei and Foiani, 2008).

Proper activation of NHEJ or HR at the correct cell cycle phase is crucial for eukaryotic cells to defend against genotoxic stress. Disruption of these processes could result in chromatin relocation, genome instability and cell death. For example, mutants that are defective in either NHEJ or HR express higher sensitivity to ionized radiation (IR) during G0/G1 phase or S/G2 phase respectively (Branzei and Foiani, 2008). In chicken DT40 cells, a Ku70 knockout mutant (NHEJ defective) is extremely sensitive to IR during G0/G1 phase, suggesting a protecting role of NHEJ at this cell cycle phase (Branzei and Foiani, 2008; Takata et al., 1998). In contrast, a

Rad54 knockout mutant (HR defective) exhibit higher IR sensitivity exclusively during S/G2 phase (Branzei and Foiani, 2008; Takata et al., 1998). Similarly, NHEJ defective mouse cells also showed elevated IR sensitivity during G0/G1 phase but not in S/G2 phase cells (Branzei and Foiani, 2008; Singh et al., 2009). In yeast, haploid cells during G0/G1 phase reply on NHEJ to repair DSBs, whereas diploid cells upregulate HR and suppress NHEJ (Astrom et al., 1999; Branzei and Foiani, 2008; Lee et al., 1999). These reports illustrated a cell cycle dependent activation of NHEJ or HR upon DSBs.

Besides repair deficiencies, inappropriate activation of NHEJ may also lead to problems. In contrast to HR, which is directed by homology based DNA repair, NHEJ simply re-ligates two random DNA break ends at proximity (Lieber, 2010). Therefore, it is error prone and likely to introduce DNA mutations, insertions or deletions (Lieber, 2010). It has been previous shown that PARP1 deletion or inhibition leads to massive cell death in HR deficient cells, due to increased DSBs and over-activation of NHEJ (Bunting et al., 2010; Patel et al., 2011). Moreover, abrogation of NHEJ by 53BP1 knockout has been shown to restore HR and promote cell survival upon PAPR1 inhibition, suggesting a toxic role of NHEJ in genome instability (Bunting et al., 2010).

In the previous chapter, I characterized HR and NHEJ efficiencies in S/G2 phase HGPS SMCs. In this chapter, I aim to establish a complete cell dependent activation profile of HR and NHEJ in HGPS cells. Here, I present data showing that the cell cycle dependent activation of NHEJ or HR is completely disrupted in HGPS

fibroblasts. HR is defective in both G0/G1 and S/G2 phase HGPS fibroblasts, whereas NHEJ is defective during G0/G1 phase but active in S/G2 phase.

4.2 Results

4.2.1 Homologous recombination is deficient during G0/G1 and S/G2 phase HGPS fibroblasts.

To assay HGPS HR activity at different cell cycle stages, I incubated normal and HGPS fibroblasts with BrdU for 30min. G0/G1 phase and S/G2 phase cells were indicated by BrdU negative and positive staining respectively. After BrdU labeling, cells were then treated with 1μM doxorubicin (Dox), a topoisomerase II inhibitor, for DSB induction. To specifically examine HR efficiency, I tested the recruitment dynamics of BRCA1 and Rad51 (two important HR factors) at 30min, 120min and 360min after Dox treatment. As shown in Figure 4-1 A, normal cells displayed a gradual increase of BRCA1 foci count during G0/G1 phase (BrdU negative), while HGPS fibroblasts failed to show any BRCA1 formation. Quantification of foci number showed a significant reduction of BRCA1 foci formation in HGPS fibroblasts (Figure 4-1B). Similar activation pattern was also observed on Rad51 recruitment (Figure 4-2). These data indicate that HR is inactive in G0/G1 phase HGPS fibroblasts upon DSBs.

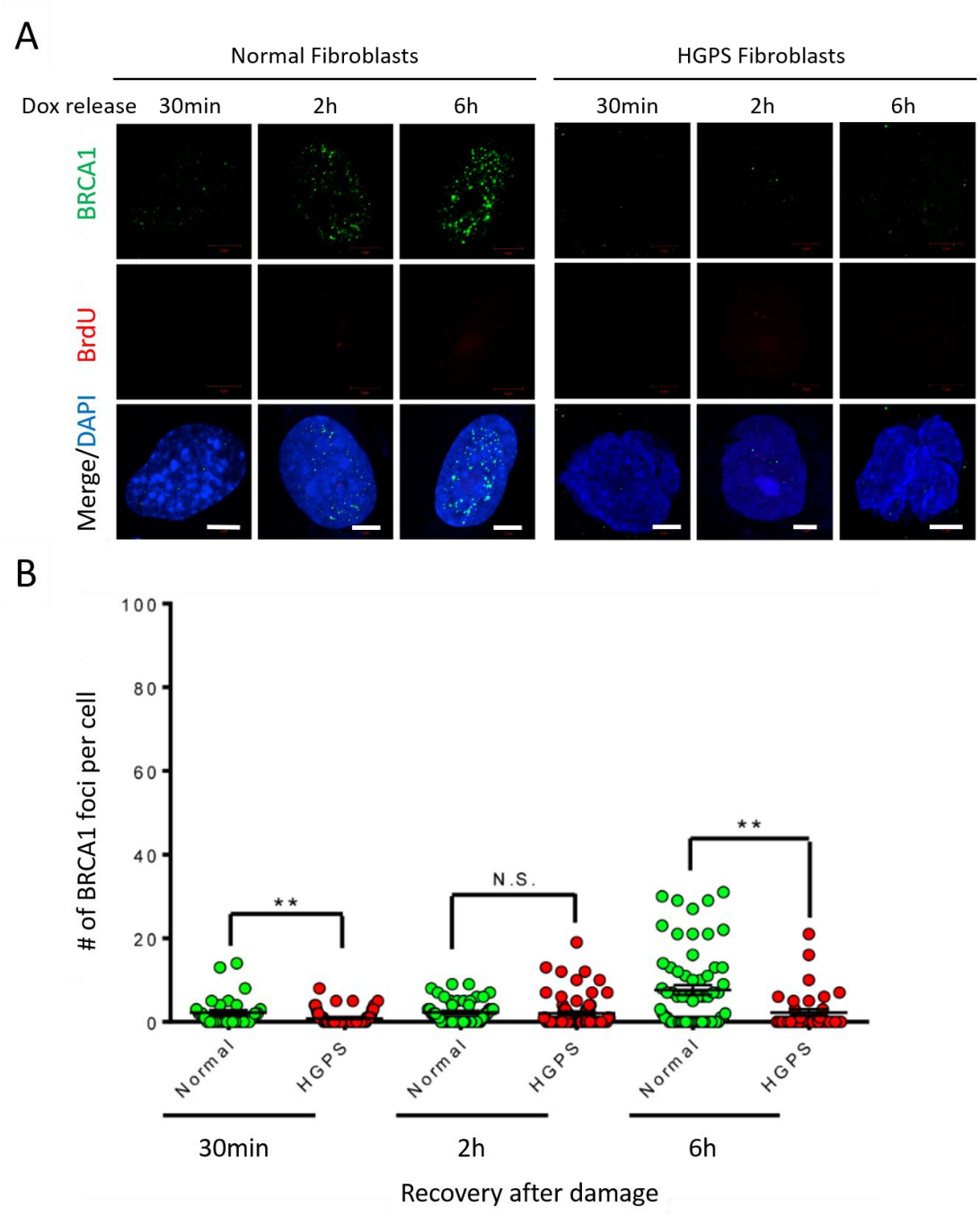

Figure 4-1: HR is deficient in G0/G1 phase HGPS fibroblasts. (A). Representative image showing immunofluorescence staining with anti-BrdU and BRCA1 antibodies on normal and HGPS fibroblasts recovered for various amounts of time after 1μM Dox treatment. (Scale bar, 5 μm.). (B). Quantification of (A) showing the number of BRCA1 foci per nuclei in normal and HGPS fibroblasts.

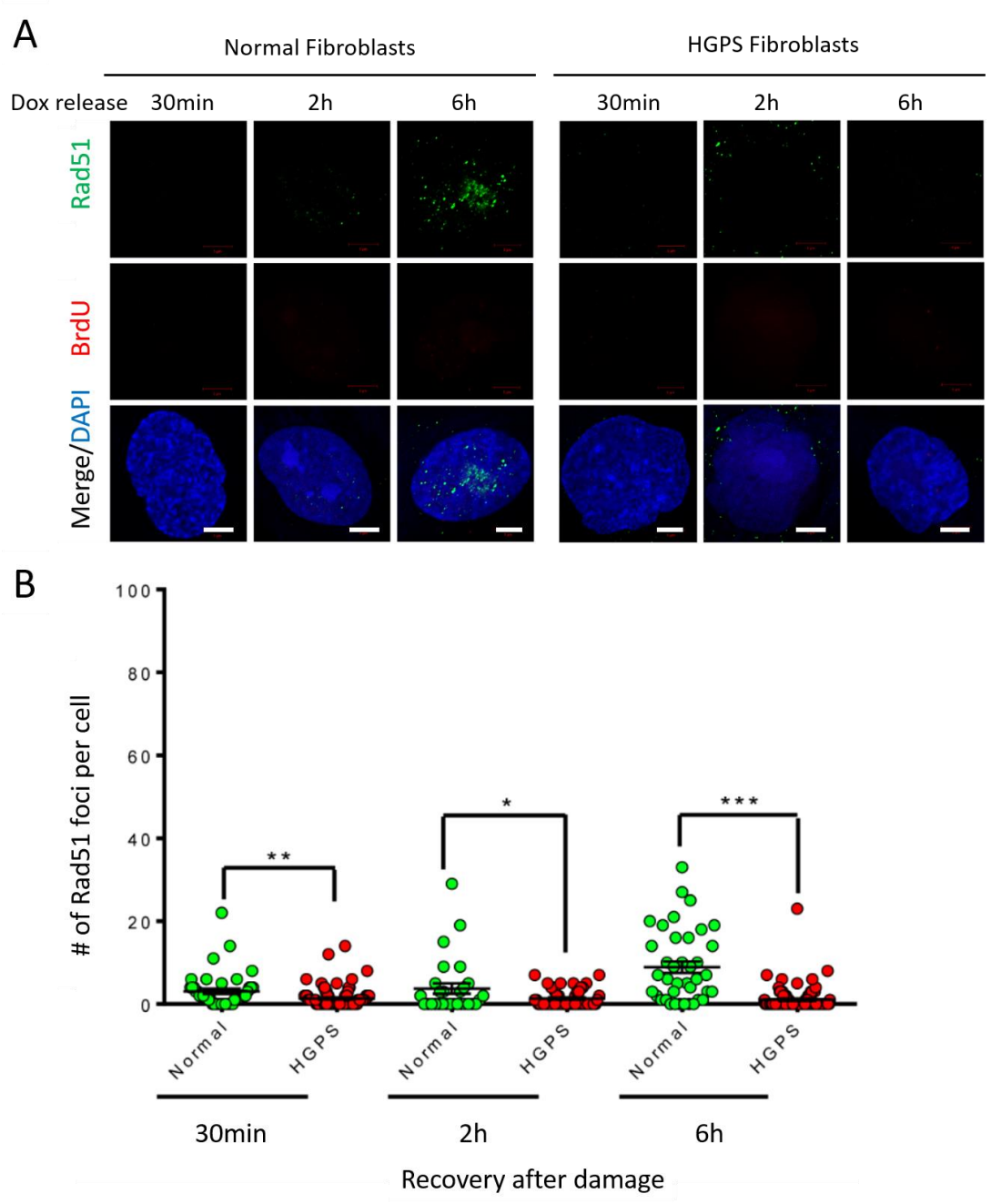

Figure 4-2: HR is deficient in G0/G1 phase HGPS fibroblasts. (A). Representative image showing immunofluorescence staining with anti-BrdU and Rad51 antibodies on normal and HGPS fibroblasts recovered for various amounts of time after 1μM Dox treatment. (Scale bar, 5 μm.). (B). Quantification of (A) showing the number of Rad51 foci per nuclei in normal and HGPS fibroblasts.

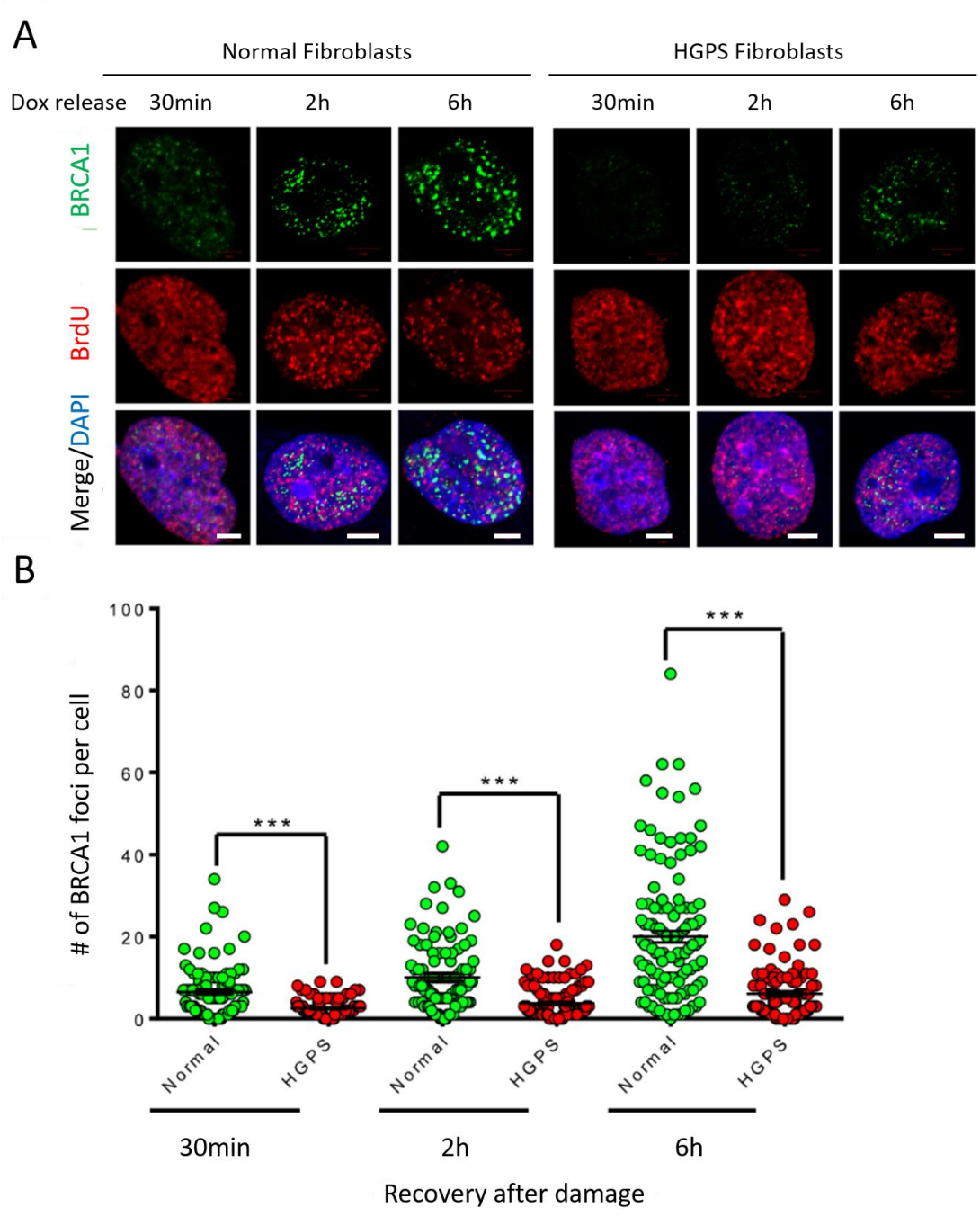

Figure 4-3: HR is deficient in S/G2 phase HGPS fibroblasts. (A). Representative image showing immunofluorescence staining with anti-BrdU and BRCA1 antibodies on normal and HGPS fibroblasts recovered for various amounts of time after 1μM Dox treatment. (Scale bar, 5 μm.). (B). Quantification of (A) showing the number of BRCA1 foci per nuclei in normal and HGPS fibroblasts.

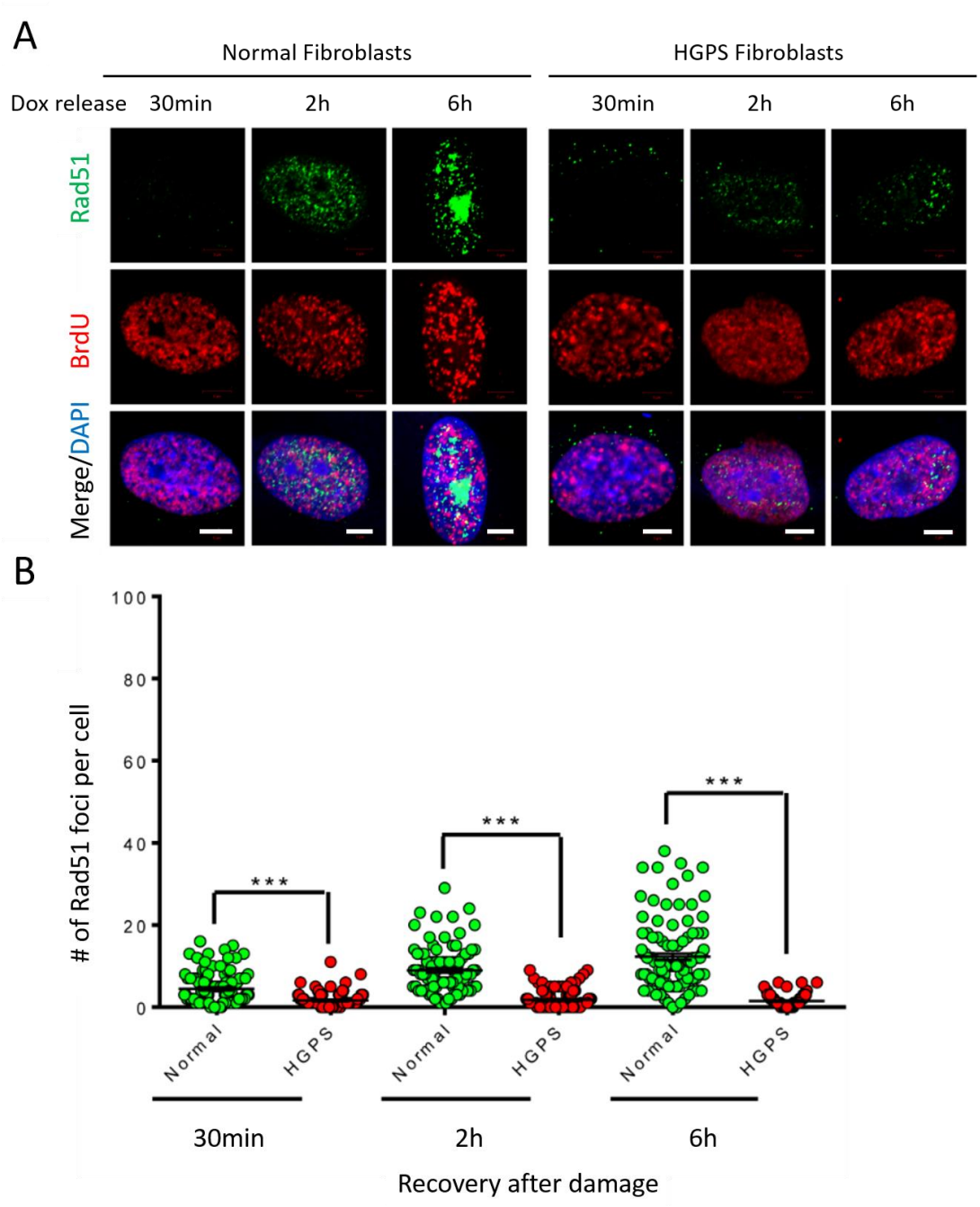

Figure 4-4: HR is deficient in S/G2 phase HGPS fibroblasts. (A). Representative image showing immunofluorescence staining with anti-BrdU and Rad51 antibodies on normal and HGPS fibroblasts recovered for various amounts of time after 1μM Dox treatment. (Scale bar, 5 μm.). (B). Quantification of (A) showing the number of Rad51 foci per nuclei in normal and HGPS fibroblasts.

I next examined HR activities in S/G2 phase cells. As shown in Figure 4-3, normal fibroblasts at S/G2 phase (BrdU positive staining) started to show a robust BRCA1 foci formation as early as early 2h after Dox treatment, whereas such event did not start in corresponding HGPS fibroblasts until four hours later, suggesting a delayed HR in HGPS during S/G2 phase. Similar activation pattern was also observed on Rad51 recruitment (Figure 4-4). Notably, both normal and HGPS cells exhibit significantly stronger BRCA1 and Rad51 recruitments during S/G2 phase in comparison to G0/G1 phase, supporting a predominant role of HR during S/G2 phase (Figure 4-1 – 4-4) (Branzei and Foiani, 2008).

To elucidate the molecular mechanism underlying HGPS HR deficiency, I performed western blotting analysis to measure the protein level of BRCA1 and Rad51 in HGPS fibroblast. Interestingly, both BRCA1 and Rad51 displayed a significant reduction in HGPS fibroblasts (Figure 4-5A). Moreover, RT-qPCR revealed that the mRNA level of these two HR factors were also significantly reduced in HGPS fibroblasts, suggesting that progerin might impact the expression of BRCA1 and Rad51. Protein level reduction of HR factors could at least partially explain HR deficiency in HGPS.

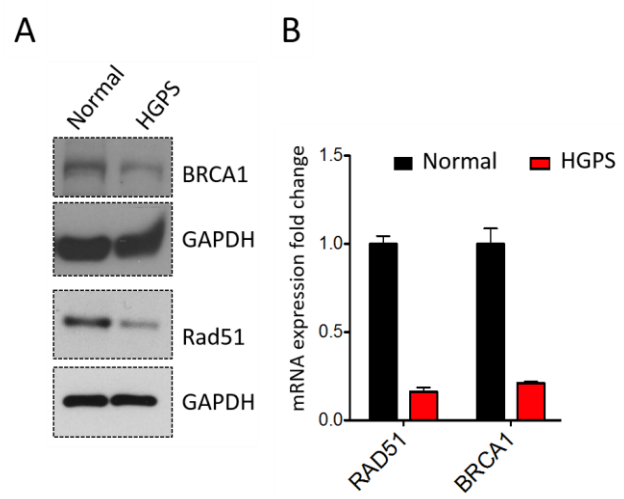

Figure 4-5: BRCA1 and Rad51 are down-regulated in HGPS fibroblasts. (A). Western blotting analysis with an anti-BRCA1 or Rad51 antibody on passage matched normal and HGPS fibroblasts. (B). RT-qPCR with BRCA1 and Rad51 specific primers on passage matched normal and HGPS fibroblasts.

4.2.2 Non-homologous end joining is deficient in G0/G1 phase but functional in S/G2 phase HGPS fibroblasts.

To characterize HGPS NHEJ efficiencies at different cell cycle phases, I examined the recruitment dynamics of RIF1, an NHEJ specific promoting protein, at 10min, 30min 2h and 6h after Dox treatment. As shown in Figure 4-6A & B, G0/G1 phase (BrdU negative staining) normal fibroblasts displayed robust recruitment of RIF1 as early as 10min after Dox treatment. This recruitment then further increased over time and peaked at 2h after Dox treatment. On the other hand, a comparable recruitment of RIF1 did not start in G0/G1 phase HGPS fibroblasts until two hours later (Figure 4-6), indicating a significant delay of NHEJ in HGPS fibroblasts during the G0/G1 phase.

In Chapter III, I revealed an over-activation of NHEJ in HGPS SMCs during S/G2 phase, which resulted in chromosome relocation and cell death (Figure 3-13 – 3-14). To further explore this phenotype, I examined the recruitment dynamics of RIF1 during S/G2 phase after Dox treatment. As shown in Figure 4-7, HGPS fibroblasts displayed a gradual formation of RIF1 foci in S/G2 phase after Dox treatment. These RIF1 recruitments were comparable to those in normal fibroblasts at every tested time points, indicating an active NHEJ in HGPS fibroblasts during S/G2 phase.

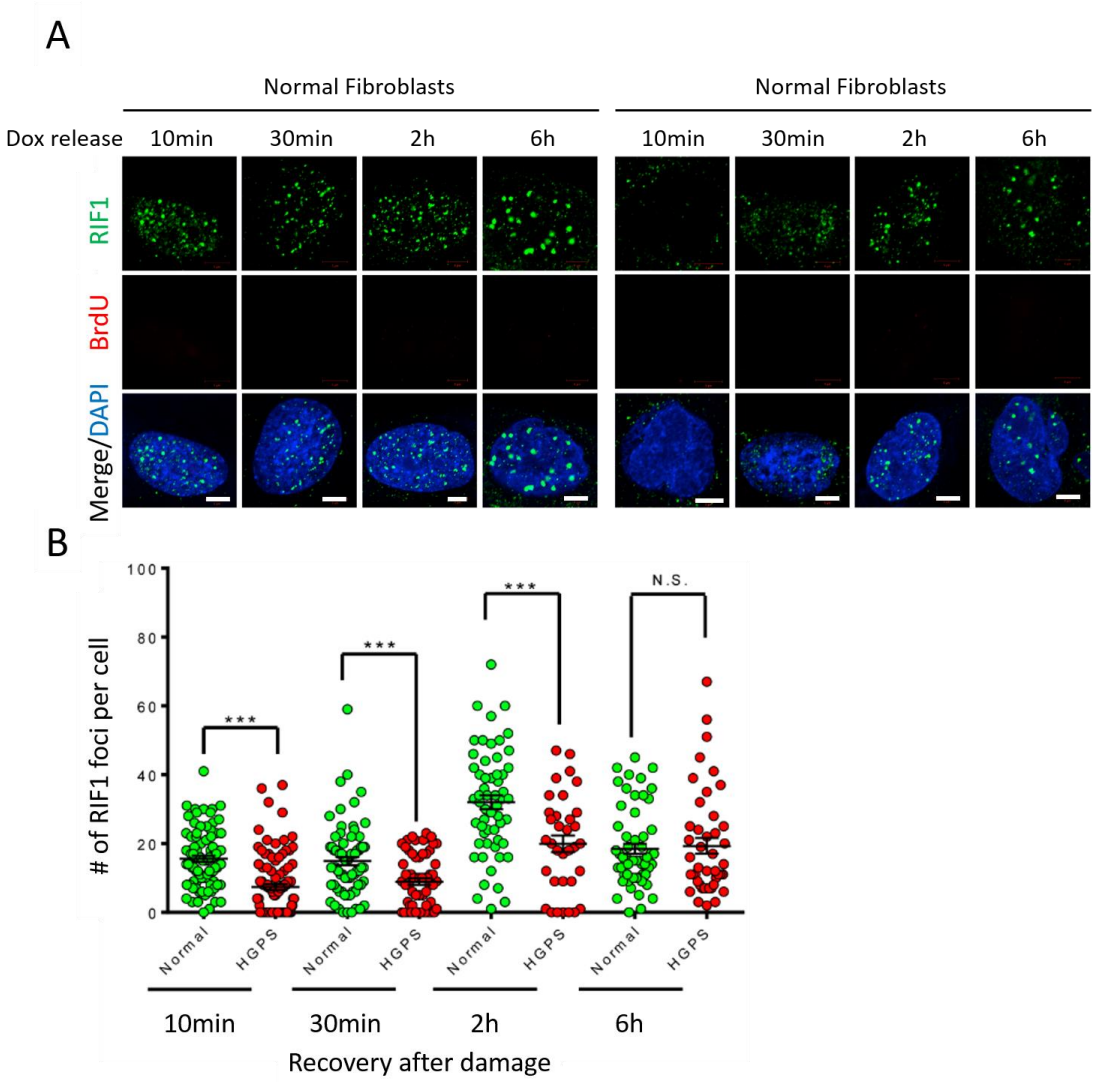

Figure 4-6: NHEJ is impaired in G0/G1 phase HGPS fibroblasts. (A). Representative image showing immunofluorescence staining with anti-BrdU and RIF1 antibodies on normal and HGPS fibroblasts recovered for various amounts of time after 1μM Dox treatment. (Scale bar, 5 μm.). (B). Quantification of (A) showing the number of RIF1 foci per nuclei in normal and HGPS fibroblasts.

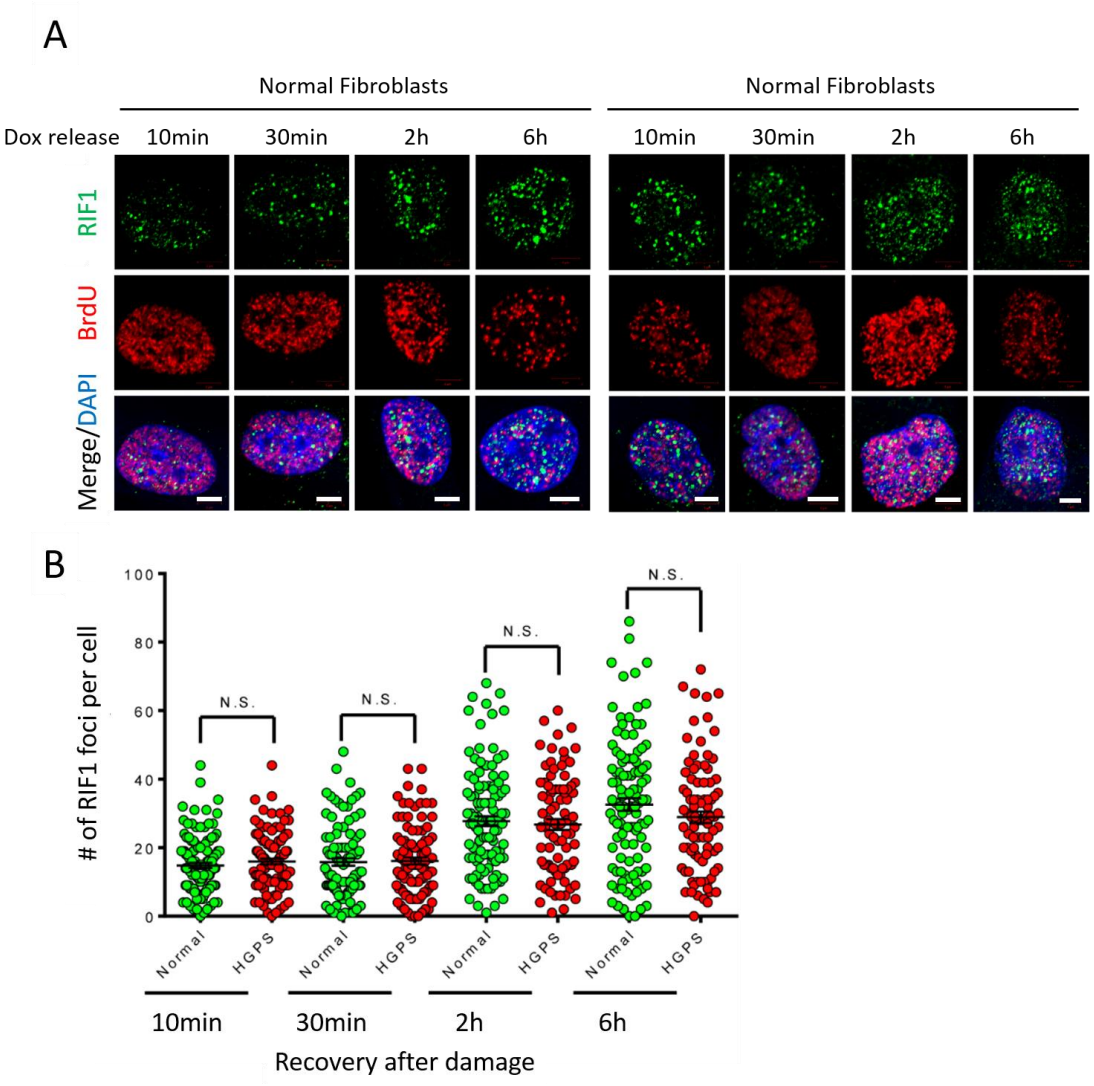

Figure 4-7: NHEJ is active in S/G2 phase HGPS fibroblasts. (A). Representative image showing immunofluorescence staining with anti-BrdU and RIF1 antibodies on normal and HGPS fibroblasts recovered for various amounts of time after 1μM Dox treatment. (Scale bar, 5 μm.). (B). Quantification of (A) showing the number of RIF1 foci per nuclei in normal and HGPS fibroblasts.

4.3 Discussion

4.3.1 Mis-regulated NHEJ and HR throughout the cell cycle in HGPS.

A proper cell cycle dependent activation of NHEJ and HR is a critical to maintain genome integrity and cellular homeostasis (Branzei and Foiani, 2008; Chapman et al., 2012; Escribano-Diaz et al., 2013; Takata et al., 1998). Deficiencies in NHEJ or HR increase cellular IR sensitivity during G0/G1 or S/G2 phase respectively (Branzei and Foiani, 2008). Significantly, mis-regulation of the NHEJ and HR pathway has been proposed to contribute to the premature aging and other defective phenotypes in HGPS animal models (Krishnan et al., 2011; Liu et al., 2005; Liu et al., 2013a; Liu et al., 2013b). In agreement with these reports, in the previous chapter, I demonstrated that deficient HR and over-activated NHEJ is responsible for the cell death phenotype in iPSC driven HGPS SMCs (Zhang et al., 2014). To portrait a comprehensive cell cycle dependent activation pattern of NHEJ and HR in HGPS, I introduced DSBs in BrdU labeled HGPS fibroblasts and measured NHEJ and HR using RIF1 and BRCA1/Rad51 as indicators respectively. My results demonstrated that HR is completely inactive in G0/G1 phase and significantly impaired in S/G2 phase HGPS fibroblasts. As for NHEJ, I found it to be drastically impaired in G0/G1 phase, but completely unaffected in S/G2 phase HGPS fibroblasts. These changes are illustrated in Figure 4-8.

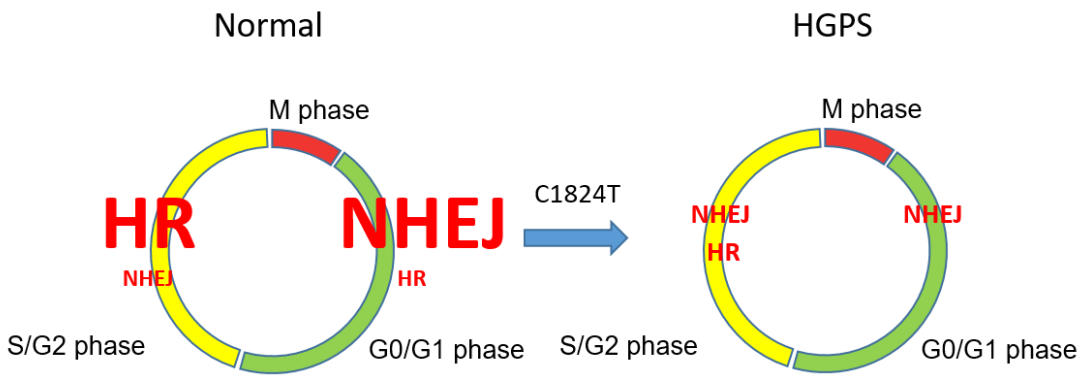

Figure 4-8: Scheme of the cell cycle dependent activation of NHEJ and HR in normal and HGPS cells. In normal cells, NHEJ is predominantly activated in G0/G1 phase with a slight activity in S/G2 phase while HR is mostly active in S/G2 phase. In HGPS, NHEJ is significantly impaired in G0/G1 phase and active in S/G2 phase. HGPS HR is also significantly impaired in S/G2 phase and completely undetectable in G0/G1 phase. The efficiencies of NHEJ in S/G2 phase HGPS cells are cell type dependent. HGPS SMCs display over activated NHEJ during S/G2 phase while S/G2 phase HGPS fibroblasts display comparable NHEJ efficiency to that in normal.

4.3.2 Mis-regulated NHEJ and HR induce various cellular defects in HGPS.

HR deficiency during S/G2 phase is particularly toxic to cellular homeostasis, as it allows the error prone NHEJ to fix DSBs and increases the frequency of chromosome breaks and relocation (Bunting et al., 2010; Cao et al., 2009; Patel et al., 2011). Consequently, aberrant chromosome structure may trigger a mechanism termed mitotic catastrophe and result in mitotic cell death (Castedo et al., 2004; Imreh et al., 2011; Vakifahmetoglu et al., 2008). This mechanism provides a plausible explanation for the cell death phenotype in HGPS SMCs (Zhang et al., 2014). Interestingly, the activity of NHEJ in S/G2 phase HGPS fibroblasts seems to be weaker than that in HGPS SMCs, since HGPS SMCs displayed significantly stronger NHEJ activity than corresponding normal SMCs whereas HGPS fibroblasts only exhibited a similar NHEJ activation to the normal control. This differential NHEJ

activation during S/G2 phase might explain the differential severity of cell death between HGPS SMCs and HGPS fibroblasts. Defective NHEJ during G0/G1 phase is also problematic, as unfixed DSBs triggers sustained DNA damage response (DDR), which results in either apoptosis or cellular senescence (Chen et al., 2007; Jackson, 2002; Robles and Adami, 1998).

The molecular mechanism underlying HGPS NHEJ and HR disruption remains unclear. My preliminary study revealed that both BRCA1 and Rad51 were significantly down-regulated in HGPS fibroblasts, pointing out a potential mechanism that could contribute to HGPS HR deficiency. However, whether this down-regulation is the only cause and how progerin induces such down-regulation remains to be uncovered. As for NHEJ, previous reports proposed that abnormal histone modifications and compact chromatin conformation serves as a barrier preventing the NHEJ regulator 53BP1 from loading to the damaged DNA lesion (Krishnan et al., 2011; Liu et al., 2012; Liu et al., 2005; Liu et al., 2013a; Liu et al., 2013b). Direct evidence that determines the role of progerin in NHEJ deficiency is still missing.

Chapter V: Reduced ATM and γH2AX DDR signals delay NHEJ in G0/G1 phase HGPS fibroblasts

5.1 Introduction

Defective DNA damage response (DDR) has been closely associated with genome instability and premature aging (Lombard et al., 2005). Abnormal DDR has been observed in HGPS fibroblast *in vitro* cultures and animal models (Krishnan et al., 2011; Liu et al., 2005; Zhang et al., 2014). Specifically, in response to ionized irradiation, the recruitments of 53BP1 and Rad51, were significantly delayed in those cells, supporting compromised NHEJ and HR DSB repair pathways (Krishnan et al., 2011; Liu et al., 2005; Zhang et al., 2014). I also observed a drastic delay in Rad51 recruitment to DSBs in HGPS iPSC-differentiated smooth muscle cells, suggesting that the defective HR is a universal phenotype associated with multiple HGPS lineages (see Chapter III). Moreover, ectopic expression of progerin in HeLa cells also significantly impaired 53BP1 recruitment to DSBs and a direct inhibitory role of progerin in DNA damage repair was suggested (Manju et al., 2006).

In the previous chapter, I characterized the efficiencies of NHEJ and HR at different cell cycle phases, using RIF1 and BRCA1/Rad51 as indicators respectively. Specifically, I revealed that NHEJ was impaired in G0/G1 phase, but still functional in S/G2 phase HGPS fibroblast. This finding is in accordance with previous reports that 53BP1 recruitment was delayed in unsynchronized HGPS fibroblasts upon ionized irradiation (Krishnan et al., 2011; Liu et al., 2005). Although tremendous efforts have been spent to understand this phenotype, the underlying molecular mechanism remains largely unknown.

In this chapter, I aim to elucidate a molecular mechanism to explain the NHEJ deficiency in HGPS cells. As discussed in 1.4.6, phosphorylation of the histone H2A

variant H2AX at Serine 139 (γH2AX) is a crucial histone modification that occurs very rapidly at DSBs (Kinner et al., 2008; Mah et al., 2010). As an upstream DDR signal, γH2AX plays an essential role in initiating NHEJ DSB repair pathways (Mah et al., 2010). In a previous study, embryonic stem cells from H2AX deficient ($H2AX^{\Delta/\Delta}$) mice displayed a delayed recruitment of DNA damage repair players, elevated sensitivity to ionizing irradiation and compromised genome integrity (Bassing et al., 2002). Mechanistically, H2AX phosphorylation was believed to recruit several down-stream DNA damage repair proteins including NBS1, MDC1, 53BP1 and BRCA1 to the DSB site to fix DSBs (Bassing et al., 2002; Chapman and Jackson, 2008; Paull et al., 2000). Three kinases, ATM, ATR or DNAPK have been shown to carry out the phosphorylation of H2AX at DSBs (Burma et al., 2001; Kinner et al., 2008; Stiff et al., 2004; Ward and Chen, 2001). In addition, ATM kinase can mediate phosphorylation of adjacent H2AX, thereby amplifying γH2AX signals and creating a positive feedback loop (Falck et al., 2005; Kinner et al., 2008; You et al., 2005). γH2AX was also reported to facilitate DSB end joining by anchoring DNA break ends in close proximities and reducing chromosome density (Banath et al., 2004; Bassing and Alt, 2004; Bouquet et al., 2006; Kinner et al., 2008; Mah et al., 2010; Xie et al., 2004). Given such importance of H2AX phosphorylation in DNA damage repair, I identify γH2AX signaling as a target to study NHEJ deficiency in HGPS.

Here I report a reduction in γH2AX signal strength in HGPS fibroblasts upon treatment with Doxorubicin (Dox), a DSB inducing agent. Interestingly, this phenotype is predominantly observed in G0/G1 phase cells but not in S phase HGPS

cells, consistent with their NHEJ deficiency pattern. A similar reduction in γH2AX response is also observed in G0/G1 phase HGPS cells upon treatment with Camptothecin (CPT), a different DSB inducing agent. The reduced amplification of γH2AX signals consequently leads to a delay in NHEJ player recruitment and DSB repair. Furthermore, ATM activation is found to be impaired in HGPS fibroblasts upon DSBs. Finally, I show evidence supporting that the observed ATM inactivation in HGPS is closely correlated with the loss of H3K9me3 in HGPS fibroblasts. Restoration of H3K9me3 through treatment with methylene blue (MB), an anti-oxidant known to rescue HGPS heterochromatin loss, can restore ATM activation, γH2AX signal strength, and NHEJ in HGPS fibroblasts. My data identified γH2AX signal mis-regulation as an underlying molecular mechanism to explain NHEJ deficiency in HGPS and also suggested a novel connection between the two prominent phenotypes (H3K9me3 loss and NHEJ deficiency) and provides mechanistic insights underlying the complex phenotypes in HGPS cells.

5.2 Results

5.2.1 HGPS fibroblasts show reduced γH2AX responses upon Dox treatment.

To study γH2AX signals in HGPS, I first examined the basal number of γH2AX foci in primary HGPS and normal control fibroblasts by immunofluorescence staining. As shown in Figure 5-1A & B, HGPS fibroblasts showed a slight but significant increase in the number of γH2AX foci than the normal control (normal: 2.5±0.3 vs. HGPS: 4.6±0.7 foci/cell), which is consistent with previous reports that HGPS cells accumulated more DSBs (Liu et al., 2006; Liu et al., 2008; Musich and Zou, 2011). To further study γH2AX responses upon DSBs, I induced DSBs in HGPS and normal control fibroblasts by treating cells with Dox, a DNA damage-inducing agent that causes DSBs by inhibiting topoisomerase II (Kurz et al., 2004). Immunofluorescence staining and confocal microscopy analysis revealed that Dox treatment induced rapid and robust γH2AX responses in normal fibroblasts (Figure 5-2A). Notably, HGPS fibroblasts displayed significantly weaker γH2AX signals compared with normal cells (Figure 5-2A). Quantitative fluorescence analysis measuring the total fluorescence intensity of γH2AX further supported this reduction in HGPS (Figure 5-2B). Western blotting analysis showed that γH2AX responses were reduced in HGPS cells (Figure 5-2C & D), while total H2AX was unchanged (Figure 5-3), suggesting that the phenotype was due to a functional deficiency in phosphorylation instead of overall H2AX reduction.

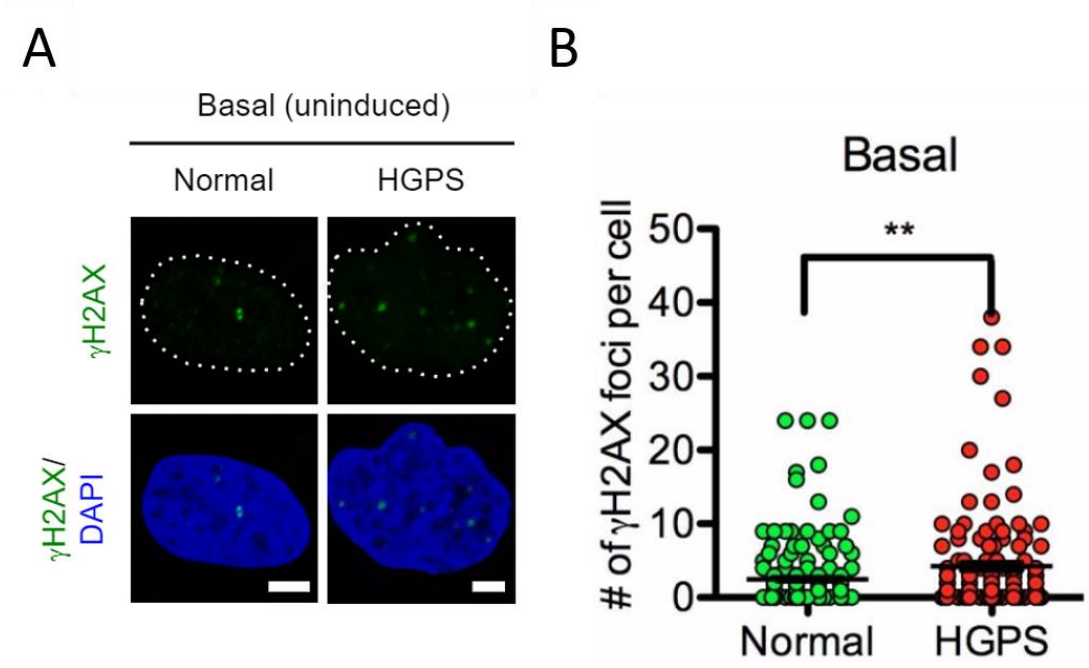

Figure 5-1: HGPS fibroblasts bear a slightly elevated basal level of γH2AX. Representative fluorescence images of basal γH2AX foci in normal and HGPS fibroblasts. Scale Bar: 5μm. Quantification of (A) showing the number of γH2AX foci in each nucleus in normal and HGPS fibroblasts at the basal level. More than 100 cells were randomly picked for quantification. Results were presented as mean ± SEM. **P < 0.01.

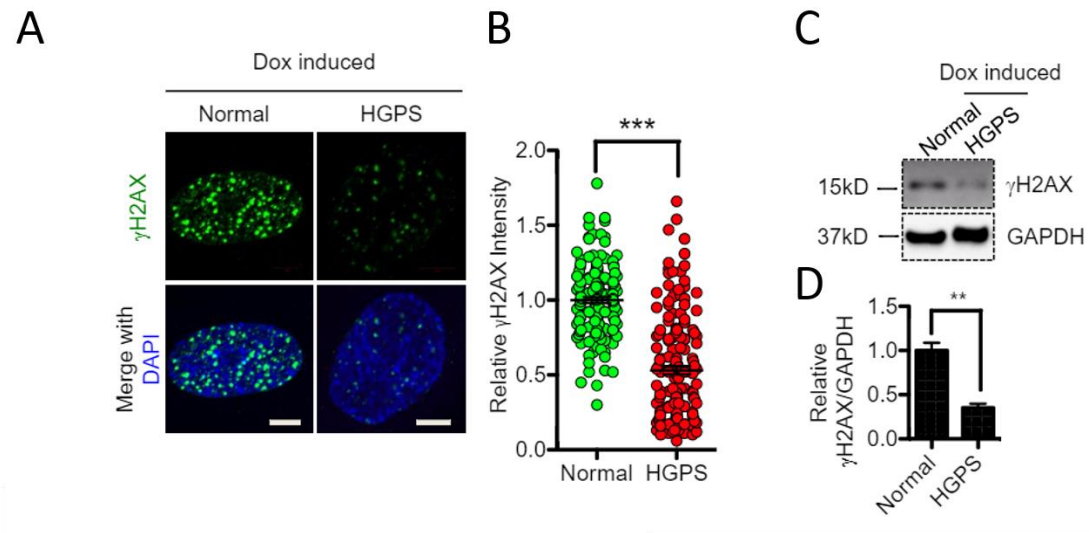

Figure 5-2: HGPS fibroblasts bear reduced γH2AX response upon Dox treatment. (A). Representative fluorescence images of γH2AX foci in normal and HGPS fibroblasts after Dox treatment. Scale Bar: 5μm. (B). Quantification of (A), showing relative γH2AX green fluorescence intensities in normal and HGPS fibroblasts after Dox treatment. More than 100 cells were randomly picked for quantification. Results were presented as mean ± SEM. ***P < 0.001. (C). Western blotting analysis with anti-γH2AX and anti-GAPDH antibodies on normal and HGPS fibroblasts after Dox treatment. (D). Quantification of (C), showing the relative γH2AX band intensity in normal and HGPS fibroblasts after Dox treatment (normalized to GAPDH). Three independent experiments were performed. Results were presented as mean ± SEM. **P < 0.01.

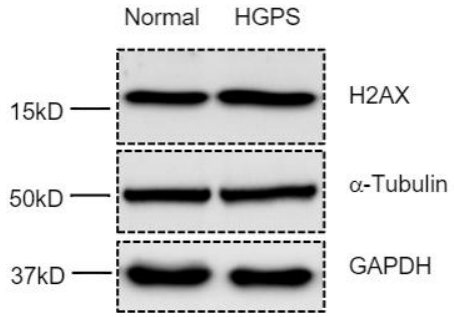

Figure 5-3: Total H2AX level is comparable between normal and HGPS fibroblasts.

I speculated that the reduction in γH2AX signals could potentially interfere with down-stream DNA damage repair in HGPS. To test this, HGPS and control fibroblasts were treated with 1μM Dox for an hour and allowed to recover for 10min, 30min, 2h, 6h, and 24h respectively. I then quantified the number of γH2AX foci per nuclei at each time point. As shown in Figure 5-4 A & B, in normal cells, the numbers of γH2AX foci decreased gradually over time, indicating successful repair of the DSBs induced by Dox treatment. In contrast, while HGPS cells displayed weaker γH2AX signals at the beginning (10 min), these signals stayed largely unfixed even after 24h. This observation was in agreement with a number of previous reports

describing defective DNA damage repair in HGPS (Krishnan et al., 2011; Liu et al., 2005; Liu et al., 2013a; Manju et al., 2006).

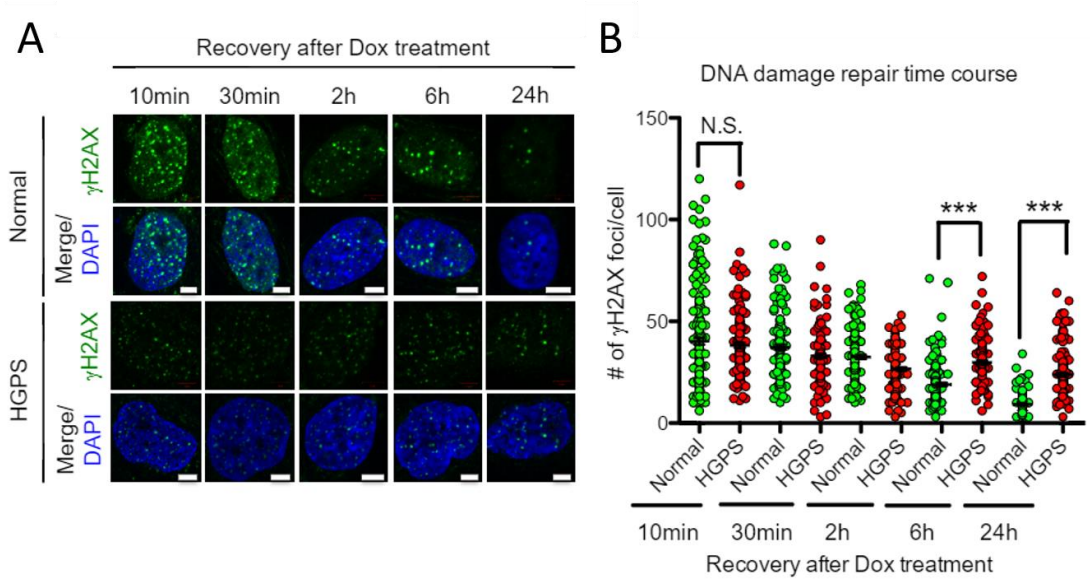

Figure 5-4: Reduced γH2AX response delays DNA damage repair in HGPS fibroblasts. (A). Representative fluorescence images of γH2AX foci in normal and HGPS fibroblasts that were allowed to recover for indicated amounts of time after Dox treatment. Scale Bar: 5μm. (B). Quantification of (E), showing the number of γH2AX foci in each nucleus at each time point. More than 100 cells were randomly picked for quantification. Results were presented as mean ± SEM. ***P < 0.001.

5.2.2 γH2AX reduction is predominantly observed in G0/G1 phase HGPS fibroblasts.

In Chapter IV, I revealed that NHEJ was delayed in G0/G1 but not in S/G2 phase HGPS fibroblasts. I next wondered whether the HGPS γH2AX signal reduction followed this pattern. To investigate the γH2AX signal reduction phenotype in HGPS during the cell cycle, I labeled S/G2 phase cells with BrdU for 30min and then examined γH2AX signals in response to Dox treatment by immunofluorescence

staining. I found that the BrdU-negative, G0/G1 phase HGPS fibroblasts displayed a significant reduction in γH2AX staining (Figure 5-5A & B left panel). To my surprise, the BrdU-positive, S/G2 phase HGPS fibroblasts showed a similar level of γH2AX signals as normal control cells (Figure 5-5A & B right panel). To further verify the phenotype in G0/G1 phase, I synchronized normal and HGPS fibroblasts to the G0/G1 phase using serum starvation. Western blotting study revealed that γH2AX was significantly weaker in these G0/G1 synchronized HGPS fibroblasts, compared to that in the normal control cells (Figure 5-5C). Taken together, these data suggest that the reduction in γH2AX responses mainly takes place during G0/G1 phase but not S/G2 phase in HGPS cells. This is in agreement with the NHEJ mis-regulation pattern in HGPS.

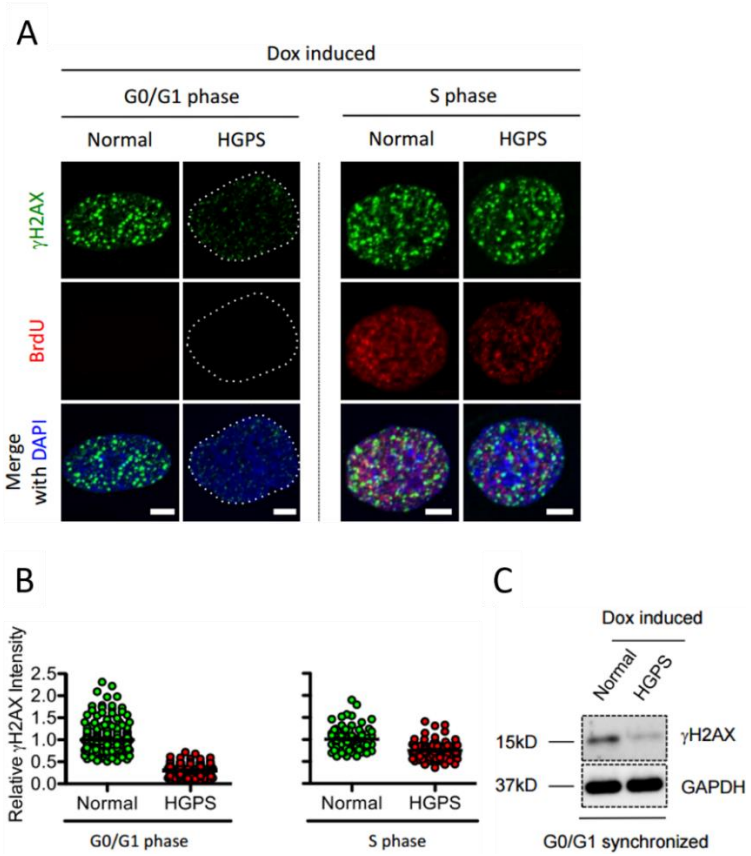

Figure 5-5: Reduction of γH2AX response is cell cycle dependent in HGPS fibroblasts. (A). Representative fluorescence images of γH2AX foci and BrdU staining in normal and HGPS fibroblasts after Dox treatment. G0/G1 and S phase were indicated by BrdU negative and positive staining respectively. Scale Bar: 5μm. (B). Quantification of (A), showing relative γH2AX green fluorescence intensity. More than 40 cells were counted for each group. Results were presented as mean ± SEM. (CN). Western blotting analysis with anti-γH2AX and anti-GAPDH antibodies on serum starvation synchronized normal and HGPS fibroblasts after Dox treatment.

5.2.3 The amplification of γH2AX signal is reduced in G0/G1 phase HGPS fibroblasts.

The reduction in γH2AX signaling could be caused by either fewer number of γH2AX foci or reduced intensities of individual foci. To distinguish between these two possibilities, I synchronized normal and HGPS fibroblasts to G0/G1 phase and quantified the number and the fluorescence intensity of γH2AX foci after Dox treatment. My analysis showed that HGPS and normal control fibroblasts had comparable γH2AX foci counts (normal: 40±1.6 vs. HGPS: 38±1.2), suggesting that similar numbers of DSBs were induced by Dox treatment in HGPS and normal cells. The result further implicated that the initial phosphorylation of H2AX at DSBs was unaffected in HGPS. On the other hand, the γH2AX signal amplification was disturbed in HGPS as reflected by reduced size and fluorescence intensity of individual foci (Figure 5-6A). Line-profile analysis and quantification of the average γH2AX foci intensity confirmed this observation (Figure 5-6B & C). To rule out the possibility that this phenotype was only specific to Dox-induced DSBs, I treated synchronized G0/G1 phase HGPS and normal control fibroblasts with Camptothecin (CPT), a distinct DSB inducing agent which created DSBs by inhibiting

topoisomerase I. Upon CPT treatment, HGPS and normal cells showed comparable γH2AX foci counts (normal: 18±0.6 vs. HGPS: 21±0.9). Consistent with Dox, CPT treatment induced significantly weaker γH2AX foci in HGPS G0/G1 phase fibroblasts (Figure 5-6D-F). These reductions upon either Dox or CPT treatment were further validated by western blotting analysis (Figure 5-6G). Together, these experiments suggested that it was not the initiation, but the amplification of γH2AX signaling upon DSBs that was affected in G0/G1 phase HGPS cells.

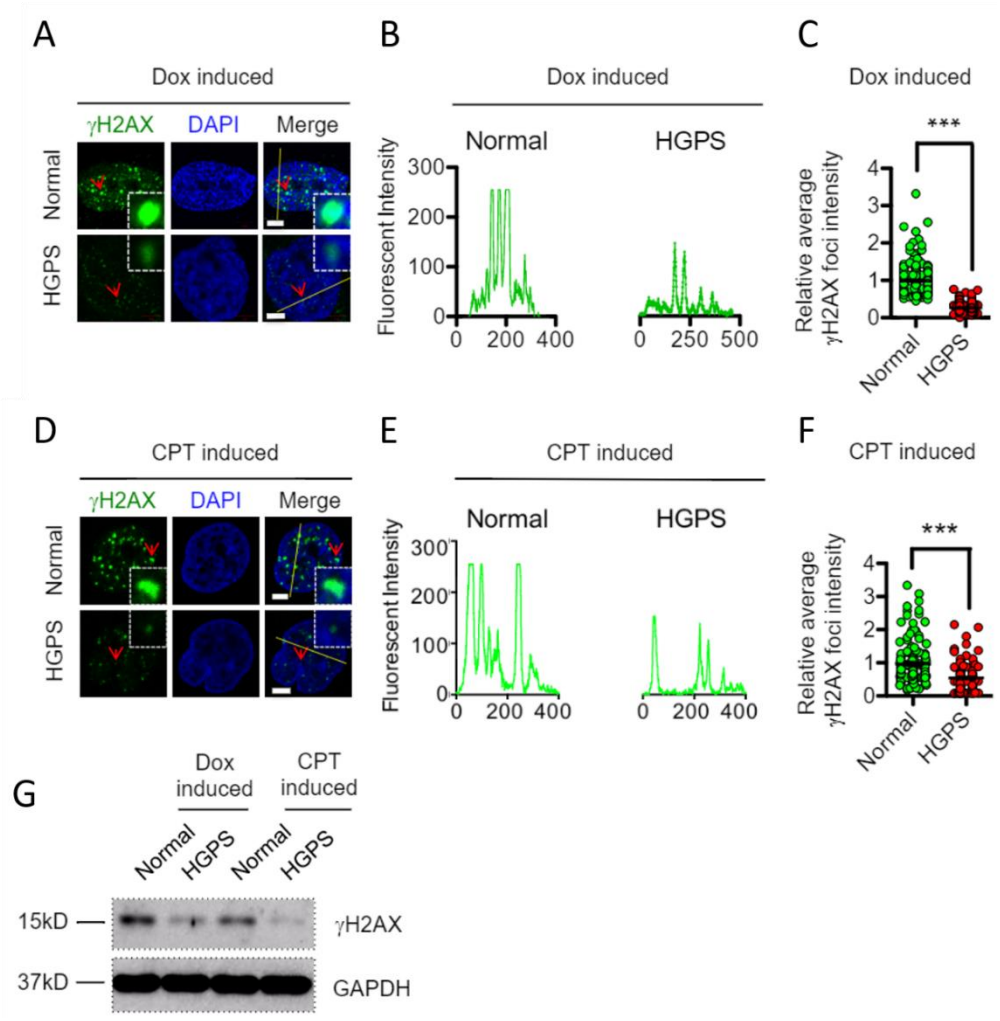

Figure 5-6: The amplification of γH2AX signal is reduced in G0/G1 phase HGPS cells after Dox and CPT treatment. (A). Representative fluorescence images of γH2AX foci in serum starvation synchronized normal and HGPS fibroblasts after Dox treatment. Arrow points to the single γH2AX foci in the enlarged square. Scale Bar: 5μm. (B). Line profile analysis of (A), showing the reduced γH2AX foci fluorescence strength in HGPS fibroblasts after Dox treatment. Green fluorescence intensity (y axis) was plotted against distance (x axis) along the yellow line in (A). (C). γH2AX foci intensity analysis of (A). Each dot represents the average fluorescence intensity of individual γH2AX foci in a single nucleus. More than 100 cells were randomly picked for quantification. Results were presented as mean ± SEM. ***P < 0.001. (D). Representative fluorescence images of γH2AX foci in serum starvation synchronized normal and HGPS fibroblasts after CPT treatment. Arrow points to the single γH2AX foci in the enlarged square. Scale Bar: 5μm. (E). Line profile analysis of (D), showing the reduced γH2AX foci fluorescence strength in HGPS fibroblasts after CPT treatment. Green fluorescence intensity (y axis) was plotted against distance (x axis) along the yellow line in (D). (F). γH2AX foci intensity analysis of (D). Each dot represents the average fluorescence intensity of individual γH2AX foci in a single nucleus. More than 100 cells were randomly picked for quantification. Results were presented as mean ± SEM. ***P < 0.001. (G). Western blotting analysis with anti-γH2AX and anti-GAPDH antibodies on serum starvation synchronized normal and HGPS fibroblasts after Dox or CPT treatment.

5.2.4 Weakened γH2AX leads to a delayed recruitment of non-homologous end joining factors in G0/G1 HGPS cells.

Non-homologous end joining (NHEJ) is the predominant DSB repair pathway in G0/G1 phase (Bassing et al., 2002; Chapman et al., 2012; Felgentreff et al., 2014; Mao et al., 2008; Zhang et al., 2014). To investigate the effect of the impaired γH2AX signal amplification on NHEJ pathway, I examined the recruitment of RIF1, an NHEJ specific promoting protein. Co-localization analysis indicated that in normal cells, RIF1 was efficiently loaded onto DSBs and co-localized with strong γH2AX foci (Figure 5-7A). Line-profile analysis confirmed this co-localization (Figure 5-7B). In contrast, HGPS fibroblasts didn't show an apparent recruitment of RIF1 to DSBs,

despite the presence of weak γH2AX foci (Figure 5-7A & B). Notably, RIF1 protein level was unchanged in HGPS fibroblasts (Figure 5-8). Therefore, this delay was a functional deficiency instead of a decrease in protein amount.

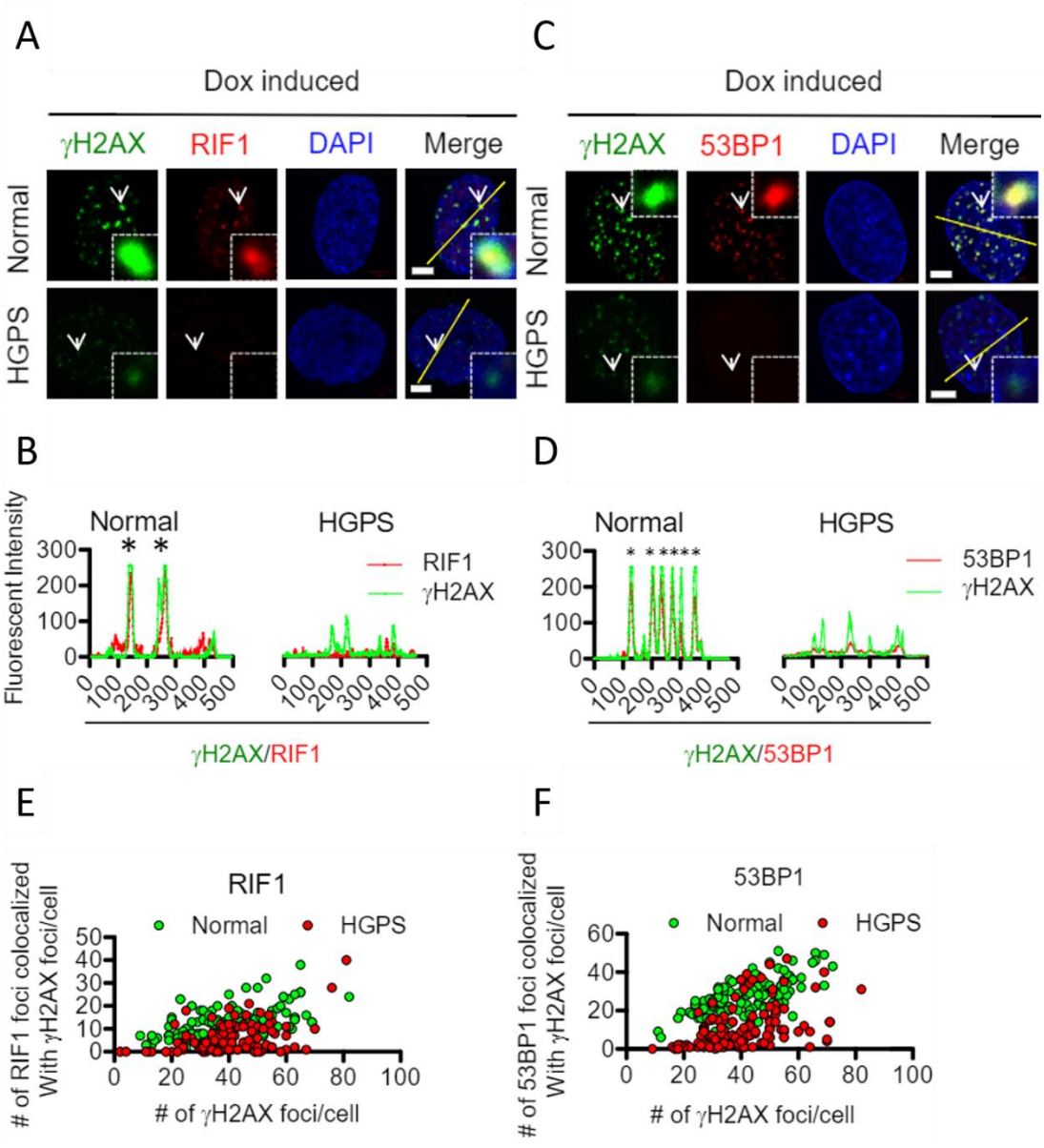

Figure 5-7: Weakened γH2AX leads to a delayed recruitment of non-homologous end joining (NHEJ) factors in G0/G1 HGPS cells. (A). Representative fluorescence images of γH2AX foci and RIF1 foci in serum starvation synchronized normal and HGPS fibroblasts after Dox treatment. Arrow points to the single γH2AX or RIF1 foci in the enlarged square. Scale Bar: 5μm. (B). Line profile analysis of (A), showing the reduced recruitment of RIF1 to γH2AX foci in HGPS fibroblasts. Green (γH2AX) and red (RIF1) fluorescence intensities (y axis) were plotted against distance (x axis) along the yellow line in (A). Stars indicated strong co-localization of RIF1 and γH2AX. (C). Representative fluorescence images of γH2AX foci and 53BP1 foci in serum starvation synchronized normal and HGPS fibroblasts after Doxorubicin treatment. Arrow points to the single γH2AX or 53BP1 foci in the enlarged square. Scale Bar: 5μm. (D). Line profile analysis of (C), showing the reduced recruitment of 53BP1 to γH2AX foci in HGPS fibroblasts. Green (γH2AX) and red (53BP1) fluorescence intensities (y axis) were plotted against distance (x axis) along the yellow line in (C). Stars indicated strong co-localization of 53BP1 and γH2AX. (E). Quantification of (A), showing the number of γH2AX (x axis) foci and co-localized RIF1 (y axis) foci per nuclei in normal and HGPS fibroblasts after Dox treatment. More than 100 cells were randomly picked for quantification. (F). Quantification of (C), showing the number of γH2AX (x axis) foci and co-localized 53BP1 (y axis) foci per nuclei in normal and HGPS fibroblasts after Dox treatment. More than 100 cells were randomly picked for quantification.

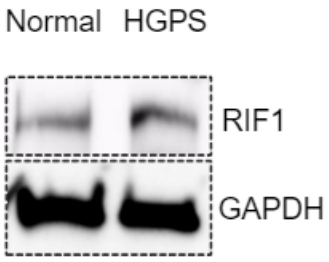

Figure 5-8: RIF1 protein level was comparable between normal and HGPS fibroblasts.

Similar to RIF1, 53BP1, an important NHEJ player upstream of RIF1 (Chapman et al., 2013; Escribano-Diaz et al., 2013; Zimmermann et al., 2013), was also found to be inefficiently recruited to γH2AX foci in HGPS G0/G1 phase cells (Figure 5-7C & D). This observation was in agreement with a previous report that 53BP1 recruitment was disrupted in H2AX deficient mouse embryonic stem cells (Ward et al., 2003).

Quantification indicated that at the same level of DNA damage, normal cells were able to recruit more RIF1 and 53BP1 to DSB sites than HGPS fibroblasts (Figure 5-7E & F). Collectively, these data suggest that compromised amplification of γH2AX signals upon DSBs affects the recruitment of NHEJ factors and delay DNA damage repair in G0/G1 phase HGPS fibroblasts.

5.2.5 γH2AX reduction is associated with defective ATM activation in HGPS.

Three types of kinases (ATM, ATR and DNAPK) have been previously reported to phosphorylate H2AX upon DSBs (Burma et al., 2001; Kinner et al., 2008; Stiff et al., 2004; Ward and Chen, 2001). To determine which kinase mediates the phosphorylation of H2AX upon Dox treatment in G0/G1 cells, western blotting analysis was performed to examine the activation of these three kinases in G0/G1 synchronized normal and HGPS fibroblasts. Upon Dox treatment, ATM was activated in normal cells as shown by an increased amount of phosphorylated ATM (pATM, S1981) (Figure 5-9A & B) (Bakkenist and Kastan, 2003). In contrast, pATM was significantly weaker in HGPS fibroblasts after Dox treatment (Figure 5-9A & B). Dosage-dependent Dox treatment further confirmed this difference between normal and HGPS fibroblasts (Figure 5-9C). These results were in agreement with a previous report that Zmpste24 deficient mouse embryonic fibroblasts (a progeroid like MEF that mimics HGPS) exhibited lower ATM activation upon ionized irradiation (Liu et al., 2013a). Interestingly, the level of total ATM seemed to be reduced in HGPS cells (Figure 5-9A & C). This down-regulation of protein amount could potentially contribute to the reduced pATM. However, the ratio between pATM and total ATM

was still significantly lower in HGPS cells, implying additional mechanisms to impede ATM activation upon Dox treatment (Figure 5-9B). In contrast to ATM activation, I didn't detect observable activation of the other two kinases: ATR and DNAPK, upon Dox treatment (Figure 5-9D & E) (Chan et al., 2002; Zhao and Piwnica-Worms, 2001).

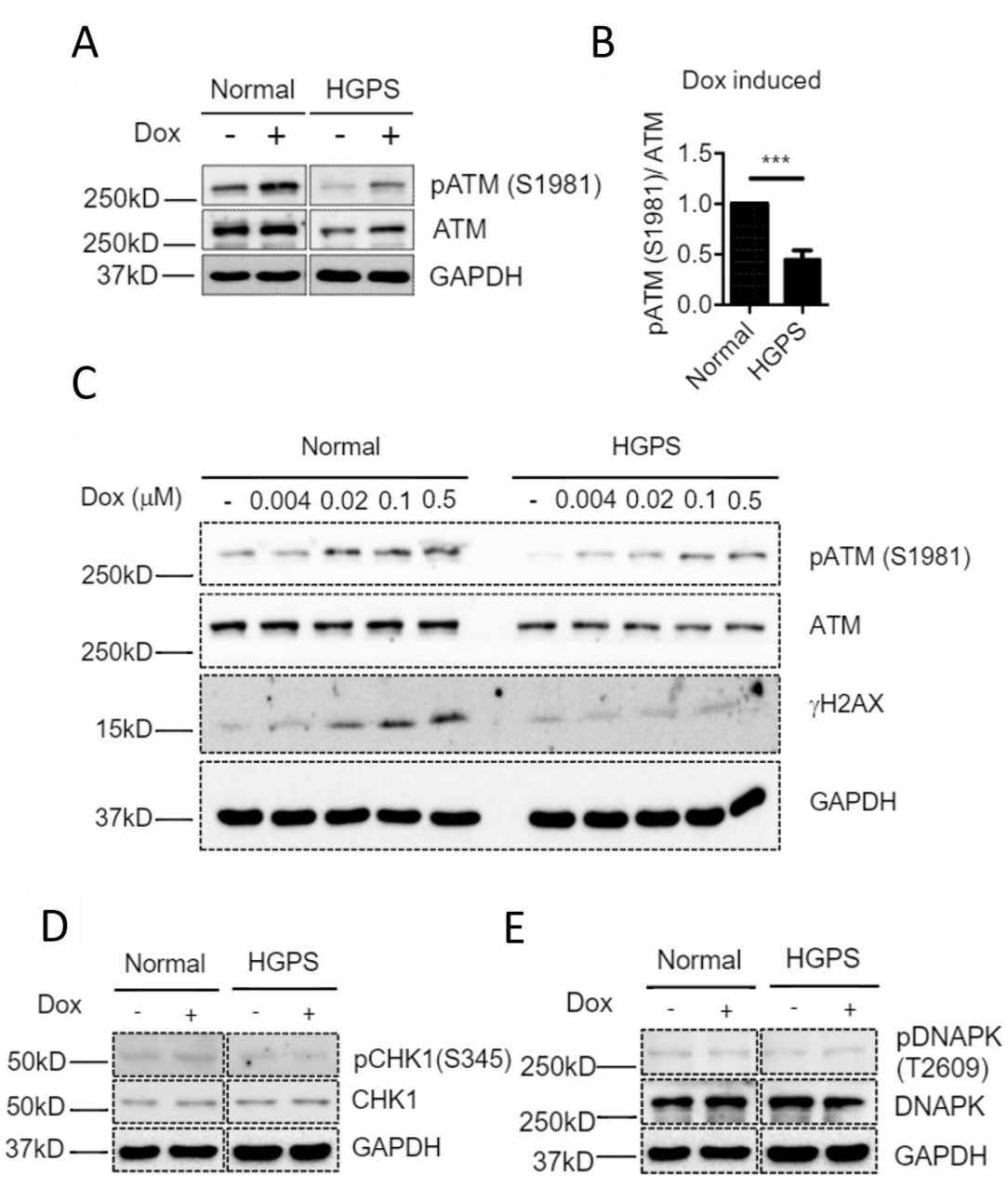

Figure 5-9: γH2AX signal reduction was caused by defective ATM activation in HGPS. (A). Western blotting analysis with anti-pATM(S1981), anti-ATM and anti-GAPDH antibodies on serum starvation synchronized normal and HGPS fibroblasts with or without Dox treatment. ATM activation was indicated by phosphorylated ATM(S1981). (B). Quantification of relative pATM(S1981) band intensity (normalized to total ATM) in normal and HGPS fibroblasts after Dox treatment. Five independent experiments were performed. Results were presented as mean ± SEM. ***P < 0.001. (C). Western blotting analysis with anti-pATM(S1981), anti-ATM, anti-γH2AX and anti-GAPDH antibodies in normal and HGPS fibroblasts treated with indicated concentrations of Dox. (D). Western blotting analysis with anti-pCHK1(S345), anti-CHK1 and anti-GAPDH antibodies on normal and HGPS fibroblasts after Dox treatment. ATR activation was indicated by phosphorylation of CHK1(S345). (E). Western blotting analysis with anti-pDNAPK(T2609), anti-DNAPK and anti-GAPDH antibodies on normal and HGPS fibroblasts after Dox treatment. DNAPK activation was indicated by phosphorylation of DNAPK(T2609).

Next, to directly assay whether the amplification of H2AX phosphorylation was dependent on ATM activation, I examined γH2AX responses in the presence of an ATM-specific inhibitor (KU-55933). As expected, incubation with the ATM inhibitor prior to Dox treatment led to a significant reduction in γH2AX signals in both normal and HGPS fibroblasts (Figure 5-10A). Quantification showed a gradual reduction of both pATM and γH2AX with increasing amounts of the ATM inhibitor (Figure 5-10B). Since γH2AX signals were crucial for 53BP1 recruitment at DSBs, I wondered whether ATM inhibitor could directly impair 53BP1 recruitment. Notably, normal fibroblasts treated with ATM inhibitor showed a significantly reduced recruitment of 53BP1 to DSBs compared to non-treated control (non-treated: 84% vs. ATM inhibitor: 27%, showing more than five 53BP1 foci/cell) (Figure 5-11A-C). These results were in agreement with previous reports that ATM activity was crucial for γH2AX signal amplification and 53BP1 recruitment (Hartlerode et al., 2015; Kurz et al., 2004).

Consistent with Figure 5-9D & E, I found that ATR and DNAPK inhibitors didn't have an impact on γH2AX signals (Figure 5-10C & D).

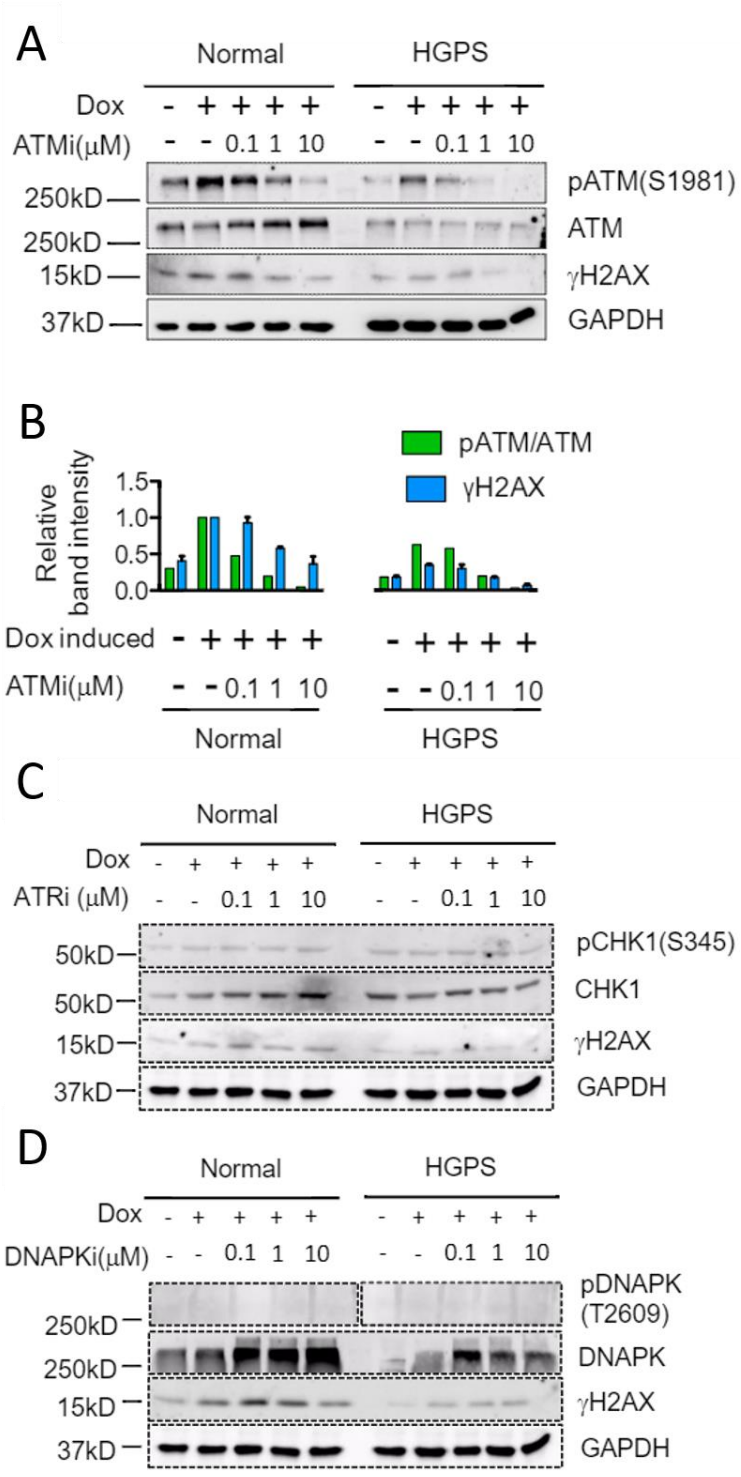

Figure 5-10: γH2AX signal reduction was caused by defective ATM activation in HGPS. (A). Western blotting analysis with anti-pATM(S1981), anti-ATM, anti-γH2AX and anti-GAPDH antibodies on serum starvation synchronized normal and HGPS fibroblasts. Cells were pre-incubated with ATM inhibitor at indicated concentrations for 24h prior to Dox treatment. (B). quantification of relative pATM(S1981) band intensity (normalized to total ATM) and relative γH2AX band intensity (normalized to GAPDH). (C). Western blotting analysis with anti-pCHK1(S345), anti-CHK1, anti-γH2AX and anti-GAPDH antibodies on normal and HGPS fibroblasts pre-incubated with indicated concentrations of ATR inhibitor for 24h prior to Dox treatment. (D). Western blotting with anti-pDNAPKcs1(T2609), anti-DNAPKcs, anti-γH2AX and anti-GAPDH antibodies on normal and HGPS fibroblasts pre-incubated with indicated concentrations of DNAPKcs inhibitor for 24h prior to Dox treatment.

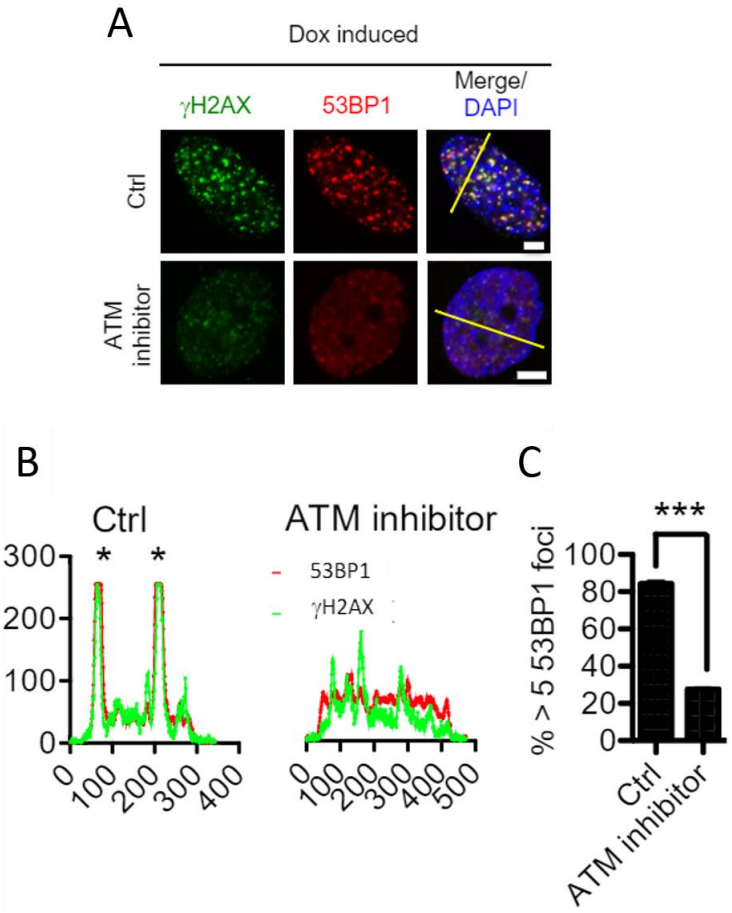

Figure 5-11: Inhibition of ATM impairs 53BP1 recruitment upon Dox treatment. (A). Representative fluorescence images of γH2AX and 53BP1 in normal fibroblasts pre-incubated with or without 10μM ATM specific inhibitor prior to Dox treatment. Scale Bar: 5μm. (B). Line profile analysis of (A), showing the reduced recruitment of 53BP1 to γH2AX foci in ATM inhibitor treated fibroblasts. Green (γH2AX) and red (53BP1) fluorescence intensities (y axis) were plotted against distance (x axis) along the yellow line in (A). Stars indicated strong co-localization of 53BP1 and γH2AX. (C). Quantification of the percentage of thr population that displayed more than five 53BP1 foci in control or ATM inhibitor treated fibroblasts. Results were presented as mean ± SEM. ***P < 0.001.

Furthermore, to understand why the γH2AX reduction in HGPS is G0/G1 phase specific, I checked the level of pATM in G0/G1 and S phase HGPS fibroblasts upon Dox treatment. As shown in Figure 5-12A & B, the immunofluorescence staining illustrated that ATM activation was significantly inhibited in G0/G1 phase but not in S phase HGPS fibroblasts, which was in high accordance with the observed differential levels of γH2AX and NHEJ activation in G0/G1 and S phases HGPS cells (Figure 5-5 – 5-7). Together, these results indicate that ATM activation is responsible for the amplification of γH2AX signals upon Dox treatment and that in G0/G1 phase HGPS cells, proper ATM activation was impaired.

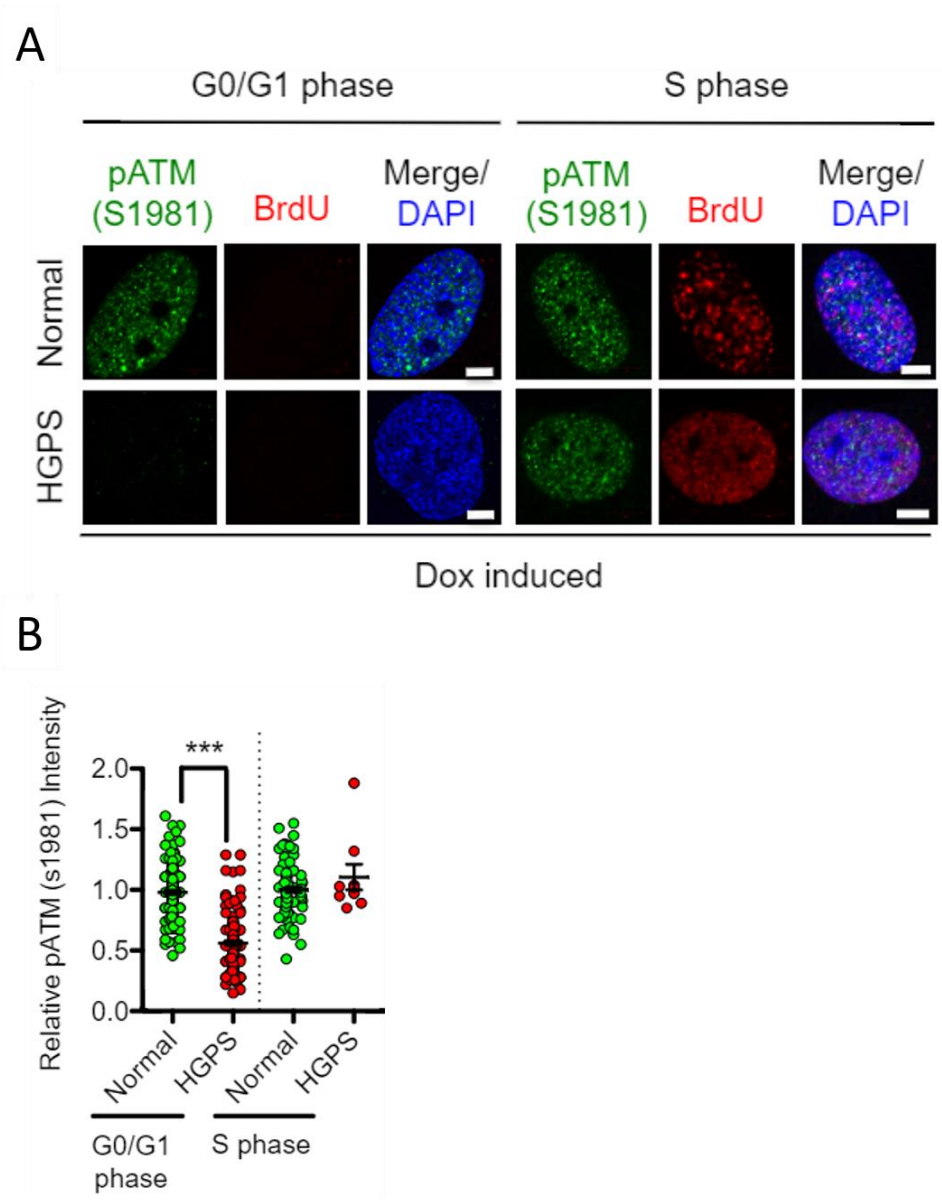

Figure 5-12: ATM activation defect is cell cycle dependent in HGPS fibroblasts. (A). Representative fluorescence images of pATM (S1981) and BrdU staining in normal and HGPS fibroblasts after Dox treatment. G0/G1 and S phase were indicated by BrdU negative and positive staining respectively. Scale Bar: 5μm. (B). Quantification of (A), showing relative pATM(S1981) green fluorescence intensity. More than 100 cells were randomly picked in each group for quantification except for S phase HGPS fibroblasts because very few S phase cells were found in that population. Results were presented as mean ± SEM. ***P < 0.001.

5.2.6 Loss of H3K9me3 contributes to impaired ATM activation in HGPS.

It has been recently shown that histone H3 trimethylated on lysine 9 (H3K9me3) was crucial for ATM activation (Ayrapetov et al., 2014; Sun et al., 2009), in particular, the removal of H3K9me3 by SUV39h1 depletion completely blocked ATM activation upon DSBs (Sun et al., 2009). It is worth mentioning that the trimethyl mark of H3K9 is diluted during replication in the S phase, and the newly synthesized histones become fully methylated only in the next G1 phase (Zee et al., 2012). In HGPS cells, a dramatic loss of H3K9me3 has been observed frequently (Kelley et al., 2011; McCord et al., 2013; Shumaker et al., 2006; Xiong et al., 2015). Based on this information, I hypothesized that loss of H3K9me3 in HGPS cells caused the consequent blockage of ATM activation, resulting in insufficient γH2AX signals at the DSBs and delayed DNA damage repair.

To test this hypothesis, I first examined the correlation between H3K9me3 and γH2AX signals in normal and HGPS cells. As shown in Figure 5-13A, I found that after Dox treatment cells with robust γH2AX responses almost always displayed decent H3K9me3 staining, and weak γH2AX staining was often observed in cells with decreased H3K9me3. Correlative analysis based on the fluorescence intensities of both indicated a significant positive correlation between H3K9me3 and γH2AX in both normal and HGPS fibroblasts (Figure 5-13B). It has been previously established that premature senescence, chromatin disorganization and epigenetic abnormalities (loss of H3K9me3 and H3K27me3) worsen in HGPS cells as progerin accumulated with increased cellular passages (McClintock et al., 2006; McCord et al., 2013; Rodriguez et al., 2009; Shumaker et al., 2006). I asked whether ATM activation and

H2AX phosphorylation also followed this pattern. To test this, I synchronized early, middle and late passage HGPS and normal control fibroblasts to G0/G1 phase, treated them with Dox and examined their levels of pATM and γH2AX. In agreement with the previous report, H3K9me3 level was high and similar to the controls at early passage, but became gradually reduced at middle and late passages (Figure 5-13C) (Shumaker et al., 2006). Moreover, both pATM and γH2AX signals displayed a similar pattern of deterioration in HGPS cells with increased cellular passages (Figure 5-13D & E). These results support my hypothesis that the loss of H3K9me3, a well-documented phenotype in HGPS cells, could play a role in blocking ATM activation and H2AX phosphorylation.

To provide some insights into the down-regulation of H3K9me3 in HGPS cells, I first examined SUV39h1, the methyltransferase that methylates H3K9. My analysis indicated that the expression of SUV39h1 was similar in normal and HGPS cells (Figure 5-13C), suggesting that the reduction in H3K9me3 might not be caused by a decrease in its methylation. I next measured heterochromatin protein 1α (HP1α), a heterochromatin binding protein that had been shown to play a crucial role in maintaining H3K9me3 (Zhang et al., 2015). Interestingly, HP1α displayed a passage dependent reduction in HGPS fibroblasts, suggesting that the down-regulation of HP1α might be responsible for H3K9me3 loss in HGPS (Figure 5-13C & E). Significantly, these reductions were accompanied by a passage dependent accumulation of progerin in HGPS, further supporting an inhibitory role of progerin in this pathway (Figure 5-14).

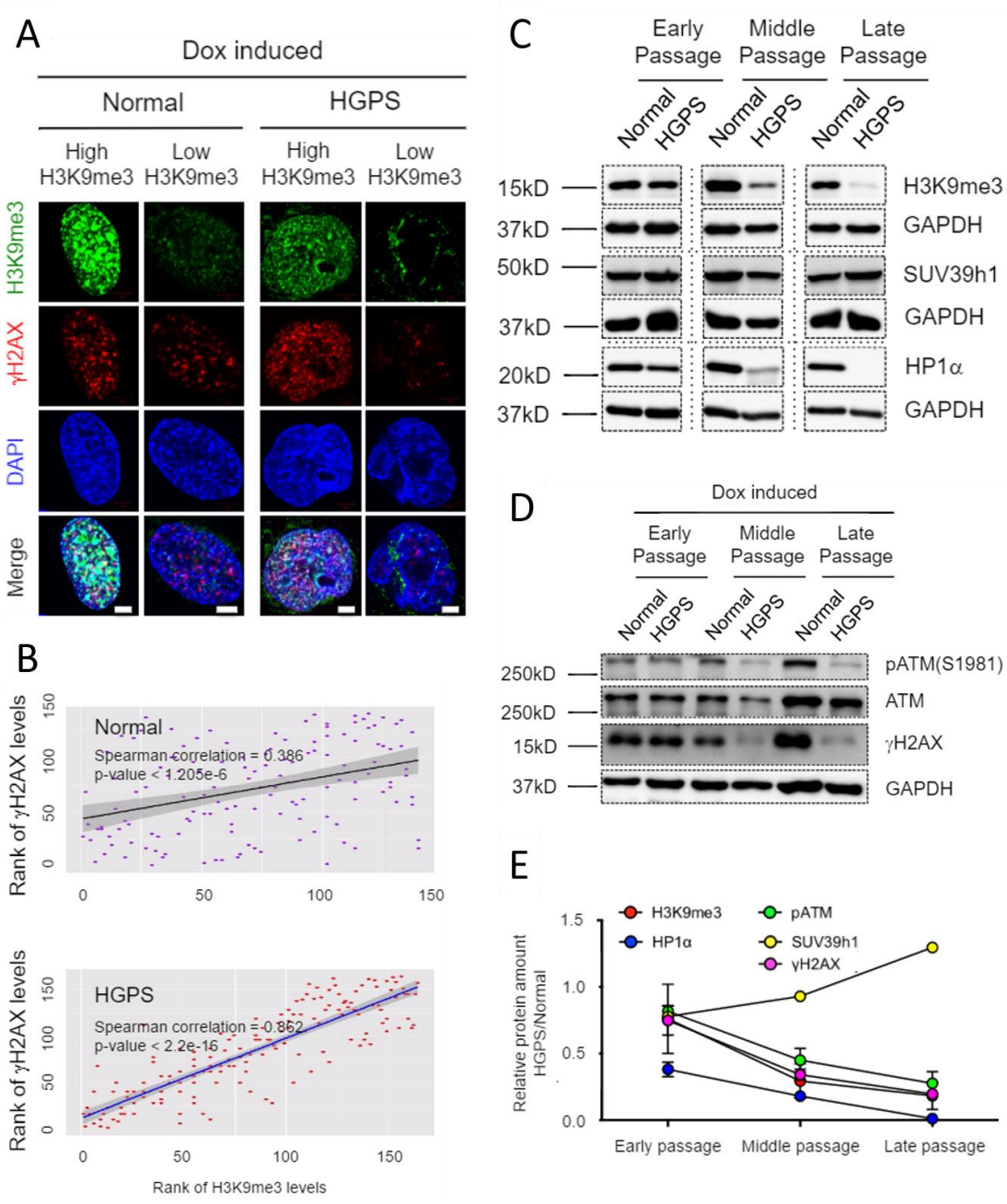
A
Dox induced
Normal
HGPS
High H3K9me3
Low H3K9me3
High H3K9me3
Low H3K9me3
H3K9me3
γH2AX
DAPI
Merge
B
Normal
Spearman correlation = 0.386
p-value < 1.205e-6
Rank of γH2AX levels
HGPS
Spearman correlation = 0.862
p-value < 2.2e-16
Rank of γH2AX levels
Rank of H3K9me3 levels
C
Early Passage
Middle Passage
Late Passage
Normal
HGPS
15kD
37kD
50kD
37kD
20kD
37kD
H3K9me3
GAPDH
SUV39h1
GAPDH
HP1α
GAPDH
D
Dox induced
Early Passage
Middle Passage
Late Passage
Normal
HGPS
250kD
250kD
15kD
37kD
pATM(S1981)
ATM
γH2AX
GAPDH
E
H3K9me3
HP1α
pATM
SUV39h1
γH2AX
Relative protein amount HGPS/Normal
Early passage
Middle passage
Late passage

Figure 5-13: Loss of H3K9me3 contributes to impaired ATM activation in HGPS. (A). Representative fluorescence images of γH2AX and H3K9me3 in normal and HGPS fibroblasts after Dox treatment. Scale Bar: 5μm. (B). Quantification of (A), showing the Spearman rank correlations between H3K9me3 green fluorescence intensity and γH2AX red fluorescence intensity in normal and HGPS fibroblasts. More than 100 cells were randomly picked for quantification in each group. (C). Western blotting analysis with anti-H3K9me3, anti-SUV39h1, anti-HP1α and anti-GAPHD antibodies on normal and HGPS fibroblasts at early, middle and late passages respectively. (D). Western blotting analysis with anti-pATM(S1981), anti-ATM, anti-γH2AX and anti-GAPDH antibodies on serum starvation synchronized normal and HGPS fibroblasts at early, middle and late passages after Dox treatment. (E). Quantification of (C) and (D), showing relative pATM(S1981) (normalized to ATM), γH2AX, H3K9me3, SUV39h1 and HP1α (normalized to GAPDH) band intensities in normal and HGPS fibroblasts at early, middle and late passages respectively.

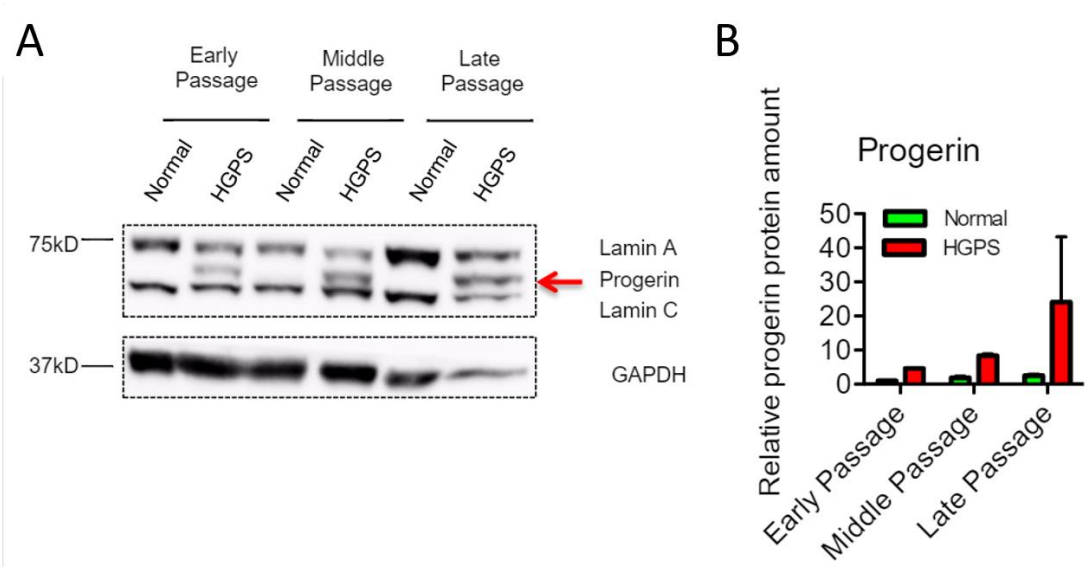

Figure 5-14: Progerin accumulates in HGPS fibroblasts with increased passage. (A). Western blotting analysis with anti-Lamin A/C and anti-GAPDH antibodies on normal and HGPS fibroblasts at early, middle and late passages, showing the passage dependent accumulation of progerin in HGPS. (B). Quantification of (A), showing the relative band intensity of progerin (normalized to GAPDH) in early, middle and late passage HGPS fibroblasts.

5.2.7 Methylene blue restores H3K9me3 and rescues ATM activation, γH2AX signaling, and NHEJ deficiency in HGPS fibroblasts.

Methylene blue (MB) has been previously shown by our group to enhance HP1α and H3K9me3 levels and rescue heterochromatin loss in HGPS fibroblasts (Xiong et al., 2015). Furthermore, MB treatment has been shown to maintain progerin level but increase its solubility in HGPS cells (Xiong et al., 2015). I were interested in examining whether MB treatment would be able to rescue the downstream defects of H3K9me3 loss, including the weakened ATM and H2AX phosphorylation and the delayed DNA damage repair in HGPS.

Normal and HGPS fibroblasts were treated with 100nM MB for 30 days and then tested for ATM and γH2AX response upon Dox treatment. As expected, after 30 days of treatment, MB significantly increased HP1α and H3K9me3 levels in HGPS G0/G1 phase fibroblasts (Figure 5-15A). Importantly pATM (S1981) and γH2AX responses were significantly restored in G0/G1 synchronized HGPS fibroblasts after MB treatment (Figure 5-15A). To test whether the up-regulation of γH2AX responses by MB was sufficient to overcome NHEJ deficiency in HGPS, I measured 53BP1 recruitment in MB treated HGPS fibroblasts. As shown in Figure 5-15B, 53BP1 was rapidly recruited to γH2AX foci, suggesting a functional NHEJ in HGPS after MB treatment. Line profile analysis also confirmed the co-localization between 53BP1 and γH2AX in MB treated HGPS fibroblasts (Figure 5-15C). Next, I investigated whether NHEJ efficiency was restored in HGPS after MB treatment by examining γH2AX foci turn over in MB treated normal and HGPS fibroblasts. As shown in Figure 5-15D & E, within 24h after Dox treatment, γH2AX foci count dropped

drastically from 44±1.7/cell to 16±0.7/cell in MB treated HGPS fibroblasts. In contrast, non-treated HGPS fibroblasts exhibited a significant delay in DNA damage repair as shown by retaining a substantial amount of γH2AX foci (31±1.1) after 24hours recovery (Figure 5-15E). In comparison, normal fibroblasts showed active NHEJ with/without MB treatment (24h after Dox treatment, -MB: 16±0.5 and +MB: 12±0.5) (Figure 5-15E). Taken together, these data provided additional support to my hypothesis that increasing H3K9me3 could promote ATM activation and γH2AX amplification and rescue NHEJ deficiency in HGPS cells.

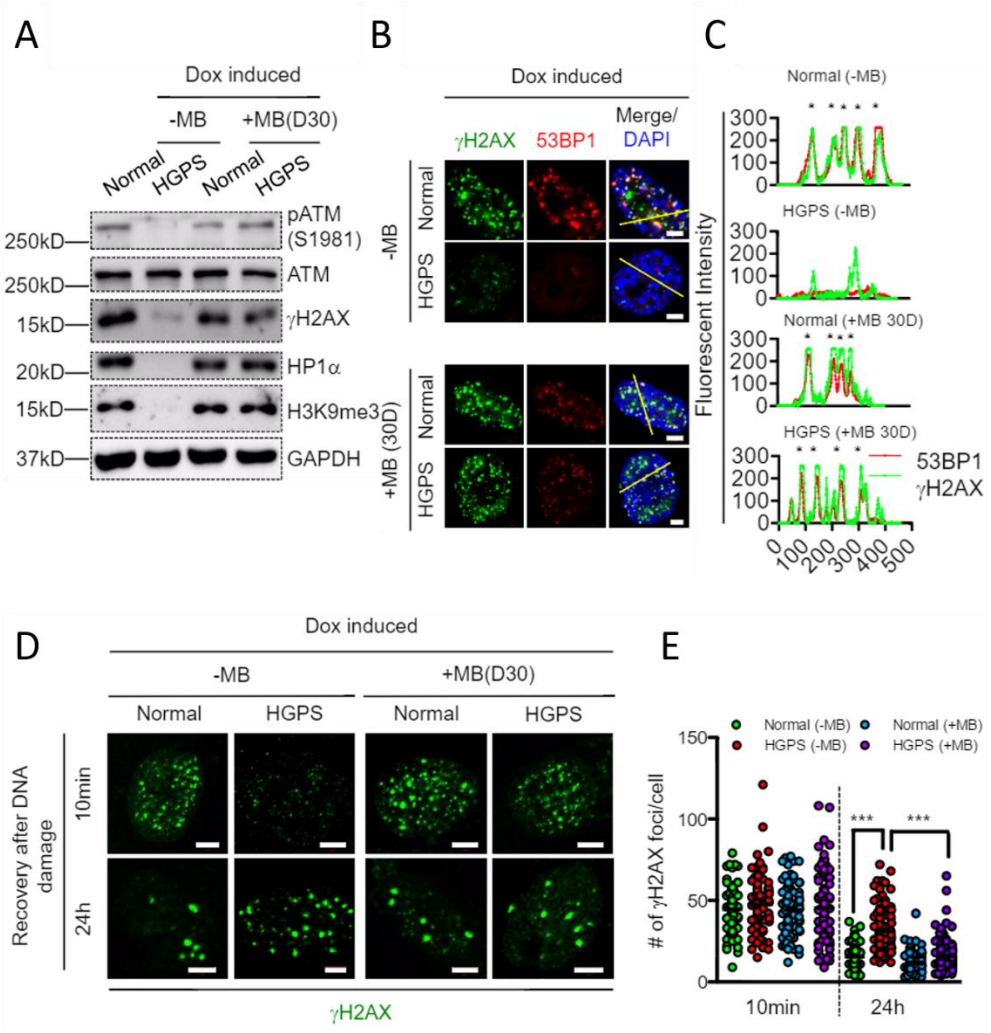

Figure 5-15: Methylene blue restores H3K9me3 and rescues ATM activation, γH2AX signaling and NHEJ in HGPS fibroblasts. (A). Western blotting analysis with anti-pATM(S1981), anti-ATM, anti-γH2AX, anti-HP1α, anti-H3K9me3 and anti-GAPDH antibodies on normal and HGPS fibroblasts treated with or without MB for 30 days. Cells were treated with Dox to induce DSBs before analysis. (B). Representative fluorescence images of γH2AX foci and 53BP1 foci in normal and HGPS fibroblasts treated with or without MB for 30 days. Cells were treated with Dox to induce DSBs before analysis. Scale Bar: 5μm. (C). Line profile analysis of (B), showing the robust recruitment of 53BP1 to γH2AX in MB treated HGPS fibroblasts. Green (γH2AX) and red (53BP1) fluorescence intensities (y axis) were plotted against distance (x axis) along the yellow line in (B). Stars indicated strong co-localization of 53BP1 to γH2AX. (D). Representative fluorescence images of γH2AX foci in normal and HGPS fibroblasts treated with or without MB for 30 days. Cells were then treated with Dox to induce DSBs and allowed to recover for indicated amounts of time before analysis. Scale Bar: 5μm. (E). Quantification of (D), showing the number of γH2AX foci in each nucleus at each time point. More than 100 cells were randomly picked for quantification in each group. Results were presented as mean ± SEM. ***P < 0.001.

5.3 Discussion

5.3.1 γH2AX response to DSBs is impaired in HGPS.

As the most conspicuous histone modification at DSBs, γH2AX plays a critical function in DDR (Bassing et al., 2002; Kinner et al., 2008; Paull et al., 2000). Loss of γH2AX signals has been shown to disrupt the recruitment of NHEJ players to DSBs and compromise genome integrity (Bassing et al., 2002; Ward et al., 2003). To investigate γH2AX signals in HGPS cells, I induced global DSBs in HGPS and normal control fibroblasts by DNA damaging agents. My results demonstrated that the G0/G1 phase HGPS fibroblasts displayed significantly reduced γH2AX signals than normal control cells under the same Dox-treatment condition (Figure 5-5A & B).

Importantly, weak γH2AX response was associated with reduced recruitments of RIF1 and 53BP1, two critical NHEJ regulators (Figure 5-7), suggesting that the weakened γH2AX signals affected normal NHEJ in HGPS cells during the G0/G1 phase.

Previous studies have reported an increased basal level of DNA damage in HGPS models (Liu et al., 2005; Liu et al., 2006; Liu et al., 2008; Osorio et al., 2011; Varela et al., 2005). In my study, I also observed an elevated basal count of γH2AX foci in HGPS fibroblasts (Figure 5-1). This increase likely reflects a dysfunctional DNA damage repair and sustained DSBs in HGPS models. Different from the Dox-induced widespread γH2AX signals described in this paper, the basal γH2AX signals are much more limited, which mark the naturally occurred DSBs under the normal condition. In this study, I applied Dox or CPT to induce global DSBs and studied the immediate γH2AX responses after induction. My results revealed a weakened immediate γH2AX response at DSBs, which consequently caused delayed NHEJ, sustained γH2AX foci and compromised genome integrity. Thus, my study provided mechanistic insights into the previously described phenotype of increased basal level γH2AX in HGPS (Liu et al., 2005; Liu et al., 2006; Liu et al., 2008; Osorio et al., 2011; Varela et al., 2005).

5.3.2 Reductions in γH2AX response and ATM activity in HGPS cells are cell-cycle dependent.

To elucidate the upstream clue of weakened γH2AX signals in HGPS, I examined three kinases that had been implied to phosphorylate H2AX: ATM, ATR,

and DNAPK (Burma et al., 2001; Kinner et al., 2008; Stiff et al., 2004; Ward and Chen, 2001). My experiments indicated that only ATM was activated upon Dox induction, which was responsible for γH2AX signals (Figure 5-9 and Figure 5-10). Moreover, I found that ATM activation was inhibited in G0/G1 phase HGPS fibroblasts (Figure 5-12).

Unlike G0/G1 phase cells, S phase HGPS fibroblasts displayed normal γH2AX signals and ATM activation upon Dox induction (Figure 5-5). An intriguing question is why ATM activation is not blocked in the S phase HGPS cells? One possibility is that the chromatin compaction and organization are different between G0/G1 and S phase cells. For instance, during the process of DNA replication, chromatin opens up and renders a more flexible structure, which has been shown to favor the recruitment of DNA damage repair pathway proteins (Alabert and Groth, 2012). Supporting this idea, the previous study has demonstrated that "opening up" chromatin by depleting histone H1 or treating cells with histone deacetylase (HDAC) inhibitor TSA was able to significantly enhance γH2AX signals upon DSBs (Murga et al., 2007). Apart from γH2AX, alterations in chromatin structure also directly impact ATM activity. "Opening up" chromatin through TSA treatment has been shown to activate ATM either with or without the presence of DSBs (Bakkenist and Kastan, 2003; Lee, 2007). Thus, it is likely that the chromatin structure remodeling during S phase might facilitate ATM activation and phosphorylate H2AX upon DSBs, alleviating the inhibition in HGPS.

5.3.3 The association of H3K9me3 loss and ATM activation in G0/G1 phase HGPS cells.

Recent studies have highlighted the role of H3K9me3 in regulating ATM activation in response to DNA damage (Ayrapetov et al., 2014; Sun et al., 2009). Removal of H3K9me3 by knocking out its methyltransferase SUV39h1 has been shown to completely abolish ATM activation upon ionizing irradiation (Sun et al., 2009). Interestingly, loss of the pericentric heterochromatin marker H3K9me3 is a major epigenetic abnormality in HGPS cells, which has been described by multiple independent groups (Kelley et al., 2011; Shumaker et al., 2006; Xiong et al., 2015). I found a significant positive correlation between the H3K9me3 level and γH2AX signal strength in both normal and HGPS fibroblasts after Dox treatment (Figure 5-13). Moreover, similar to H3K9me3, both the ATM activity and H2AX phosphorylation followed a trend of deterioration with increased cellular passage and accumulation of progerin in HGPS fibroblasts (Figure 5-13D & E and Figure 5-14).

Based on these observations, I further hypothesized that restoration of H3K9me3 might rescue ATM functionality in HGPS cells. To test this hypothesis, I treated normal and HGPS fibroblasts with methylene blue (MB), a chemical that was recently shown to increase the solubility of progerin, enhance H3K9me3 level and rescue heterochromatin loss in HGPS fibroblasts (Xiong et al., 2015). Significantly, MB almost completely restored ATM activation in G0/G1 HGPS fibroblasts upon Dox treatment (Figure 5-15A). Moreover, downstream DNA damage response activities including γH2AX response, 53BP1 recruitment and DNA damage repair were also rescued by MB treatment (Figure 5-15). In agreement with my previous

observation that MB's effect was mostly HGPS specific (Xiong et al., 2015), I found that MB treatment didn't change NHEJ in normal fibroblasts (Figure 5-15). Based on these results, my study suggests a novel connection between the two prominent phenotypes in HGPS - H3K9me3 loss and NHEJ deficiency. My results also provide mechanistic insights underlying the complex phenotypes in HGPS cells and suggest new therapeutic target to treat DNA damage repair deficiency and protect genome integrity in HGPS cells.

Chapter VI: Summary and future perspectives

6.1 Summary

The research presented in this dissertation has three aims. To begin with, my initial goal was to elucidate the molecular mechanism underlying the frequently observed vascular smooth muscle cell loss phenotype in HGPS patients and animal models.

The research presented in Chapter II & III started from the development and characterization of an *in vitro* SMC differentiation system based on iPSCs. I established this system to circumvent the problems associated with primary HGPS SMC culture and to acquire a workable amount of HGPS SMCs. To differentiate SMCs from iPSCs, I adopted a three step lineage specific differentiation protocol and generated HGPS and normal control SMCs with high efficiency (>80% expressing SMC specific markers) (Xie et al., 2007b). Characterization on these cells confirmed classic HGPS cellular phenotypes including proliferation defects and premature senescence. Moreover, I found that HGPS SMCs bear elevated basal level of cell death, which provided a plausible *in vitro* explanation for the *in vivo* vascular SMC loss phenotype.

The mechanistic study revealed that HGPS SMC cell death was independent of Caspase 3 mediated apoptosis. Interestingly, PARP1, an important regulator involved in DNA damage repair and cellular homeostasis was found to be significantly down-regulated in HGPS SMCs (Patel et al., 2011). I determined that progerin led to PARP1 down-regulation through interfering with its nuclear translocation. It has been previously reported that deletion or inhibition of PARP1 was lethal in HR deficient cells (Bothmer et al., 2011; Bunting et al., 2010; Cao et al., 2009; Patel et al., 2011).

More importantly, HR has been shown to be impaired in HGPS fibroblasts, implying a potentially similar deficiency in HGPS SMCs (Liu et al., 2005). Based on these pieces of information, I hypothesized that down-regulation of PARP1 in HR deficient HGPS SMCs lead to genome instability, chromosome aberrations and cell death. Indeed, my data suggested that HR was completely inhibited in HGPS SMCs during S/G2 phase. Moreover, NHEJ, the error prone DSB repair pathway was over-activated in HGPS SMCs during S/G2 phase. This mis-regulation of DSB repair pathways led to abnormal chromosome structure and cell death during mitosis. This mechanistic model is illustrated in Figure 6-1. Together, these results suggested that DNA damage repair deficiency was an important factor contributing to the SMC cell loss phenotype and cardiovascular pathology in HGPS.

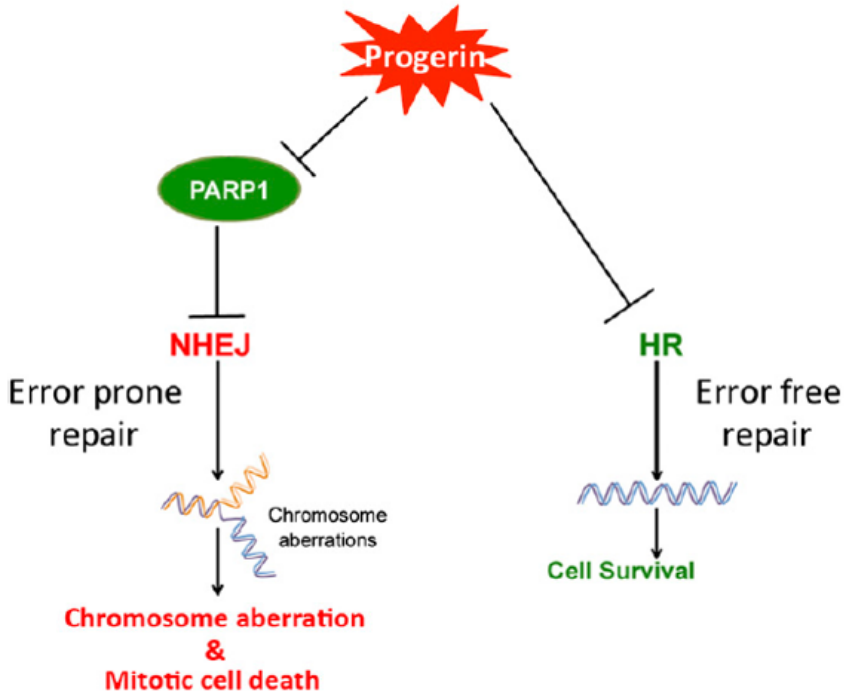

Figure 6-1: Working model of HGPS SMC cell death. The accumulation of membrane-associated progerin not only causes HR deficiency via an unknown mechanism, but also causes PARP1 down-regulation, likely through interfering with PARP1 nuclear import. This PARP1 reduction results in the activation of the NHEJ pathway in the HR-deficient HGPS SMCs, leading to error-prone DNA repair, chromosome aberration, and mitotic catastrophe in HGPS SMCs.

Chapter II & III emphasized the importance of proper regulation of NHEJ and HR during different cell cycle phases to genome integrity and cellular homeostasis (Branzei and Foiani, 2008). Based on those results, in the second aim, I proposed to fully characterize the cell cycle dependent activation pattern of NHEJ and HR in HGPS cells upon DSBs. The research presented in Chapter IV revealed a completely disrupted cell cycle dependent regulation of NHEJ and HR in HGPS fibroblasts. In detail, HR (indicated by BRCA1 & Rad51 recruitment) was almost undetectable in G0/G1 phase and significantly impaired in S/G2 phase HGPS fibroblasts. NHEJ (indicated by RIF1), on the other hand, was drastically delayed during the G0/G1 phase, but active in S/G2 phase HGPS fibroblasts (Figure 4-8). These results were in agreement with my previous findings on HGPS SMCs. The mis-regulation of NHEJ and HR could potentially induce various cellular defects in HGPS. For example, defective HR and active NHEJ during S/G2 HGPS SMCs undermine genome integrity and contribute to chromosome aberrations and mitotic catastrophe (See in Chapter III). On the other hand, deficient NHEJ during G0/G1 phase has been proposed to induce premature senescence in HGPS fibroblasts (Krishnan et al., 2011; Liu et al., 2012; Liu et al., 2005; Liu et al., 2013a; Liu et al., 2013b).

In aim three, I continued to investigate the molecular mechanism underlying NHEJ mis-regulation in HGPS (see Chapter V). In this chapter, I targeted a DDR

signal up-stream of NHEJ: γH2AX response. γH2AX is not only a popular DSB marker, but also an important signal protein that facilitates down-stream DNA repair (Kinner et al., 2008). Deletion of γH2AX signal has been shown to impair the recruitment of a variety of DNA repair factors, including 53BP1, an important player in NHEJ (Bassing et al., 2002; Kinner et al., 2008; Mah et al., 2010). To investigate γH2AX signaling in HGPS upon DNA damage, I introduced DSBs by Doxorubicin treatment. My results showed that γH2AX response followed a cell cycle dependent reduction in HGPS fibroblasts upon DSBs. HGPS γH2AX response was significantly reduced during the G0/G1 phase, but almost completely unaffected in S/G2 phase. This cell cycle dependent response of γH2AX was highly accordant with NHEJ activation pattern in HGPS. Reduced γH2AX response was correlated with delayed recruitment of 53BP1 and RIF1 and also delayed DNA damage repair in HGPS as indicated by undetectable 53BP1 or RIF1 co-localized with weak γH2AX foci in HGPS. These results suggested a role of γH2AX signal deficiency in NHEJ mis-regulation. In the upstream, γH2AX reduction was caused by a reduced ATM activation during the G0/G1 phase in HGPS fibroblasts. Inhibition of ATM, but not ATR or DNAPKcs was able to suppress γH2AX response upon Dox treatment. Interestingly, ATM activation was normal in S/G2 phase HGPS fibroblasts. This activation pattern was consistent with γH2AX response and NHEJ in HGPS. Finally, I found that ATM inactivation was highly correlated with the H3K9me3 loss, a classic epigenetic alteration in HGPS. Restoration of γH3K9me3 through methylene blue treatment was able to rescue ATM inactivation, H2AX signal reduction and 53BP1 recruitment. Together, these data elucidated an upstream signal deficiency

underlying HGPS NHEJ abnormality and provided a novel connection between the two prominent phenotypes (H3K9me3 loss and NHEJ deficiency) and mechanistic insights underlying the complex phenotypes in HGPS cells.

6.2 Future perspectives

The work presented in this dissertation not only established a plausible model to recapitulate HGPS vascular smooth muscle cell pathology, but also identified PARP1 down-regulation and disrupted HR and NHEJ as important players in HGPS SMC cell death. Furthermore, this dissertation investigated the molecular mechanism underlying HGPS NHEJ deficiency and provided a novel connection between the classic H3K9me3 loss phenotype and defective NHEJ in HGPS cells. Despite that the conclusions from this dissertation deepened our understanding of the HGPS SMC loss phenotype and HGPS DNA damage repair deficiency, there are still important questions remaining to be addressed.

Question 1: Does *in vitro* mechanism pertain to *in vivo* phenotype? In Chapter II & III, I established a 2D differentiation system to mimic the *in vivo* SMC loss phenotype and proposed a mechanistic model (Figure 6-1) to explain HGPS SMC cell death. However, whether these findings faithfully recapitulated *in vivo* situations remains unclear. Therefore, a validation of their applicability within a more physiological environment is important. BACG608G and *Lmna*^{G609G} HGPS mouse models provide a valuable tool to test these mechanistic models *in vivo*. This question can be addressed from two aspects. First, a direct comparison of the levels of PARP1

between vessel tissues from HGPS and normal control mouse models is necessary. To do this, one could perform western blotting and immunohistochemistry (IHC) analysis to detect PARP1 level on aortic tissue samples from BAC G608G mice and control mice at various ages. In IHC experiments, the intensity of PARP1 signal in each SMC will negatively correspond with the progerin signal intensity to establish a correlation between progerin and PARP1 at single cell level in vivo. Second, to assay DNA damage repair *in vivo*, one could isolate primary SMCs from BAC G608G mice and measure HR and NHEJ efficiencies as described in Chapter III.

Question II: What is the connection between HGPS SMC loss and HGPS cardiovascular pathology? Despite that BACG608G and *Lmna*^{G609G} mouse models are able to phenotypically recapitulate the vascular SMC loss phenotype in HGPS patients, they fail to display the connection between this phenotype and the cardiovascular pathology in progeria. This drawback is caused by their incapability to capture the onset and progression of SMC loss or to establish a causation relationship between SMC loss and other cardiovascular defects. Based on this notion, *in vivo* real time observation of SMC loss and other cardiovascular physiological features is a good approach to inform us about the connection between vascular SMC loss and cardiovascular pathogenesis in HGPS. Moreover, real time monitoring vascular SMC loss will allow researchers to more conveniently test new drug therapies towards HGPS. Technically, I can adopt the *in vivo* bioluminescence imaging technology to visualize vessel development and SMC loss in a real time manner. By, using a Firefly luciferase and GFP reporter driven by SMC marker specific promoter, such as SM22α and smMHC promoter, I will be able to specifically observe the changes in vascular SMC number by measuring bioluminescence intensity, under normal or HGPS genetic background.

Question III: Are there additional methods to mimic HGPS SMC loss under physiological conditions? Besides using animal models, an alternative approach to

reconstruct physiological environment is to engineer the 2D differentiated HGPS SMCs into 3D tissue engineered blood vessels (TEBVs) (Fernandez et al., 2014). These vessels are cultured in a fluid perfusion system, which allows scientists to recreate blood flow in TEBVs *in vitro*. Compared to HGPS animal models, HGPS TEBVs not only could faithfully recapitulate physiological conditions, but also are easier to generate, maintain and test. In collaboration with Dr. George Truskey at Duke University, we established a protocol to generate HGPS and control TEBVs from HGPS SMCs.

Question IV: Is HGPS SMC cell death rescuable? My mechanistic model suggested that progerin induced PARP1 down-regulation contributed to HGPS SMC cell death (Figure 6-1). Therefore, it would be interesting to over express PARP1 in HGPS SMCs and examine its effect on HGPS SMC survival.

Question V: What is the mechanism underlying HGPS HR deficiency? In chapter IV, I showed that HR was significantly impaired in S/G2 phase HGPS fibroblasts. Yet, the underlying molecular mechanism is still largely unknown. My preliminary data suggested that protein and mRNA levels of Rad51 and BRCA1 were significantly reduced in HGPS fibroblasts (Figure 4-5). However, it has been previously shown that S/G2 phase cells expressed higher amount of HR associated factors including BRCA1 and Rad51. Thus, it was unclear whether this reduction reflected a real protein down-regulation or was an artifact caused by a reduced percentage of S/G2 phase population in HGPS fibroblasts. To solve this problem, it is worthy to compare the level of HR factors between HGPS and normal control cells during S/G2 phase.

Question VI: What is the potential of Methylene blue as an HGPS therapeutic approach?

According to our previous research, methylene blue possessed significant beneficial effect to HGPS fibroblasts and was able to promote HGPS cellular proliferation, reduce HGPS ROS level and improve HGPS mitochondrial function and restore HGPS heterochromatin abnormalities. Moreover, in my research, I discovered that methylene blue could rescue the DSB repair defects in HGPS cells. Based on these beneficial effects, it would be interesting to test methylene blue's potential as a therapeutic approach to treat HGPS.

Elucidating the above questions is beyond the scope of this dissertation, but will significantly expand our knowledge about the HGPS SMC cell loss, cardiovascular pathology and DNA damage repair deficiency.

Chapter VII: Materials and methods

7.1 Chapter II & III

7.1.1 Plasmids

Retroviral vectors encoding human KLF4, SOX2, OCT4, and C-MYC were previously described in (Takahashi et al., 2007). pEGFPC1- Hutchinson–Gilford (HG) (progerin) and pEGFP-C1-lamin A (LA) were constructed based on pEGFP-C1 vector (Clontech). DsRed-HG and DsRed-LA were constructed based on DsRedmonomer-C1 vector (Clontech). pMKO.1-progerin-shRNA retroviral plasmid was constructed based on pMKO.1 vector (Addgene). pEGFP-N3-Poly(ADP-ribose) polymerase 1 (PARP1) was kindly provided by Guy Poirier at Université Laval, Quebec, Canada.

7.1.2 RT-Quantitative PCR and Primers

RNA samples were extracted from normal and Hutchinson–Gilford progeria syndrome (HGPS) smooth muscle cells (SMCs) with the Qiagen RNAeasy kit, and reverse transcribed into cDNA with the iScript Advanced cDNA Synthesis kit (170–8842; Bio-Rad). RT-quantitative PCR (RT-qPCR) was conducted in triplicate using SYBR Green Supermix (170–8880; Bio-Rad) on a CFX96 real-time system (C1000 Thermal Cycler; Bio-Rad). Primers for amplifying Endo-Sox2, Endo-Oct3/4, and Nanog were previously described (Takahashi et al., 2007). Primers for amplifying SMC–α-actin (SMA), calponin, smMHC, and SM22-α were described (Xie et al., 2007b). As an internal control, human GAPDH primer was purchased from real-time primers (VHPS-3541). Primer sequences for amplifying p16ink4a, human telomerase

reverse transcriptase (hTERT), Bax, PARP1 are listed below: human p16ink4a (F: 5′ -TAGTTACGGTCGGAGGCCGAT; R: 5′ -CTTTCAATCGGGGATGTCTGAG); human TERT (F: 5′ - TGTGCACCAACATCTACAAG; R: 5′ - GCGTTCTTGGCTTTCAGGAT); human Bax (F: 5′ - GTTTCATCCAGGATCGAGCAG; R: 5′ -CATCTTCTTCCAGATGGTGA); and human PARP1 (F: 5′ -GACCTGAAGGAGCTACTCATC; R: 5′ - TTTCTCGGAATTCCTTTGGGG).

7.1.3 SMC Differentiation from Induced Pluripotent Stem Cells

To differentiate SMCs from induced pluripotent stem (iPS) cells, I adopted a three-step indirect differentiation protocol with minor modifications (2). Briefly, embryoid bodies (EBs), generated from normal or HGPS-iPSCs, were cultured in suspension for 5–7 d and then seeded onto 0.1% gelatin-coated dishes for EB outgrowth formation. After 10 d, outgrowth cells were detached and reseeded onto Matrigel-coated plates in SMC growth medium (Lonza) and further cultured as pre-SMCs for 2 wk. The pre-SMCs can be frozen and stored for future differentiation. After 2 wk of induction, the HGPS and normal pre-SMCs were trypsinized with TrypLE Express (Life Sciences) and re-plated at a density of 1 × 106 cells per 10-cm dish (precoated by 0.1% gelatin) in SMC differentiation medium [DMEM, supplied with 5% (vol/vol) FBS] to initiate SMC differentiation. SMCs were grown for 28 d in SMC differentiation medium and passaged at 1:2 when they reached 90% confluence.

7.1.4 Western Blotting Analysis

Whole cell lysate was obtained by treating cell pellets with Laemmli buffer (161–0737; Bio-Rad), containing 5% (vol/vol) β-mercaptoethanol. Protein samples were then separated in 10% or 15% SDS/PAGE gels and transferred onto a nitrocellulose membrane (Bio-Rad) for primary and secondary antibody incubation as described. Signal intensity was quantified using ImageJ software (National Institutes of Health, NIH).

7.1.5 Contractility Assay and Ca2+ Image

SMC contractility was tested by angiotensin II treatment. Briefly, normal and HGPS SMCs were seeded onto gelatin-coated 35-mm glass-bottom dishes (NC0409658; Fisher Scientific) at days 14 and 21. Twenty-four hours later, cells were treated with 10 μM angiotensin II and phase contrast pictures were taken every 10 min until 30 min after treatment. Pictures were taken with a Zeiss AX10 microscope. To image Ca2+ flow in SMCs, flow3 Ca2+ fluorescent indicator (Invitrogen) was adopted. Briefly, normal and HGPS SMCs were washed with standard tyrode solution (100502-380; VWR) and incubated with 2 μM fluo-3-Ca2+ indicator [diluted in tyrode solution containing 0.02% Pluronic F-127 (8409400; Fisher Scientific)] at room temperature for 20 min. Cells were then washed with tyrode solution three times and imaged for angiotensin II-stimulated Ca2+ flow signal by UltraVIEW VoX system (PerkinElmer) attached to an inverted microscope (Eclipse Ti; Nikon) as previously described (Fernandes et al., 2011).

7.1.6 SMC Differentiation Efficiency Test

SMC cells were detached from plates at day 14, washed with PBS, fixed in 4% (vol/vol) paraformaldehyde in PBS for 20 min, and permeabilized with 0.2% Triton X-100 in PBS for 5 min. Cells were then incubated with primary anti-SMA (Sigma) or anti-calponin (Millipore) antibody overnight at 4 °C. Samples without primary antibodies were included as blank controls. Alexa Fluor 488-tagged secondary antibody (Life Sciences) was then added to all samples for 1 h at room temperature. Finally, samples were rinsed with PBS and scored by flow cytometry (FACSCanto II; BD). Positive signals were determined according to the blank controls.

7.1.7 Senescence-Associated β-Galactosidase Activity Assay

Senescence-Associated β-Galactosidase Activity Assay. SA–β-gal activity was assayed weekly on normal and HGPS SMCs according to the manufacturer's protocol (9860; Cell Signaling). Images were taken with a Zeiss AX10 microscope. Cell Cycle Analysis. Cell cycle analysis was conducted on normal and HGPS SMCs weekly during SMC differentiation. Cells were harvested, rinsed with PBS, and resuspended in 0.5 mL PBS. Then, 4.5 mL of 70% (vol/vol) ice-cold ethanol was added to the cell suspension for fixation. This mixture was incubated on ice for 10–15 min. Then cells were pelleted, rinsed with PBS, and re-suspended in propidium iodide (PI) DNA staining buffer (50 μg/mL PI and 100 μg/mL DNase-free RNase in PBS) for 30 min at 37 °C. Flow cytometry was performed with FACS CantoII (BD) and the data were analyzed by FlowJo software.

7.1.8 PI-annexin V Assay

PI-annexin V Assay. PI-annexin V assay was performed weekly on normal and HGPS SMCs according to the manufacturer's protocol (556547; BD). Briefly, normal and HGPS SMCs were harvested and rinsed with PBS (with extreme care to minimize cell injury). Then cells were re-suspended and stained with 100 μl of 1× annexin V binding buffer containing 5 μl of annexin V and 5 μL of PI for 25 min in the dark at room temperature. After the staining, these samples were scored by FACS CantoII (BD) and the data were processed by FlowJo software.

7.1.9 Caspase 3 Activity Assay

Caspase 3 activity was assayed on normal and HGPS SMCs using a caspase 3 Colorimetric Activity kit following instructions from the manufacturer (APT165; Millipore). Briefly, for basal caspase 3 activity measurement, differentiated SMCs at day 21 were harvested and lysed in lysis buffer. Protein concentration was determined by Nanodrop 2000 spectrophotometer (Thermo Scientific), and different amounts of protein samples were added into 96-well plates with a caspase 3 substrate. After a 24-h incubation at 37 °C, these mixtures were measured for light absorbance at 405 nm by SpectraMax M5e (Molecular Devices). To measure caspase 3 activity upon apoptotic induction, normal and HGPS SMCs were first treated with 20 μM camptothecin (CPT) for indicated periods of time before lysis buffer addition.

7.1.10 Clonogenic Assay

Normal and HGPS fibroblasts (passage 16) were seeded into six-well plates at a density of 500 cells per well. Cells were incubated for 5–7 h. Then, fresh fibroblast medium with indicated concentration of PARP1 inhibitor (AZD2281; Olaparib) was added to the cells for 72 h. After the inhibitor was removed, cells were further cultured for 10–14 d to allow colony formation. To count the number of colonies, cells were stained with Hoechst 33342 and cell clusters that contain more than 20 cells were counted as a positive colony. The number of colonies in each treatment was normalized to untreated control to calculate the survival rate.

7.1.11 SMC Transfection

Electroporation was performed with a Amaxa NHDF Nucleofector kit (F-09376; Lonza) on a Nucleofector 2b machine (Lonza). Roughly 1 × 106 normal SMC cells were collected and transfected with 2 μg pEGFP-HG or pEGFP-LA for a single transfection, and with 0.5 μg pEGFP-N3-PARP1 plus 1.5 μg DsRed-LA, DsRed-HG, or DsRed-HG-SSIM, a nonfarnesylatable mutant of progerin that carries a cysteine to serine mutation on the CSIM motif at the C terminus for a double transfection. Seventy-two hours after transfection, cells were examined by Western immunoblotting or with confocal microscopy (Zeiss LSM 710). For farnesyltransferase inhibitor (FTI) treatment, after SMCs were transfected, 2 μM FTI was immediately applied to the transfected cells, and cells were examined by confocal microscopy (Zeiss LSM 710) 72 h later.

7.1.12 Immunofluorescence Quantification

To quantify immunofluorescence intensity, pictures were analyzed by ImageJ software (NIH) using color histogram function. Fluorescent intensities were subtracted with background signals and plotted. ForRan gradient (Ran N/C) quantification, fluorescent signals of both nuclear and cytoplasmic Ran were quantified. To quantify immunofluorescence intensity, pictures were analyzed by ImageJ

7.1.13 Quantification of DNA Damage and HR Repair Efficiency

Cells were seeded 2 d before CPT treatment and fixed and permeabilized at various time points (10 min, 30 min, 120 min, and 720 min) post-CPT treatment. Immunofluorescence was conducted as follows. Fixed cells were incubated in blocking buffer [either 5% (vol/vol) donkey serum or 4% (vol/vol) BSA in TBS] for 1 h, and co-stained with anti-γH2AX and anti-Rad51 antibodies for 2–3 h at room temperature. Corresponding secondary antibodies were then applied for 1 h before mounting. Images were taken by a Zeiss LSM 710 confocal microscope and analyzed by ImageJ software (NIH). The numbers of γH2AX foci in each normal or HGPS SMC cell were counted using the “find maxima” function. Only those Rad51 foci that colocalized with γH2AX foci were scored. More than 100 nuclei were analyzed at each time point.

7.1.14 BrdU Pulse-Chase Assay

Normal and HGPS SMCs were incubated with SMC differentiation medium containing 10 μM BrdU for 18 h. Upon BrdU removal, cells were incubated and fixed at denoted time points. To visualize BrdU, cells were treated with 2 M HCl before blocking buffer to open up DNA double strand and to expose the BrdU epitope. Cells were then processed with the standard immunofluorescence protocol using the anti-BrdU antibody. Fluorescence images were taken and analyzed with a Zeiss AX10 microscope.

7.1.15 Life cell imaging

Normal and HGPS SMCs were seeded in 35-mm glass-bottom dishes (NC0409658; Fisher Scientific) and imaged by the UltraVIEW VoX system (PerkinElmer) attached to an inverted microscope (Eclipse Ti; Nikon) as previously described (Fernandes et al., 2011).

7.2 Chapter IV & V

7.2.1 Cell culture

Primary HGPS human skin fibroblast cells that carry the classic 1824 C->T mutation (HGADFN167) and normal control cells (HGFDFN168, father of HGADFN167) were obtained from Progeria Research Foundation (PRF) and cultured in conditions as previously described (Xiong et al., 2015). For passaging, cells were

split at a ratio of 1:2 at 95% confluency. Normal and HGPS fibroblasts at passages 13-15, 18-20 and 22-24 were referred to as early, middle and late passage fibroblasts respectively.

7.2.2 Drugs

Drugs used in this study are listed as below: Doxorubicin (Dox, Sigma), Camptothecin (CPT, Sigma), ATM specific inhibitor (KU55933, Selleck Chem), ATR specific inhibitor (VE-821, Selleck Chem), DNAPK specific inhibitor (NU7441, Selleck Chem) and Methylene Blue (MB; Acros Organics).

7.2.3 Antibodies

Antibodies used in western blotting and immunofluorescence analysis were obtained from the following sources: mouse anti-lamin A/C (Mab3211, Millipore), mouse anti-γH2AX (05-636, Upstate), rabbit anti-γH2AX (ab11174, Abcam), rabbit anti-H2AX (2595, cell signaling), mouse anti- α -tubulin (DM1α, Santa Cruz), mouse anti-GAPDH (ab8245, Abcam), mouse anti-BrdU (555627, BD Pharmingen), rabbit anti-RIF1 (A300-568A, Bethyl Laboratory), rabbit anti-53BP1 (sc-22760, Santa Cruz), rabbit anti-ATM (ab32420, Abcam), rabbit anti-pATM (S1981) (ab81292, Abcam), mouse anti-DNAPK (sc-390495, Santa Cruz), mouse anti-pDNAPK (T2609) (ab18356, Abcam), mouse anti-CHK1 (sc-8408, Santa Cruz), rabbit anti-pCHK1(S345) (2341S, Cell Signaling), rabbit anti-H3K9me3 (ab8898, Abcam), rabbit anti-HP1α (2616S, Cell Signaling), rabbit anti-SUV39h1 (A302-127A, Bethyl Laboratory).

7.2.4 G0/G1 phase synchronization & Cell cycle analysis

Passage-matched normal and HGPS fibroblasts were cultured in serum free MEM (Life Technologies) medium, supplemented with 2mM L-Glutamine (Life Technologies), for 24h for G0/G1 phase synchronization. Cell cycle analysis was then performed as previously described to examine the effect of serum starvation(Zhang et al., 2014). Briefly, normal and HGPS fibroblasts were harvested by TrypLE Express (Life Technologies) and washed with PBS (HyClone). Cell pellets were re-suspended in 0.5ml PBS and then added with 4.5ml 70% (vol/vol) ice-cold ethonal. The mixture was incubated for 10-15min at 4°C, washed with PBS and then re-suspended in 50μl propidium iodide (Invitrogen) staining buffer (50μg/ml propidium iodide and 100μg/ml DNAse-free RNAse in PBS). The mixture was then allowed to incubate for 30min at 37°C. Flow cytometry was performed with FACS CantoII (BD) and cell cycle data analysis was performed with FlowJo software.

7.2.5 Doxorubicin, Camptothecin and kinase inhibitor treatment

For immunofluorescence staining analysis, 1μM Doxorubicin or 20μM Camptothecin were applied on passage-matched normal and HGPS fibroblasts (G0/G1 synchronized or unsynchronized) for 1h. Cells were then allowed to recover for 10min (or as indicated in time course experiments) before fixation. For western blotting analysis, 0.5μM Doxorubicin or 50μM Camptothecin were applied on passage-matched normal and HGPS fibroblasts for 2h before harvest. For kinase inhibition experiments, ATM, ATR or DNAPK specific inhibitors were individually

applied to passage-matched normal and HGPS fibroblasts at indicated concentrations for 24h prior to Doxorubicin treatment.

7.2.6 Methylene blue treatment

Methylene blue treatment was conducted as previously described (Xiong et al., 2015). Briefly, MB was dissolved in PBS and added into growth medium at a final concentration of 100nM. Middle passage normal and HGPS fibroblasts were cultured in MB containing medium and passaged at 95% confluency. Cells were treated with MB for 30 days before analysis.

7.2.7 Immunofluorescence staining

Passage-matched normal and HGPS fibroblasts were seeded in chamber slides (BD Falcon) for immunofluorescence staining. Cells were fixed with 4% PFA/PBS for 25-30min, permeabilized with 0.5% Triton X-100 (EMD chemicals Inc.) for 5min and then blocked with 4% BSA/TBS for 1h at room temperature. Cells were then incubated with primary antibodies for overnight at 4°C. Corresponding secondary antibodies were then applied for 1h at room temperature. Fluorescence Images were taken by Zeiss LSM 710 confocal microscope.

7.2.8 BrdU labeling

For BrdU labeling, cells were pre-incubated with 10μM BrdU (BD Biosciences) for 30min before Doxorubicin treatment. To visualize BrdU, cells were treated with 2M hydrochloric acid for 30min before blocking to expose BrdU epitope. Cells were

then proceeded with standard immunofluorescence staining protocol with anti-BrdU antibody. Fluorescence images were taken by Zeiss LSM 710 confocal microscope.

7.2.9 Fluorescence image analysis

Fluorescence signal intensity was quantified through the "color histogram" function of Image J software (National Institute of Health, NIH). Fluorescence intensities were subtracted with background signals and plotted. The number of DNA damage associated foci (γH2AX, RIF1 or 53BP1) was counted through the "find maxima" function of Image J software. Average intensity of individual foci was calculated as the ratio between total fluorescence intensity and the number of foci in each nucleus. Line profile analysis was conducted through the "Line profile" plugin of Image J software.

7.2.10 Western blotting analysis

Western blotting analysis was performed as previously described (Zhang et al., 2014). Briefly, cells were directly lysed in Laemmli buffer (161–0737; Bio-Rad), containing 5% (vol/vol) β-mercaptoethanol. Protein samples were separated in 7.5% or 10% SDS-PAGE gels and transferred onto nitrocellulose membrane (Bio-Rad). Membranes were blocked with 5% milk in TBST and then incubated with primary antibodies for overnight at 4°C. Protein band intensities were quantified through Image J software (NIH).

7.2.11 Statistical analysis

Two-tailed Student t test was used to analyze difference between normal and HGPS. A p value ≤ 0.05 was considered as significant. Statistical analysis was conducted through GraphPad Prism 5.0 software.

7.2.12 Correlation analysis

Spearman rank correlation analysis was performed to capture the association between H3K9me3 and γH2AX signals and estimate the correlation coefficients. I used correlation functions in R to perform the analysis and ggplot2 package to make the plots in R.

Appendices

Besides the above study, I am also involved in designing two additional projects:

I. The roles of microtubule in nuclear morphology maintenance

Nuclear blebbing is a hallmark of HGPS cellular phenotypes (Capell and Collins, 2006). Besides nuclear lamina meshwork, cytoskeleton network is also involved in nuclear structure maintenance (Starr and Fridolfsson, 2010). For example, microtubules have been shown to mediate nuclear lobulation in granulopoesis (Olins and Olins, 2004). Microtubules are also connected with the nuclear lamina meshwork through LINC complex, a protein complex that spans across the nuclear envelope and bridge between nuclear lamina and cytoskeleton network (Starr and Fridolfsson, 2010). This information suggest that microtubules play a role in regulating nuclear morphology. In this project, we aimed to investigate the effect of lamin A-microtubule interaction on nuclear morphology maintenance.

II. Development of tissue engineered blood vessels (TEBVs) from iPSC differentiated SMCs

As discussed in 6.2 Question III, TEBV is a plausible system to mimic HGPS SMC loss under physiological conditions. To realize HGPS TEBVs, I collaborated with Dr. George Truskey at Duke University. In this project, we were able to establish normal and HGPS TEBVs, based on which, we were able to perform

physiological, biochemical, molecular and cellular tests to validate our *in vitro* mechanistic model (Figure 6-1) in a 3D environment.

Bibliography

Alabert, C., and Groth, A. (2012). Chromatin replication and epigenome maintenance. Nat Rev Mol Cell Biol *13*, 153-167.

Ame, J.C., Rolli, V., Schreiber, V., Niedergang, C., Apiou, F., Decker, P., Muller, S., Hoger, T., Menissier-de Murcia, J., and de Murcia, G. (1999). PARP-2, A novel mammalian DNA damage-dependent poly(ADP-ribose) polymerase. J Biol Chem *274*, 17860-17868.

Andres, V., and Gonzalez, J.M. (2009). Role of A-type lamins in signaling, transcription, and chromatin organization. J Cell Biol *187*, 945-957.

Astrom, S.U., Okamura, S.M., and Rine, J. (1999). Yeast cell-type regulation of DNA repair. Nature *397*, 310.

Atkins, L. (1954). Progeria: report of a case with post-mortem findings. N Engl J Med *250*, 1065-1069.

Ayrapetov, M.K., Gursoy-Yuzugullu, O., Xu, C., Xu, Y., and Price, B.D. (2014). DNA double-strand breaks promote methylation of histone H3 on lysine 9 and transient formation of repressive chromatin. Proc Natl Acad Sci U S A *111*, 9169-9174.

Baker, D.J., Wijshake, T., Tchkonia, T., LeBrasseur, N.K., Childs, B.G., van de Sluis, B., Kirkland, J.L., and van Deursen, J.M. (2011). Clearance of p16Ink4a-positive senescent cells delays ageing-associated disorders. Nature *479*, 232-236.

Bakkenist, C.J., and Kastan, M.B. (2003). DNA damage activates ATM through intermolecular autophosphorylation and dimer dissociation. Nature *421*, 499-506.

Banath, J.P., Macphail, S.H., and Olive, P.L. (2004). Radiation sensitivity, H2AX phosphorylation, and kinetics of repair of DNA strand breaks in irradiated cervical cancer cell lines. Cancer Res *64*, 7144-7149.

Bassing, C.H., and Alt, F.W. (2004). H2AX may function as an anchor to hold broken chromosomal DNA ends in close proximity. Cell Cycle *3*, 149-153.

Bassing, C.H., Chua, K.F., Sekiguchi, J., Suh, H., Whitlow, S.R., Fleming, J.C., Monroe, B.C., Ciccone, D.N., Yan, C., Vlasakova, K., *et al.* (2002). Increased ionizing radiation sensitivity and genomic instability in the absence of histone H2AX. Proc Natl Acad Sci U S A *99*, 8173-8178.

Bennett, M.R. (1999). Apoptosis of vascular smooth muscle cells in vascular remodelling and atherosclerotic plaque rupture. Cardiovasc Res *41*, 361-368.

Boamah, E.K., Kotova, E., Garabedian, M., Jarnik, M., and Tulin, A.V. (2012). Poly(ADP-Ribose) polymerase 1 (PARP-1) regulates ribosomal biogenesis in Drosophila nucleoli. PLoS Genet *8*, e1002442.

Bothmer, A., Robbiani, D.F., Di Virgilio, M., Bunting, S.F., Klein, I.A., Feldhahn, N., Barlow, J., Chen, H.T., Bosque, D., Callen, E., *et al.* (2011). Regulation of DNA end joining, resection, and immunoglobulin class switch recombination by 53BP1. Mol Cell *42*, 319-329.

Bothmer, A., Robbiani, D.F., Feldhahn, N., Gazumyan, A., Nussenzweig, A., and Nussenzweig, M.C. (2010). 53BP1 regulates DNA resection and the choice between classical and alternative end joining during class switch recombination. J Exp Med *207*, 855-865.

Bouquet, F., Muller, C., and Salles, B. (2006). The loss of gammaH2AX signal is a marker of DNA double strand breaks repair only at low levels of DNA damage. Cell Cycle *5*, 1116-1122.

Bouwman, P., Aly, A., Escandell, J.M., Pieterse, M., Bartkova, J., van der Gulden, H., Hiddingh, S., Thanasoula, M., Kulkarni, A., Yang, Q., *et al.* (2010). 53BP1 loss rescues BRCA1 deficiency and is associated with triple-negative and BRCA-mutated breast cancers. Nat Struct Mol Biol *17*, 688-695.

Branzei, D., and Foiani, M. (2008). Regulation of DNA repair throughout the cell cycle. Nat Rev Mol Cell Biol *9*, 297-308.

Bunting, S.F., Callen, E., Kozak, M.L., Kim, J.M., Wong, N., Lopez-Contreras, A.J., Ludwig, T., Baer, R., Faryabi, R.B., Malhowski, A., *et al.* (2012). BRCA1 functions independently of homologous recombination in DNA interstrand crosslink repair. Mol Cell *46*, 125-135.

Bunting, S.F., Callen, E., Wong, N., Chen, H.T., Polato, F., Gunn, A., Bothmer, A., Feldhahn, N., Fernandez-Capetillo, O., Cao, L., *et al.* (2010). 53BP1 inhibits homologous recombination in Brca1-deficient cells by blocking resection of DNA breaks. Cell *141*, 243-254.

Burke, B., and Stewart, C.L. (2013). The nuclear lamins: flexibility in function. Nat Rev Mol Cell Biol *14*, 13-24.

Burma, S., Chen, B.P., Murphy, M., Kurimasa, A., and Chen, D.J. (2001). ATM phosphorylates histone H2AX in response to DNA double-strand breaks. J Biol Chem *276*, 42462-42467.

Burtner, C.R., and Kennedy, B.K. (2010). Progeria syndromes and ageing: what is the connection? Nat Rev Mol Cell Biol *11*, 567-578.

Caldecott, K.W. (2008). Single-strand break repair and genetic disease. Nat Rev Genet *9*, 619-631.

Campisi, J. (2001). From cells to organisms: can we learn about aging from cells in culture? Exp Gerontol *36*, 607-618.

Cao, K., Blair, C.D., Faddah, D.A., Kieckhaefer, J.E., Olive, M., Erdos, M.R., Nabel, E.G., and Collins, F.S. (2011a). Progerin and telomere dysfunction collaborate to trigger cellular senescence in normal human fibroblasts. J Clin Invest *121*, 2833-2844.

Cao, K., Capell, B.C., Erdos, M.R., Djabali, K., and Collins, F.S. (2007). A lamin A protein isoform overexpressed in Hutchinson-Gilford progeria syndrome interferes with mitosis in progeria and normal cells. Proc Natl Acad Sci U S A *104*, 4949-4954.

Cao, K., Graziotto, J.J., Blair, C.D., Mazzulli, J.R., Erdos, M.R., Krainc, D., and Collins, F.S. (2011b). Rapamycin reverses cellular phenotypes and enhances mutant

protein clearance in Hutchinson-Gilford progeria syndrome cells. Sci Transl Med *3*, 89ra58.

Cao, L., Xu, X., Bunting, S.F., Liu, J., Wang, R.H., Cao, L.L., Wu, J.J., Peng, T.N., Chen, J., Nussenzweig, A., *et al.* (2009). A selective requirement for 53BP1 in the biological response to genomic instability induced by Brca1 deficiency. Mol Cell *35*, 534-541.

Capanni, C., Cenni, V., Mattioli, E., Sabatelli, P., Ognibene, A., Columbaro, M., Parnaik, V.K., Wehnert, M., Maraldi, N.M., Squarzoni, S., *et al.* (2003). Failure of lamin A/C to functionally assemble in R482L mutated familial partial lipodystrophy fibroblasts: altered intermolecular interaction with emerin and implications for gene transcription. Exp Cell Res *291*, 122-134.

Capell, B.C., and Collins, F.S. (2006). Human laminopathies: nuclei gone genetically awry. Nat Rev Genet *7*, 940-952.

Capell, B.C., Erdos, M.R., Madigan, J.P., Fiordalisi, J.J., Varga, R., Conneely, K.N., Gordon, L.B., Der, C.J., Cox, A.D., and Collins, F.S. (2005). Inhibiting farnesylation of progerin prevents the characteristic nuclear blebbing of Hutchinson-Gilford progeria syndrome. Proc Natl Acad Sci U S A *102*, 12879-12884.

Capell, B.C., Olive, M., Erdos, M.R., Cao, K., Faddah, D.A., Tavarez, U.L., Conneely, K.N., Qu, X., San, H., Ganesh, S.K., *et al.* (2008). A farnesyltransferase inhibitor prevents both the onset and late progression of cardiovascular disease in a progeria mouse model. Proc Natl Acad Sci U S A *105*, 15902-15907.

Castedo, M., Perfettini, J.L., Roumier, T., Andreau, K., Medema, R., and Kroemer, G. (2004). Cell death by mitotic catastrophe: a molecular definition. Oncogene *23*, 2825-2837.

Chan, D.W., Chen, B.P., Prithivirajsingh, S., Kurimasa, A., Story, M.D., Qin, J., and Chen, D.J. (2002). Autophosphorylation of the DNA-dependent protein kinase catalytic subunit is required for rejoining of DNA double-strand breaks. Genes Dev *16*, 2333-2338.

Chapman, J.R., Barral, P., Vannier, J.B., Borel, V., Steger, M., Tomas-Loba, A., Sartori, A.A., Adams, I.R., Batista, F.D., and Boulton, S.J. (2013). RIF1 is essential for 53BP1-dependent nonhomologous end joining and suppression of DNA double-strand break resection. Mol Cell *49*, 858-871.

Chapman, J.R., and Jackson, S.P. (2008). Phospho-dependent interactions between NBS1 and MDC1 mediate chromatin retention of the MRN complex at sites of DNA damage. EMBO Rep *9*, 795-801.

Chapman, J.R., Taylor, M.R., and Boulton, S.J. (2012). Playing the end game: DNA double-strand break repair pathway choice. Mol Cell *47*, 497-510.

Chen, C.Y., Chi, Y.H., Mutalif, R.A., Starost, M.F., Myers, T.G., Anderson, S.A., Stewart, C.L., and Jeang, K.T. (2012). Accumulation of the inner nuclear envelope protein Sun1 is pathogenic in progeric and dystrophic laminopathies. Cell *149*, 565-577.

Chen, J.H., Hales, C.N., and Ozanne, S.E. (2007). DNA damage, cellular senescence and organismal ageing: causal or correlative? Nucleic Acids Res *35*, 7417-7428.

Chen, L., Nievera, C.J., Lee, A.Y., and Wu, X. (2008). Cell cycle-dependent complex formation of BRCA1.CtIP.MRN is important for DNA double-strand break repair. J Biol Chem *283*, 7713-7720.

Chen, Z.J., Wang, W.P., Chen, Y.C., Wang, J.Y., Lin, W.H., Tai, L.A., Liou, G.G., Yang, C.S., and Chi, Y.H. (2014). Dysregulated interactions between lamin A and SUN1 induce abnormalities in the nuclear envelope and endoplasmic reticulum in progeric laminopathies. J Cell Sci *127*, 1792-1804.

Clarke, M.C., Figg, N., Maguire, J.J., Davenport, A.P., Goddard, M., Littlewood, T.D., and Bennett, M.R. (2006). Apoptosis of vascular smooth muscle cells induces features of plaque vulnerability in atherosclerosis. Nat Med *12*, 1075-1080.

Cooke, M.S., Evans, M.D., Dizdaroglu, M., and Lunec, J. (2003). Oxidative DNA damage: mechanisms, mutation, and disease. Faseb j *17*, 1195-1214.

d'Adda di Fagagna, F. (2008). Living on a break: cellular senescence as a DNA-damage response. Nat Rev Cancer *8*, 512-522.

Dechat, T., Adam, S.A., and Goldman, R.D. (2009). Nuclear lamins and chromatin: when structure meets function. Adv Enzyme Regul *49*, 157-166.

Dechat, T., Pfleghaar, K., Sengupta, K., Shimi, T., Shumaker, D.K., Solimando, L., and Goldman, R.D. (2008). Nuclear lamins: major factors in the structural organization and function of the nucleus and chromatin. Genes Dev *22*, 832-853.

Dimitrova, N., Chen, Y.C., Spector, D.L., and de Lange, T. (2008). 53BP1 promotes non-homologous end joining of telomeres by increasing chromatin mobility. Nature *456*, 524-528.

Dimri, G.P., Lee, X., Basile, G., Acosta, M., Scott, G., Roskelley, C., Medrano, E.E., Linskens, M., Rubelj, I., Pereira-Smith, O., *et al.* (1995). A biomarker that identifies senescent human cells in culture and in aging skin in vivo. Proc Natl Acad Sci U S A *92*, 9363-9367.

Driscoll, M.K., Albanese, J.L., Xiong, Z.M., Mailman, M., Losert, W., and Cao, K. (2012). Automated image analysis of nuclear shape: what can we learn from a prematurely aged cell? Aging (Albany NY) *4*, 119-132.

Eriksson, M., Brown, W.T., Gordon, L.B., Glynn, M.W., Singer, J., Scott, L., Erdos, M.R., Robbins, C.M., Moses, T.Y., Berglund, P., *et al.* (2003). Recurrent de novo point mutations in lamin A cause Hutchinson-Gilford progeria syndrome. Nature *423*, 293-298.

Escribano-Diaz, C., Orthwein, A., Fradet-Turcotte, A., Xing, M., Young, J.T., Tkac, J., Cook, M.A., Rosebrock, A.P., Munro, M., Canny, M.D., *et al.* (2013). A cell cycle-dependent regulatory circuit composed of 53BP1-RIF1 and BRCA1-CtIP controls DNA repair pathway choice. Mol Cell *49*, 872-883.

Falck, J., Coates, J., and Jackson, S.P. (2005). Conserved modes of recruitment of ATM, ATR and DNA-PKcs to sites of DNA damage. Nature *434*, 605-611.

Felgentreff, K., Du, L., Weinacht, K.G., Dobbs, K., Bartish, M., Giliani, S., Schlaeger, T., DeVine, A., Schambach, A., Woodbine, L.J., *et al.* (2014). Differential role of nonhomologous end joining factors in the generation, DNA damage response, and myeloid differentiation of human induced pluripotent stem cells. Proc Natl Acad Sci U S A *111*, 8889-8894.

Fernandes, M.C., Cortez, M., Flannery, A.R., Tam, C., Mortara, R.A., and Andrews, N.W. (2011). Trypanosoma cruzi subverts the sphingomyelinase-mediated plasma membrane repair pathway for cell invasion. J Exp Med *208*, 909-921.

Fernandez, C.E., Achneck, H.E., Reichert, W.M., and Truskey, G.A. (2014). Biological and engineering design considerations for vascular tissue engineered blood vessels (TEBVs). Curr Opin Chem Eng *3*, 83-90.

Filesi, I., Gullotta, F., Lattanzi, G., D'Apice, M.R., Capanni, C., Nardone, A.M., Columbaro, M., Scarano, G., Mattioli, E., Sabatelli, P., *et al.* (2005). Alterations of nuclear envelope and chromatin organization in mandibuloacral dysplasia, a rare form of laminopathy. Physiol Genomics *23*, 150-158.

Fradet-Turcotte, A., Canny, M.D., Escribano-Diaz, C., Orthwein, A., Leung, C.C., Huang, H., Landry, M.C., Kitevski-LeBlanc, J., Noordermeer, S.M., Sicheri, F., *et al.* (2013). 53BP1 is a reader of the DNA-damage-induced H2A Lys 15 ubiquitin mark. Nature *499*, 50-54.

Game, J.C., and Mortimer, R.K. (1974). A genetic study of x-ray sensitive mutants in yeast. Mutat Res *24*, 281-292.

Gibbs-Seymour, I., Markiewicz, E., Bekker-Jensen, S., Mailand, N., and Hutchison, C.J. (2015). Lamin A/C-dependent interaction with 53BP1 promotes cellular responses to DNA damage. Aging Cell *14*, 162-169.

Goldman, R.D., Gruenbaum, Y., Moir, R.D., Shumaker, D.K., and Spann, T.P. (2002). Nuclear lamins: building blocks of nuclear architecture. Genes Dev *16*, 533-547.

Goldman, R.D., Shumaker, D.K., Erdos, M.R., Eriksson, M., Goldman, A.E., Gordon, L.B., Gruenbaum, Y., Khuon, S., Mendez, M., Varga, R., *et al.* (2004). Accumulation of mutant lamin A causes progressive changes in nuclear architecture in Hutchinson-Gilford progeria syndrome. Proc Natl Acad Sci U S A *101*, 8963-8968.

Gordon, L.B., Kleinman, M.E., Miller, D.T., Neuberg, D.S., Giobbie-Hurder, A., Gerhard-Herman, M., Smoot, L.B., Gordon, C.M., Cleveland, R., Snyder, B.D., *et al.* (2012). Clinical trial of a farnesyltransferase inhibitor in children with Hutchinson-Gilford progeria syndrome. Proc Natl Acad Sci U S A *109*, 16666-16671.

Gordon, L.B., McCarten, K.M., Giobbie-Hurder, A., Machan, J.T., Campbell, S.E., Berns, S.D., and Kieran, M.W. (2007). Disease progression in Hutchinson-Gilford progeria syndrome: impact on growth and development. Pediatrics *120*, 824-833.

Gu, J., Lu, H., Tippin, B., Shimazaki, N., Goodman, M.F., and Lieber, M.R. (2007). XRCC4:DNA ligase IV can ligate incompatible DNA ends and can ligate across gaps. Embo j *26*, 1010-1023.

Hagting, A., Jackman, M., Simpson, K., and Pines, J. (1999). Translocation of cyclin B1 to the nucleus at prophase requires a phosphorylation-dependent nuclear import signal. Curr Biol *9*, 680-689.

Haince, J.F., McDonald, D., Rodrigue, A., Dery, U., Masson, J.Y., Hendzel, M.J., and Poirier, G.G. (2008). PARP1-dependent kinetics of recruitment of MRE11 and NBS1 proteins to multiple DNA damage sites. J Biol Chem *283*, 1197-1208.

Hartlerode, A.J., Morgan, M.J., Wu, Y., Buis, J., and Ferguson, D.O. (2015). Recruitment and activation of the ATM kinase in the absence of DNA-damage sensors. Nat Struct Mol Biol *22*, 736-743.

Herbig, U., Ferreira, M., Condel, L., Carey, D., and Sedivy, J.M. (2006). Cellular senescence in aging primates. Science *311*, 1257.

Hochegger, H., Dejsuphong, D., Fukushima, T., Morrison, C., Sonoda, E., Schreiber, V., Zhao, G.Y., Saberi, A., Masutani, M., Adachi, N., *et al.* (2006). Parp-1 protects homologous recombination from interference by Ku and Ligase IV in vertebrate cells. Embo j *25*, 1305-1314.

Hutchison, C.J. (2002). Lamins: building blocks or regulators of gene expression? Nat Rev Mol Cell Biol *3*, 848-858.

Imreh, G., Norberg, H.V., Imreh, S., and Zhivotovsky, B. (2011). Chromosomal breaks during mitotic catastrophe trigger gammaH2AX-ATM-p53-mediated apoptosis. J Cell Sci *124*, 2951-2963.

Jackson, S.P. (2002). Sensing and repairing DNA double-strand breaks. Carcinogenesis *23*, 687-696.

Jeyapalan, J.C., Ferreira, M., Sedivy, J.M., and Herbig, U. (2007). Accumulation of senescent cells in mitotic tissue of aging primates. Mech Ageing Dev *128*, 36-44.

Kelley, J.B., Datta, S., Snow, C.J., Chatterjee, M., Ni, L., Spencer, A., Yang, C.S., Cubenas-Potts, C., Matunis, M.J., and Paschal, B.M. (2011). The defective nuclear lamina in Hutchinson-gilford progeria syndrome disrupts the nucleocytoplasmic Ran gradient and inhibits nuclear localization of Ubc9. Mol Cell Biol *31*, 3378-3395.

Kennedy, B.K., Barbie, D.A., Classon, M., Dyson, N., and Harlow, E. (2000). Nuclear organization of DNA replication in primary mammalian cells. Genes Dev *14*, 2855-2868.

Kennedy, R.D., and D'Andrea, A.D. (2006). DNA repair pathways in clinical practice: lessons from pediatric cancer susceptibility syndromes. J Clin Oncol *24*, 3799-3808.

Kinner, A., Wu, W., Staudt, C., and Iliakis, G. (2008). Gamma-H2AX in recognition and signaling of DNA double-strand breaks in the context of chromatin. Nucleic Acids Res *36*, 5678-5694.

Kolas, N.K., Chapman, J.R., Nakada, S., Ylanko, J., Chahwan, R., Sweeney, F.D., Panier, S., Mendez, M., Wildenhain, J., Thomson, T.M., *et al.* (2007). Orchestration of the DNA-damage response by the RNF8 ubiquitin ligase. Science *318*, 1637-1640.

Kraemer, K.H., Patronas, N.J., Schiffmann, R., Brooks, B.P., Tamura, D., and DiGiovanna, J.J. (2007). Xeroderma pigmentosum, trichothiodystrophy and Cockayne syndrome: a complex genotype-phenotype relationship. Neuroscience *145*, 1388-1396.

Krishnan, V., Chow, M.Z., Wang, Z., Zhang, L., Liu, B., Liu, X., and Zhou, Z. (2011). Histone H4 lysine 16 hypoacetylation is associated with defective DNA repair and premature senescence in Zmpste24-deficient mice. Proc Natl Acad Sci U S A *108*, 12325-12330.

Kurz, E.U., Douglas, P., and Lees-Miller, S.P. (2004). Doxorubicin activates ATM-dependent phosphorylation of multiple downstream targets in part through the generation of reactive oxygen species. J Biol Chem *279*, 53272-53281.

Lee, J.S. (2007). Activation of ATM-dependent DNA damage signal pathway by a histone deacetylase inhibitor, trichostatin A. Cancer Res Treat *39*, 125-130.

Lee, S.E., Paques, F., Sylvan, J., and Haber, J.E. (1999). Role of yeast SIR genes and mating type in directing DNA double-strand breaks to homologous and non-homologous repair paths. Curr Biol *9*, 767-770.

Li, X., and Heyer, W.D. (2008). Homologous recombination in DNA repair and DNA damage tolerance. Cell Res *18*, 99-113.

Lieber, M.R. (2010). The mechanism of double-strand DNA break repair by the nonhomologous DNA end-joining pathway. Annu Rev Biochem *79*, 181-211.

Lin, M.T., and Beal, M.F. (2006). Mitochondrial dysfunction and oxidative stress in neurodegenerative diseases. Nature *443*, 787-795.

Liu, B., Ghosh, S., Yang, X., Zheng, H., Liu, X., Wang, Z., Jin, G., Zheng, B., Kennedy, B.K., Suh, Y., *et al.* (2012). Resveratrol rescues SIRT1-dependent adult stem cell decline and alleviates progeroid features in laminopathy-based progeria. Cell Metab *16*, 738-750.

Liu, B., Wang, J., Chan, K.M., Tjia, W.M., Deng, W., Guan, X., Huang, J.D., Li, K.M., Chau, P.Y., Chen, D.J., *et al.* (2005). Genomic instability in laminopathy-based premature aging. Nat Med *11*, 780-785.

Liu, B., Wang, Z., Ghosh, S., and Zhou, Z. (2013a). Defective ATM-Kap-1-mediated chromatin remodeling impairs DNA repair and accelerates senescence in progeria mouse model. Aging Cell *12*, 316-318.

Liu, B., Wang, Z., Zhang, L., Ghosh, S., Zheng, H., and Zhou, Z. (2013b). Depleting the methyltransferase Suv39h1 improves DNA repair and extends lifespan in a progeria mouse model. Nat Commun *4*, 1868.

Liu, G.H., Barkho, B.Z., Ruiz, S., Diep, D., Qu, J., Yang, S.L., Panopoulos, A.D., Suzuki, K., Kurian, L., Walsh, C., *et al.* (2011). Recapitulation of premature ageing with iPSCs from Hutchinson-Gilford progeria syndrome. Nature *472*, 221-225.

Liu, Y., Drozdov, I., Shroff, R., Beltran, L.E., and Shanahan, C.M. (2013c). Prelamin A accelerates vascular calcification via activation of the DNA damage response and senescence-associated secretory phenotype in vascular smooth muscle cells. Circ Res *112*, e99-109.

Liu, Y., Rusinol, A., Sinensky, M., Wang, Y., and Zou, Y. (2006). DNA damage responses in progeroid syndromes arise from defective maturation of prelamin A. J Cell Sci *119*, 4644-4649.

Liu, Y., Wang, Y., Rusinol, A.E., Sinensky, M.S., Liu, J., Shell, S.M., and Zou, Y. (2008). Involvement of xeroderma pigmentosum group A (XPA) in progeria arising from defective maturation of prelamin A. Faseb j *22*, 603-611.

Lombard, D.B., Chua, K.F., Mostoslavsky, R., Franco, S., Gostissa, M., and Alt, F.W. (2005). DNA repair, genome stability, and aging. Cell *120*, 497-512.

Lopez-Candales, A., Holmes, D.R., Liao, S., Scott, M.J., Wickline, S.A., and Thompson, R.W. (1997). Decreased vascular smooth muscle cell density in medial degeneration of human abdominal aortic aneurysms. Am J Pathol *150*, 993-1007.

Luo, X., and Kraus, W.L. (2012). On PAR with PARP: cellular stress signaling through poly(ADP-ribose) and PARP-1. Genes Dev *26*, 417-432.

Ma, Y., Lu, H., Tippin, B., Goodman, M.F., Shimazaki, N., Koiwai, O., Hsieh, C.L., Schwarz, K., and Lieber, M.R. (2004). A biochemically defined system for mammalian nonhomologous DNA end joining. Mol Cell *16*, 701-713.

Ma, Y., Pannicke, U., Schwarz, K., and Lieber, M.R. (2002). Hairpin opening and overhang processing by an Artemis/DNA-dependent protein kinase complex in nonhomologous end joining and V(D)J recombination. Cell *108*, 781-794.

Mah, L.J., El-Osta, A., and Karagiannis, T.C. (2010). gammaH2AX: a sensitive molecular marker of DNA damage and repair. Leukemia *24*, 679-686.

Mahen, R., Hattori, H., Lee, M., Sharma, P., Jeyasekharan, A.D., and Venkitaraman, A.R. (2013). A-type lamins maintain the positional stability of DNA damage repair foci in mammalian nuclei. PLoS One *8*, e61893.

Mailand, N., Bekker-Jensen, S., Faustrup, H., Melander, F., Bartek, J., Lukas, C., and Lukas, J. (2007). RNF8 ubiquitylates histones at DNA double-strand breaks and promotes assembly of repair proteins. Cell *131*, 887-900.

Manju, K., Muralikrishna, B., and Parnaik, V.K. (2006). Expression of disease-causing lamin A mutants impairs the formation of DNA repair foci. J Cell Sci *119*, 2704-2714.

Mao, Z., Bozzella, M., Seluanov, A., and Gorbunova, V. (2008). DNA repair by nonhomologous end joining and homologous recombination during cell cycle in human cells. Cell Cycle *7*, 2902-2906.

Mathew, C.G. (2006). Fanconi anaemia genes and susceptibility to cancer. Oncogene *25*, 5875-5884.

McClintock, D., Gordon, L.B., and Djabali, K. (2006). Hutchinson-Gilford progeria mutant lamin A primarily targets human vascular cells as detected by an anti-Lamin A G608G antibody. Proc Natl Acad Sci U S A *103*, 2154-2159.

McClintock, D., Ratner, D., Lokuge, M., Owens, D.M., Gordon, L.B., Collins, F.S., and Djabali, K. (2007). The mutant form of lamin A that causes Hutchinson-Gilford progeria is a biomarker of cellular aging in human skin. PLoS One *2*, e1269.

McCord, R.P., Nazario-Toole, A., Zhang, H., Chines, P.S., Zhan, Y., Erdos, M.R., Collins, F.S., Dekker, J., and Cao, K. (2013). Correlated alterations in genome organization, histone methylation, and DNA-lamin A/C interactions in Hutchinson-Gilford progeria syndrome. Genome Res *23*, 260-269.

Meier, J., Campbell, K.H., Ford, C.C., Stick, R., and Hutchison, C.J. (1991). The role of lamin LIII in nuclear assembly and DNA replication, in cell-free extracts of Xenopus eggs. J Cell Sci *98 (Pt 3)*, 271-279.

Menissier-de Murcia, J., Molinete, M., Gradwohl, G., Simonin, F., and de Murcia, G. (1989). Zinc-binding domain of poly(ADP-ribose)polymerase participates in the recognition of single strand breaks on DNA. J Mol Biol *210*, 229-233.

Merideth, M.A., Gordon, L.B., Clauss, S., Sachdev, V., Smith, A.C., Perry, M.B., Brewer, C.C., Zalewski, C., Kim, H.J., Solomon, B., *et al.* (2008). Phenotype and course of Hutchinson-Gilford progeria syndrome. N Engl J Med *358*, 592-604.

Moir, R.D., Montag-Lowy, M., and Goldman, R.D. (1994). Dynamic properties of nuclear lamins: lamin B is associated with sites of DNA replication. J Cell Biol *125*, 1201-1212.

Moir, R.D., Spann, T.P., Herrmann, H., and Goldman, R.D. (2000). Disruption of nuclear lamin organization blocks the elongation phase of DNA replication. J Cell Biol *149*, 1179-1192.

Murga, M., Jaco, I., Fan, Y., Soria, R., Martinez-Pastor, B., Cuadrado, M., Yang, S.M., Blasco, M.A., Skoultchi, A.I., and Fernandez-Capetillo, O. (2007). Global chromatin compaction limits the strength of the DNA damage response. J Cell Biol *178*, 1101-1108.

Murphy, M.P. (2009). How mitochondria produce reactive oxygen species. Biochem J *417*, 1-13.

Musich, P.R., and Zou, Y. (2009). Genomic instability and DNA damage responses in progeria arising from defective maturation of prelamin A. Aging (Albany NY) *1*, 28-37.

Musich, P.R., and Zou, Y. (2011). DNA-damage accumulation and replicative arrest in Hutchinson-Gilford progeria syndrome. Biochem Soc Trans *39*, 1764-1769.

Newport, J.W., Wilson, K.L., and Dunphy, W.G. (1990). A lamin-independent pathway for nuclear envelope assembly. J Cell Biol *111*, 2247-2259.

Nikolova, V., Leimena, C., McMahon, A.C., Tan, J.C., Chandar, S., Jogia, D., Kesteven, S.H., Michalicek, J., Otway, R., Verheyen, F., *et al.* (2004). Defects in nuclear structure and function promote dilated cardiomyopathy in lamin A/C-deficient mice. J Clin Invest *113*, 357-369.

Olins, A.L., and Olins, D.E. (2004). Cytoskeletal influences on nuclear shape in granulocytic HL-60 cells. BMC Cell Biol *5*, 30.

Olive, M., Harten, I., Mitchell, R., Beers, J.K., Djabali, K., Cao, K., Erdos, M.R., Blair, C., Funke, B., Smoot, L., *et al.* (2010). Cardiovascular pathology in Hutchinson-Gilford progeria: correlation with the vascular pathology of aging. Arterioscler Thromb Vasc Biol *30*, 2301-2309.

Oltvai, Z.N., Milliman, C.L., and Korsmeyer, S.J. (1993). Bcl-2 heterodimerizes in vivo with a conserved homolog, Bax, that accelerates programmed cell death. Cell *74*, 609-619.

Osorio, F.G., Navarro, C.L., Cadinanos, J., Lopez-Mejia, I.C., Quiros, P.M., Bartoli, C., Rivera, J., Tazi, J., Guzman, G., Varela, I., *et al.* (2011). Splicing-directed therapy in a new mouse model of human accelerated aging. Sci Transl Med *3*, 106ra107.

Pagano, G., Talamanca, A.A., Castello, G., Cordero, M.D., d'Ischia, M., Gadaleta, M.N., Pallardo, F.V., Petrovic, S., Tiano, L., and Zatterale, A. (2014). Oxidative stress and mitochondrial dysfunction across broad-ranging pathologies: toward mitochondria-targeted clinical strategies. Oxid Med Cell Longev *2014*, 541230.

Panier, S., and Boulton, S.J. (2014). Double-strand break repair: 53BP1 comes into focus. Nat Rev Mol Cell Biol *15*, 7-18.

Parnaik, V.K. (2008). Role of nuclear lamins in nuclear organization, cellular signaling, and inherited diseases. Int Rev Cell Mol Biol *266*, 157-206.

Patel, A.G., Sarkaria, J.N., and Kaufmann, S.H. (2011). Nonhomologous end joining drives poly(ADP-ribose) polymerase (PARP) inhibitor lethality in homologous recombination-deficient cells. Proc Natl Acad Sci U S A *108*, 3406-3411.

Paull, T.T., Rogakou, E.P., Yamazaki, V., Kirchgessner, C.U., Gellert, M., and Bonner, W.M. (2000). A critical role for histone H2AX in recruitment of repair factors to nuclear foci after DNA damage. Curr Biol *10*, 886-895.

Pegoraro, G., Kubben, N., Wickert, U., Gohler, H., Hoffmann, K., and Misteli, T. (2009). Ageing-related chromatin defects through loss of the NURD complex. Nat Cell Biol *11*, 1261-1267.

Polo, S.E., and Jackson, S.P. (2011). Dynamics of DNA damage response proteins at DNA breaks: a focus on protein modifications. Genes Dev *25*, 409-433.

Ragnauth, C.D., Warren, D.T., Liu, Y., McNair, R., Tajsic, T., Figg, N., Shroff, R., Skepper, J., and Shanahan, C.M. (2010). Prelamin A acts to accelerate smooth muscle cell senescence and is a novel biomarker of human vascular aging. Circulation *121*, 2200-2210.

Ray Chaudhuri, A., Hashimoto, Y., Herrador, R., Neelsen, K.J., Fachinetti, D., Bermejo, R., Cocito, A., Costanzo, V., and Lopes, M. (2012). Topoisomerase I poisoning results in PARP-mediated replication fork reversal. Nat Struct Mol Biol *19*, 417-423.

Reddy, K.L., Zullo, J.M., Bertolino, E., and Singh, H. (2008). Transcriptional repression mediated by repositioning of genes to the nuclear lamina. Nature *452*, 243-247.

Reina-San-Martin, B., Chen, H.T., Nussenzweig, A., and Nussenzweig, M.C. (2004). ATM is required for efficient recombination between immunoglobulin switch regions. J Exp Med *200*, 1103-1110.

Rensen, S.S., Doevendans, P.A., and van Eys, G.J. (2007). Regulation and characteristics of vascular smooth muscle cell phenotypic diversity. Neth Heart J *15*, 100-108.

Richards, S.A., Muter, J., Ritchie, P., Lattanzi, G., and Hutchison, C.J. (2011). The accumulation of un-repairable DNA damage in laminopathy progeria fibroblasts is caused by ROS generation and is prevented by treatment with N-acetyl cysteine. Hum Mol Genet *20*, 3997-4004.

Rivera-Torres, J., Acin-Perez, R., Cabezas-Sanchez, P., Osorio, F.G., Gonzalez-Gomez, C., Megias, D., Camara, C., Lopez-Otin, C., Enriquez, J.A., Luque-Garcia, J.L., *et al.* (2013). Identification of mitochondrial dysfunction in Hutchinson-Gilford

progeria syndrome through use of stable isotope labeling with amino acids in cell culture. J Proteomics *91*, 466-477.

Robles, S.J., and Adami, G.R. (1998). Agents that cause DNA double strand breaks lead to p16INK4a enrichment and the premature senescence of normal fibroblasts. Oncogene *16*, 1113-1123.

Rodriguez, S., Coppede, F., Sagelius, H., and Eriksson, M. (2009). Increased expression of the Hutchinson-Gilford progeria syndrome truncated lamin A transcript during cell aging. Eur J Hum Genet *17*, 928-937.

Rogakou, E.P., Boon, C., Redon, C., and Bonner, W.M. (1999). Megabase chromatin domains involved in DNA double-strand breaks in vivo. J Cell Biol *146*, 905-916.

Rothkamm, K., Kruger, I., Thompson, L.H., and Lobrich, M. (2003). Pathways of DNA double-strand break repair during the mammalian cell cycle. Mol Cell Biol *23*, 5706-5715.

Rzucidlo, E.M., Martin, K.A., and Powell, R.J. (2007). Regulation of vascular smooth muscle cell differentiation. J Vasc Surg *45 Suppl A*, A25-32.

San Filippo, J., Sung, P., and Klein, H. (2008). Mechanism of eukaryotic homologous recombination. Annu Rev Biochem *77*, 229-257.

Scaffidi, P., and Misteli, T. (2005). Reversal of the cellular phenotype in the premature aging disease Hutchinson-Gilford progeria syndrome. Nat Med *11*, 440-445.

Scaffidi, P., and Misteli, T. (2006). Lamin A-dependent nuclear defects in human aging. Science *312*, 1059-1063.

Shoeman, R.L., and Traub, P. (1990). The in vitro DNA-binding properties of purified nuclear lamin proteins and vimentin. J Biol Chem *265*, 9055-9061.

Shumaker, D.K., Dechat, T., Kohlmaier, A., Adam, S.A., Bozovsky, M.R., Erdos, M.R., Eriksson, M., Goldman, A.E., Khuon, S., Collins, F.S., *et al.* (2006). Mutant nuclear lamin A leads to progressive alterations of epigenetic control in premature aging. Proc Natl Acad Sci U S A *103*, 8703-8708.

Singh, M., Hunt, C.R., Pandita, R.K., Kumar, R., Yang, C.R., Horikoshi, N., Bachoo, R., Serag, S., Story, M.D., Shay, J.W., *et al.* (2013). Lamin A/C depletion enhances DNA damage-induced stalled replication fork arrest. Mol Cell Biol *33*, 1210-1222.

Singh, S.K., Wu, W., Wang, M., and Iliakis, G. (2009). Extensive repair of DNA double-strand breaks in cells deficient in the DNA-PK-dependent pathway of NHEJ after exclusion of heat-labile sites. Radiat Res *172*, 152-164.

Snow, C.J., Dar, A., Dutta, A., Kehlenbach, R.H., and Paschal, B.M. (2013). Defective nuclear import of Tpr in Progeria reflects the Ran sensitivity of large cargo transport. J Cell Biol *201*, 541-557.

Spann, T.P., Moir, R.D., Goldman, A.E., Stick, R., and Goldman, R.D. (1997). Disruption of nuclear lamin organization alters the distribution of replication factors and inhibits DNA synthesis. J Cell Biol *136*, 1201-1212.

Starr, D.A., and Fridolfsson, H.N. (2010). Interactions between nuclei and the cytoskeleton are mediated by SUN-KASH nuclear-envelope bridges. Annu Rev Cell Dev Biol *26*, 421-444.

Steen, R.L., Martins, S.B., Tasken, K., and Collas, P. (2000). Recruitment of protein phosphatase 1 to the nuclear envelope by A-kinase anchoring protein AKAP149 is a prerequisite for nuclear lamina assembly. J Cell Biol *150*, 1251-1262.

Stehbens, W.E., Delahunt, B., Shozawa, T., and Gilbert-Barness, E. (2001). Smooth muscle cell depletion and collagen types in progeric arteries. Cardiovasc Pathol *10*, 133-136.

Stehbens, W.E., Wakefield, S.J., Gilbert-Barness, E., Olson, R.E., and Ackerman, J. (1999). Histological and ultrastructural features of atherosclerosis in progeria. Cardiovasc Pathol *8*, 29-39.

Stiff, T., O'Driscoll, M., Rief, N., Iwabuchi, K., Lobrich, M., and Jeggo, P.A. (2004). ATM and DNA-PK function redundantly to phosphorylate H2AX after exposure to ionizing radiation. Cancer Res *64*, 2390-2396.

Stuurman, N., Heins, S., and Aebi, U. (1998). Nuclear lamins: their structure, assembly, and interactions. J Struct Biol *122*, 42-66.

Sun, Y., Jiang, X., Xu, Y., Ayrapetov, M.K., Moreau, L.A., Whetstine, J.R., and Price, B.D. (2009). Histone H3 methylation links DNA damage detection to activation of the tumour suppressor Tip60. Nat Cell Biol *11*, 1376-1382.

Sung, P., and Klein, H. (2006). Mechanism of homologous recombination: mediators and helicases take on regulatory functions. Nat Rev Mol Cell Biol *7*, 739-750.

Takahashi, K., Tanabe, K., Ohnuki, M., Narita, M., Ichisaka, T., Tomoda, K., and Yamanaka, S. (2007). Induction of pluripotent stem cells from adult human fibroblasts by defined factors. Cell *131*, 861-872.

Takata, M., Sasaki, M.S., Sonoda, E., Morrison, C., Hashimoto, M., Utsumi, H., Yamaguchi-Iwai, Y., Shinohara, A., and Takeda, S. (1998). Homologous recombination and non-homologous end-joining pathways of DNA double-strand break repair have overlapping roles in the maintenance of chromosomal integrity in vertebrate cells. Embo j *17*, 5497-5508.

Tang, J., Cho, N.W., Cui, G., Manion, E.M., Shanbhag, N.M., Botuyan, M.V., Mer, G., and Greenberg, R.A. (2013). Acetylation limits 53BP1 association with damaged chromatin to promote homologous recombination. Nat Struct Mol Biol *20*, 317-325.

Taniura, H., Glass, C., and Gerace, L. (1995). A chromatin binding site in the tail domain of nuclear lamins that interacts with core histones. J Cell Biol *131*, 33-44.

Thompson, L.J., Bollen, M., and Fields, A.P. (1997). Identification of protein phosphatase 1 as a mitotic lamin phosphatase. J Biol Chem *272*, 29693-29697.

Ulukan, H., and Swaan, P.W. (2002). Camptothecins: a review of their chemotherapeutic potential. Drugs *62*, 2039-2057.

Vakifahmetoglu, H., Olsson, M., and Zhivotovsky, B. (2008). Death through a tragedy: mitotic catastrophe. Cell Death Differ *15*, 1153-1162.

Varela, I., Cadinanos, J., Pendas, A.M., Gutierrez-Fernandez, A., Folgueras, A.R., Sanchez, L.M., Zhou, Z., Rodriguez, F.J., Stewart, C.L., Vega, J.A., *et al.* (2005). Accelerated ageing in mice deficient in Zmpste24 protease is linked to p53 signalling activation. Nature *437*, 564-568.

Varga, R., Eriksson, M., Erdos, M.R., Olive, M., Harten, I., Kolodgie, F., Capell, B.C., Cheng, J., Faddah, D., Perkins, S., *et al.* (2006). Progressive vascular smooth muscle cell defects in a mouse model of Hutchinson-Gilford progeria syndrome. Proc Natl Acad Sci U S A *103*, 3250-3255.

Verstraeten, V.L., Broers, J.L., Ramaekers, F.C., and van Steensel, M.A. (2007). The nuclear envelope, a key structure in cellular integrity and gene expression. Curr Med Chem *14*, 1231-1248.

Vitale, I., Galluzzi, L., Castedo, M., and Kroemer, G. (2011). Mitotic catastrophe: a mechanism for avoiding genomic instability. Nat Rev Mol Cell Biol *12*, 385-392.

Vlcek, S., and Foisner, R. (2007). A-type lamin networks in light of laminopathic diseases. Biochim Biophys Acta *1773*, 661-674.

Wang, M., Wu, W., Rosidi, B., Zhang, L., Wang, H., and Iliakis, G. (2006). PARP-1 and Ku compete for repair of DNA double strand breaks by distinct NHEJ pathways. Nucleic Acids Res *34*, 6170-6182.

Ward, I.M., and Chen, J. (2001). Histone H2AX is phosphorylated in an ATR-dependent manner in response to replicational stress. J Biol Chem *276*, 47759-47762.

Ward, I.M., Minn, K., Jorda, K.G., and Chen, J. (2003). Accumulation of checkpoint protein 53BP1 at DNA breaks involves its binding to phosphorylated histone H2AX. J Biol Chem *278*, 19579-19582.

Xie, A., Hartlerode, A., Stucki, M., Odate, S., Puget, N., Kwok, A., Nagaraju, G., Yan, C., Alt, F.W., Chen, J., *et al.* (2007a). Distinct roles of chromatin-associated proteins MDC1 and 53BP1 in mammalian double-strand break repair. Mol Cell *28*, 1045-1057.

Xie, A., Puget, N., Shim, I., Odate, S., Jarzyna, I., Bassing, C.H., Alt, F.W., and Scully, R. (2004). Control of sister chromatid recombination by histone H2AX. Mol Cell *16*, 1017-1025.

Xie, C.Q., Zhang, J., Villacorta, L., Cui, T., Huang, H., and Chen, Y.E. (2007b). A highly efficient method to differentiate smooth muscle cells from human embryonic stem cells. In Arterioscler Thromb Vasc Biol (United States), pp. e311-312.

Xiong, Z.M., Choi, J.Y., Wang, K., Zhang, H., Tariq, Z., Wu, D., Ko, E., LaDana, C., Sesaki, H., and Cao, K. (2015). Methylene blue alleviates nuclear and mitochondrial abnormalities in progeria. Aging Cell.

Xiong, Z.M., Choi, J.Y., Wang, K., Zhang, H., Tariq, Z., Wu, D., Ko, E., LaDana, C., Sesaki, H., and Cao, K. (2016). Methylene blue alleviates nuclear and mitochondrial abnormalities in progeria. Aging Cell *15*, 279-290.

Yang, S.H., Meta, M., Qiao, X., Frost, D., Bauch, J., Coffinier, C., Majumdar, S., Bergo, M.O., Young, S.G., and Fong, L.G. (2006). A farnesyltransferase inhibitor improves disease phenotypes in mice with a Hutchinson-Gilford progeria syndrome mutation. J Clin Invest *116*, 2115-2121.

You, Z., Chahwan, C., Bailis, J., Hunter, T., and Russell, P. (2005). ATM activation and its recruitment to damaged DNA require binding to the C terminus of Nbs1. Mol Cell Biol *25*, 5363-5379.

Zee, B.M., Britton, L.M., Wolle, D., Haberman, D.M., and Garcia, B.A. (2012). Origins and formation of histone methylation across the human cell cycle. Mol Cell Biol *32*, 2503-2514.

Zhang, H., Kieckhaefer, J.E., and Cao, K. (2013). Mouse models of laminopathies. Aging Cell *12*, 2-10.

Zhang, H., Xiong, Z.M., and Cao, K. (2014). Mechanisms controlling the smooth muscle cell death in progeria via down-regulation of poly(ADP-ribose) polymerase 1. Proc Natl Acad Sci U S A *111*, E2261-2270.

Zhang, J., Lian, Q., Zhu, G., Zhou, F., Sui, L., Tan, C., Mutalif, R.A., Navasankari, R., Zhang, Y., Tse, H.F., *et al.* (2011). A human iPSC model of Hutchinson Gilford Progeria reveals vascular smooth muscle and mesenchymal stem cell defects. Cell Stem Cell *8*, 31-45.

Zhang, W., Li, J., Suzuki, K., Qu, J., Wang, P., Zhou, J., Liu, X., Ren, R., Xu, X., Ocampo, A., *et al.* (2015). Aging stem cells. A Werner syndrome stem cell model

unveils heterochromatin alterations as a driver of human aging. Science *348*, 1160-1163.

Zhao, H., and Piwnica-Worms, H. (2001). ATR-mediated checkpoint pathways regulate phosphorylation and activation of human Chk1. Mol Cell Biol *21*, 4129-4139.

Zhou, Y., Caron, P., Legube, G., and Paull, T.T. (2014). Quantitation of DNA double-strand break resection intermediates in human cells. Nucleic Acids Res *42*, e19.

Zimmermann, M., Lottersberger, F., Buonomo, S.B., Sfeir, A., and de Lange, T. (2013). 53BP1 regulates DSB repair using Rif1 to control 5' end resection. Science *339*, 700-704.